SP Technical Research Institute of Sweden

Assessment of concrete structures after fire

Joakim Albrektsson, Mathias Flansbjer,
Jan Erik Lindqvist and Robert Jansson

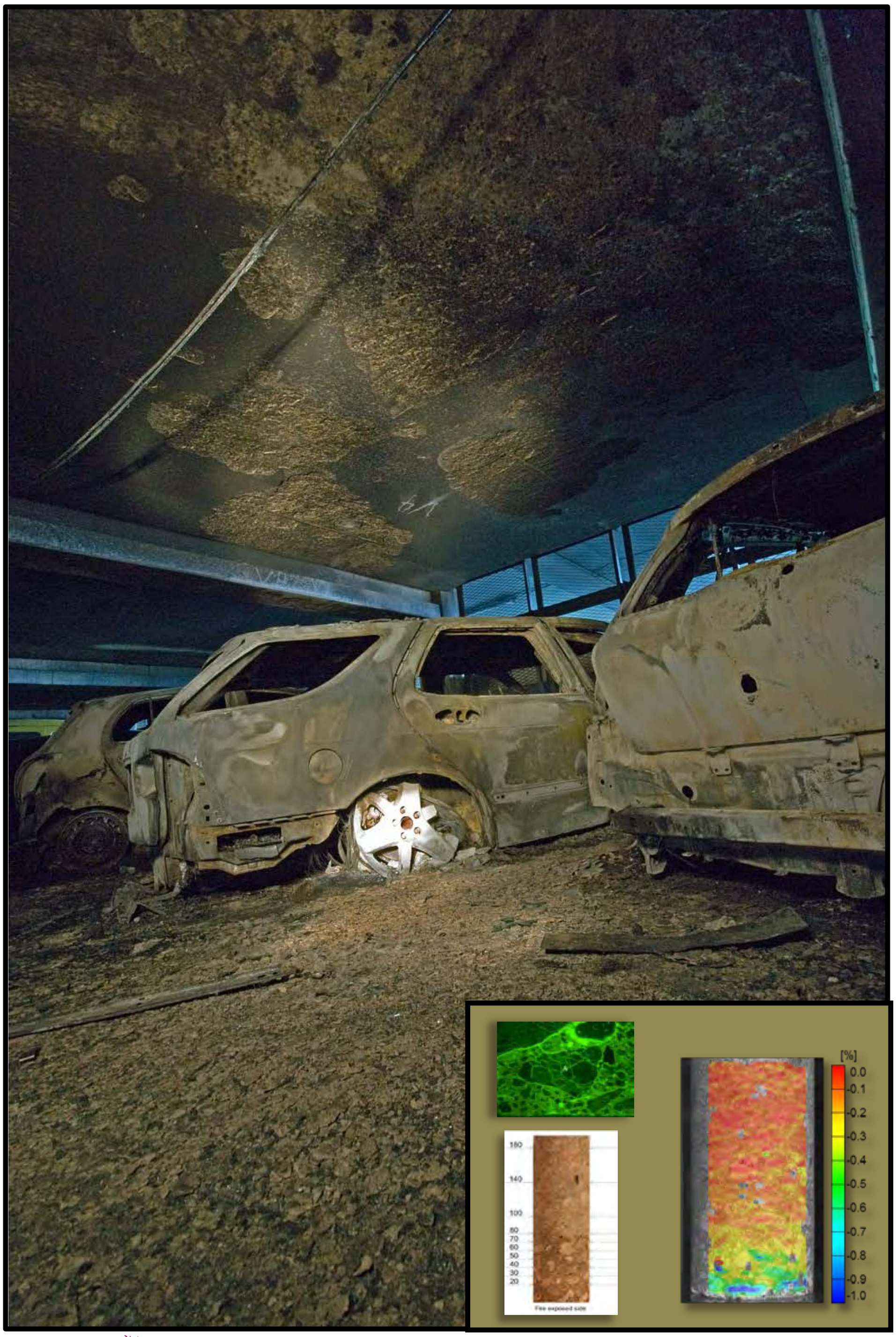

Brandforsk project number: 301-091

Fire Technology

SP Report 2011:19

Assessment of concrete structures after fire

Joakim Albrektsson, Mathias Flansbjer,
Jan Erik Lindqvist and Robert Jansson

Abstract

After a fire incident the first question from a structural point of view is whether the construction can be refurbished or, in extreme cases, needs to be replaced. The choice of action must be based on an assessment of the status of the structure. This assessment is in turn based on a mapping of damage to the construction. The mapping of damage needs to be accurate to optimise both the safety level and the best solution from an economic point of view. The work presented in this report is divided into a literature study of commonly used traditional methods to conduct such a “mapping of damage” and an experimental part where several traditional methods are compared to a new methodology which has been developed for such applications in this project. The traditional assessment methods included in the experimental part of the report are: rebound hammer, ultrasonic pulse measurements and microscopy methods. These are compared to optical full-field strain measurements during a compressive load cycle on drilled cores, i.e. the new method proposed to determine the degree of damage in a fire exposed cross-section.

Based on the results from the present study an approach with two levels of complexity is recommended. The initial level is to perform an inspection and determine the development, size and spread pattern of the fire (if possible). This should also include a visual mapping of damage, such as spalling, cracking, delaminations, deformations and other physical influence from the fire. When doing this initial investigation it is useful to have a hammer and a chisel at hand to be able to identify highly affected parts and delaminations. At complex fire scenes it is also helpful to use a damage classification system. If a slightly more detailed map of the affected areas is required at this level the rebound hammer and ultrasonic pulse velocity measurements can be helpful. It is important, however, to remember that it is difficult to use these methods for more detailed assessments of how deep the damage is to the cross-section.

In many cases the above recommended strategy gives enough information for a recommendation concerning how to restore a construction after a fire. But sometimes a more in detail picture of the degradation is needed to assess the conditions of a construction and then a second level of complexity is opened using core drilling and a battery of laboratory tests.

On site directly after drilling it is possible to do ultrasonic pulse measurement on different depths from the fire exposed side of the core to get a rough overview of the depth of damage. As this method is on site decisions to conduct further drilling can be based on the results. In the laboratory the cores can be examined by different microscopy methods. Studies of cracks and colour change can provide important information on the maximum temperature that the reinforcement may have been exposed to and information about the residual durability as high intensity of cracks amplify the sensitivity to reinforcement corrosion.

To ultimately obtain a direct coupling to mechanical properties, optical full-field strain measurements during a compressive load cycle can be performed on the drilled cores. With this measurement a true mechanical response of the material in the cross-section can be determined as the most damaged parts will deform more under load as the stiffness will be reduced. This will give a picture on the degree of damage at different depths.

Key words: Concrete, fire, damage assessment

SP Sveriges Tekniska Forskningsinstitut
SP Technical Research Institute of Sweden

SP Report 2011:19
ISBN 978-91-86622-50-3
ISSN 0284-5172
Borås 2011

Contents

Appendix

Preface

This project was supported by Brandforsk, project number 301-091, which is gratefully acknowledged.

We also wish to thank the following persons for valuable support during the project: Dr Roberto Felisetti from the University of Milano in Italy for his inspiring lecture during a visit at SP; Prof. Johan Silfwerbrand and Tec lic. Jan Trägårdh from CBI Swedish Cement and Concrete Institute; and Dr. Lars Boström at SP Fire Technology for his input during the project.

The project group had the following composition:

Robert Jansson, SP Fire Technology, Project leader
Joakim Albrektsson, SP Fire Technology
Mathias Flansbjer, SP Building Technology and Mechanics
Jan Erik Lindqvist, CBI Swedish Cement and Concrete Institute

Borås, March 2011
Robert Jansson

Sammanfattning

När en brand har påverkat en betongkonstruktion måste en tillståndsbedömning av konstruktionen göras för att säkerställa dess funktion. Efter tillståndsbedömningen kan beslut tas om konstruktionen behöver repareras eller i allvarliga fall rivas. Vid tillståndsbedömningen karteras visuella skador och resultat från mätmetoder som används för att upptäcka skador. Det är viktigt att skadenivån kan bestämmas med tillräckligt god noggrannhet både med tanke på säkerheten men även av ekonomiska skäl. Rapporten är uppdelad i två delar, en litteraturdel där provningsmetoder som är vanligt förekommande vid tillståndsbedömningar beskrivs samt en experimentell del där studshammarmätningar, ultraljudsmätningar och mikroskopi jämförs med en ny metodik som har utvecklats för att utvärdera brandpåverkad betong. Den nya metodiken, optisk deformationsmätning under tryckprov på utborrade cylindrar, möjliggör en kontinuerlig utvärdering av skadenivån i tvärsnittet av den brandpåverkade betongen.

Baserat på litteraturstudien och resultaten från den experimentella delen rekommenderas två olika nivåer på utredningen. Om nivå ett inte ger tillräcklig information rekommenderas mer komplicerade metoder. Genom en visuell granskning av brandplatsen både inkluderat den påverkade konstruktionen och andra påverkade objekt på brandplatsen samt räddningstjänstens rapport och andra iakttagelser i samband med branden kan brandens intensitet, varaktighet och utbredning uppskattas. Skador på betongen som spjälkning, deformationer, delamineringar och annan synlig påverkan dokumenteras. Med hjälp av en vanlig hammare och en huggmejsel kan delamineringar och andra svaga zoner lokaliseras. Vi komplexa brandscenarier är det lämpligt att använda ett klassificeringssystem för skadorna. I dessa fall kan det även var till hjälp att använda studshammaren och genomföra ultraljudsmätningar för att kvantifiera skadorna. Dessa metoder indikerar kraftigt påverkade zoner med ger ingen direkt information om skadornas djup.

I många fall ger undersökningen beskriven ovan tillräckligt med information för att kunna besluta om nödvändiga åtgärder för konstruktionen. I vissa fall behövs dock en noggrannare bestämning av hur djupa skadorna är. I dessa fall kan kärnor borras ur konstruktionen och utvärderas med laboratoriemetoder.

I samband med att en kärna borras ur konstruktionen kan ultraljudsmätningar på olika djup tvärs över kärna genomföras. På så vis får bedömaren en direkt uppfattning om skadans djup och har då möjlighet att korrigera provuttaget. I laboratoriet studeras sedan sprickbildningar och färgväxlingar i mikroskop vilket ger viktig information om den maximala temperaturen som armeringen har utsatts för under branden. Sprickbildningen ger även information om konstruktionens beständighet eftersom en hög sprickintensitet ger hög permeabilitet vilket ökar risken för armeringskorrosion.

För att gör en direkt mätning av hur branden har påverkat de mekaniska egenskaperna hos den brandpåverkade betongen kan kärnorna belastas i en tryckprovningsmaskin samtidigt som deformationerna mäts med ett beröringsfritt mätsystem. Detta ger den verkliga mekaniska responsen längs kärnans tvärsnitt eftersom de brandskadade delarna deformeras mer under belastning. Denna metod ger en bild av skadenivån i hela tvärsnittet vilket leder till en säkrare bedömning av resthållfastheten.

1 Introduction

Concrete is one of the main building materials in society today. It is cheap, durable and has satisfactory fire performance in most instances of fire exposure. Despite this there will always be combinations of certain constructions and fire scenarios when the concrete is seriously damaged and, in extreme cases, collapses.

After a fire incident the first question from a structural point of view is whether the construction can be refurbished or, in extreme cases, needs to be replaced. The choice of action will be based on an assessment of the status of the structure. This assessment is based on mapping of damage in the construction. This mapping of damages needs to be accurate to ensure both a good safety level and the best solution from an economic point of view can be found. There are some calculation methodologies that may assist an evaluation but the assessment should be based mainly on on-site inspections supplemented by laboratory testing when necessary (Concrete Society, 2008).

The aim of this project is to provide an overview of some traditional methods for the assessment of damage to concrete cross-sections after fire, including their pros and cons and to investigate a new method for assessing the damage to a concrete structure after exposure to a fire. This new method is directly coupled to an assessment of the mechanical properties of the concrete in contrast to the majority of traditional methods that are indirect.

It is also important to remember safety aspect when arriving at a fire site. Jones (1986) has made an illustrative flow chart, shown in Figure 1, describing the process when conducting an assessment of a structure after a fire event.

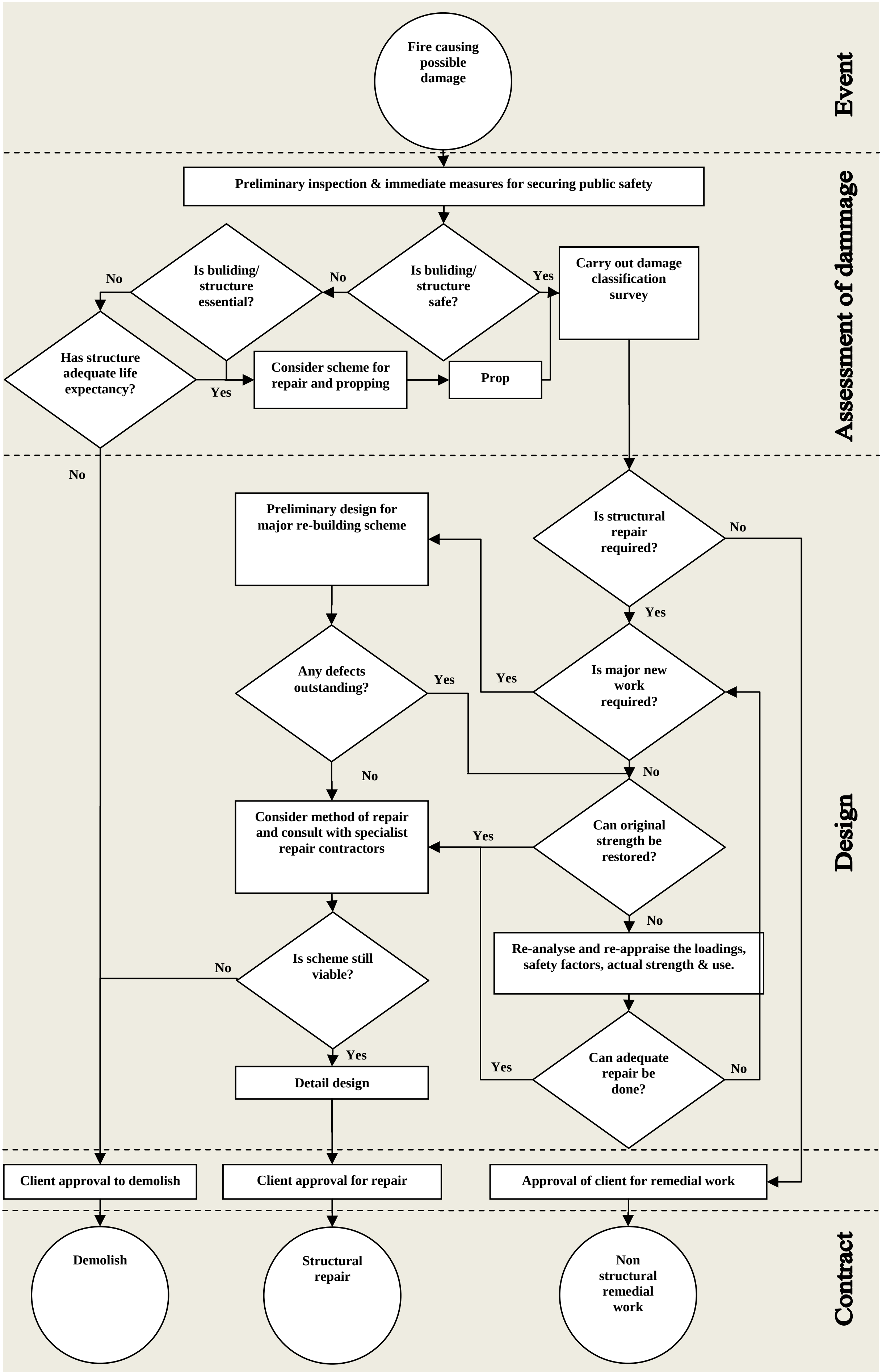

Figure 1 *Assessment procedure for fire damaged structures (Jones, 1986).*

1.1 Limitations

With a few exceptions this study is limited to material behaviour rather than the behaviour of a whole structure. If the depth of damage can be classified with good accuracy a safe and economic assessment, from a structural engineering point of view, of the whole fire exposed structure can be made based on this information.

2 Assessment of fire damaged concrete

2.1 Effect of elevated temperature

2.1.1 Concrete

During recent decades a vast amount of experiments have been undertaken to determine the thermal and mechanical properties of concrete. However, concrete is not a single material. Rather it can be considered as a family of related materials with sometimes rather different physical properties. Therefore, it is no simple matter to provide a comprehensive overview of the influence of temperature on the physical properties of all types of concrete. Further, the specific choice of test method when determining the physical properties of concrete at high temperature has an impact on the results obtained and explains some of the differences between results found in the literature.

The influence of temperature on some important properties of concrete is described in more general terms in the Eurocode 1992-1-2 (2004). The temperature dependant thermal conductivity is described in Eurocode1992-1-2 (2004) with two curves: an upper limit and a lower limit. As seen in Figure 2 the conductivity decreases with temperature as the porosity and the occurrence of micro-cracks increases. In Figure 3 the influence of temperature on the volumetric specific heat is shown. In this curve a peak from free moisture inside the concrete is included to take into account the effect from the free moisture contained in the porous system.

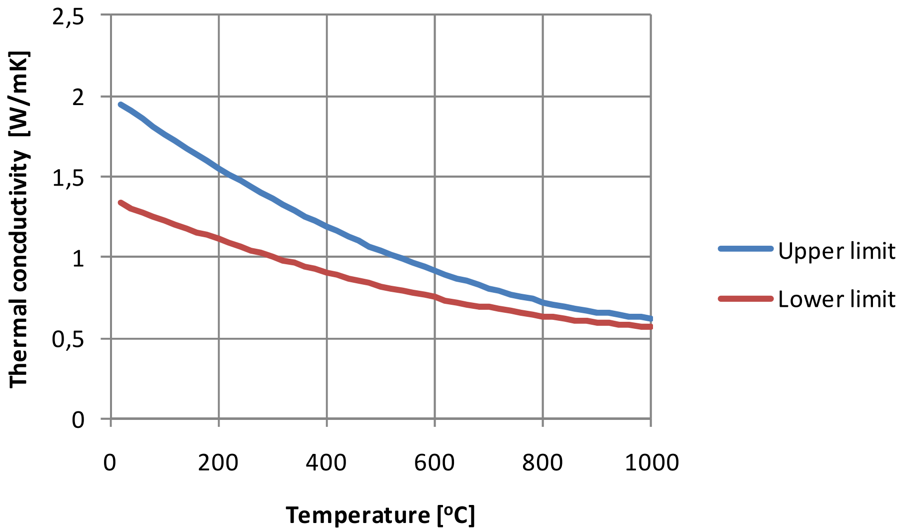

Figure 2 *Temperature dependant thermal conductivity according to EN 1992-1-2 (2004).*

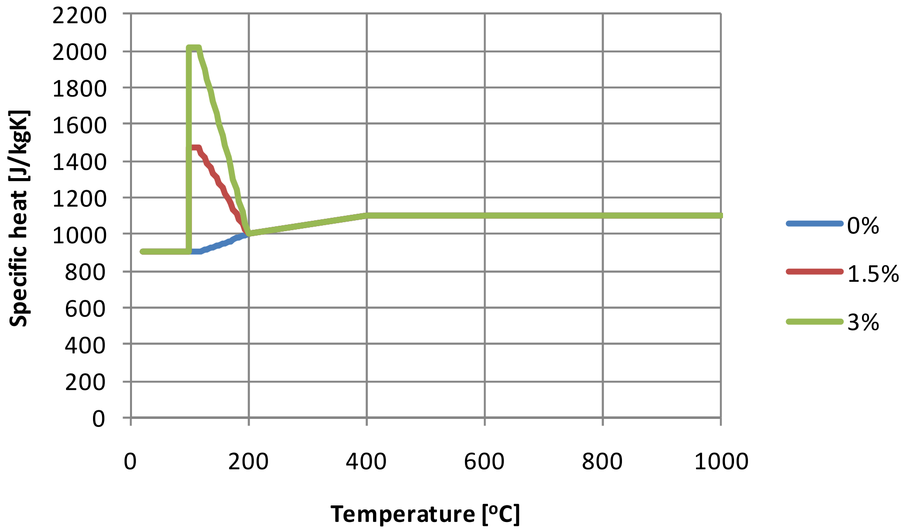

Figure 3 *Temperature dependant specific heat for concrete with 0, 1.5 and 3 % moisture content according to EN 1992-1-2.*

When conducting calculations of the heating of concrete based on the conductivity and the specific heat shown in the diagrams above, the changes in density also need to be known. In Figure 4 the temperature dependant density variation according to the Eurocode is shown. The main component in the density reduction is the loss of water.

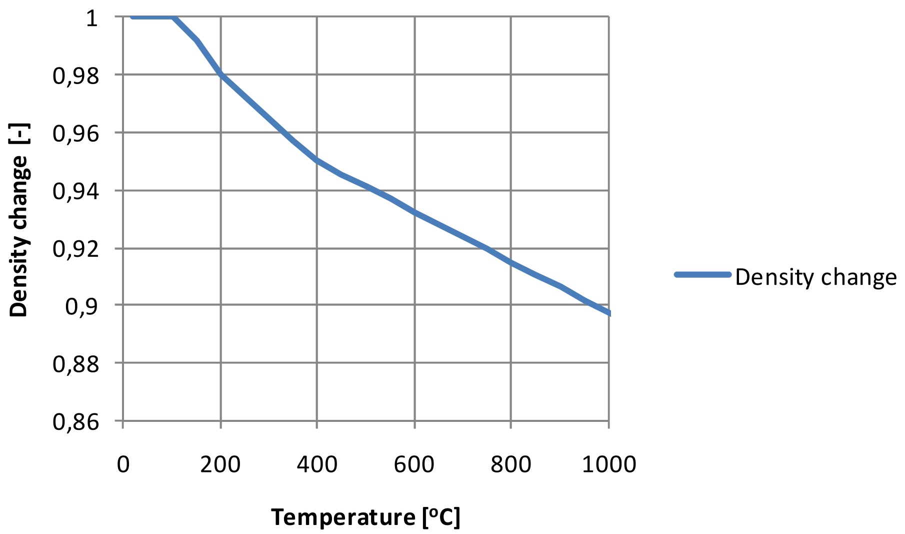

Figure 4 *Reduction of density with temperature according to EN 1992-1-2.*

The mechanical properties of concrete are changed at elevated temperatures compared to values at room temperature. The loss of compressive strength at high temperatures is defined for two types of aggregates in the Eurocode: siliceous and calcareous aggregate, see Figure 5. The values in the diagram should only be interpreted as a general trend as the reduction of compressive strength is strongly dependent on whether the concrete is loaded during heating or not (Bazant & Kaplan, 1996).

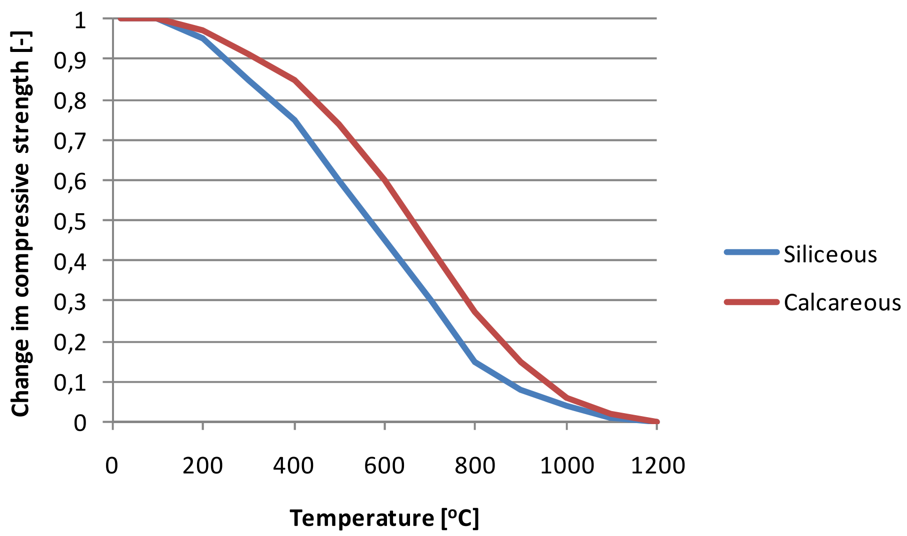

Figure 5 *Variation of compressive strength with temperature according to EN 1992-1-2(2004).*

When looking at the change of elastic modulus with temperature the values that can be derived from the temperature dependant stress strain relationship defined in the Eurocode EN 1992-1-2 (2004) are not applicable. This is because the effect of transient creep is implicitly taken into account as a reduction in stiffness. When looking at experimentally determined values for the elastic modulus a large variation is found in the literature. To summarize the results Figure 6 shows a region in the reduction curve where most of the results can be found.

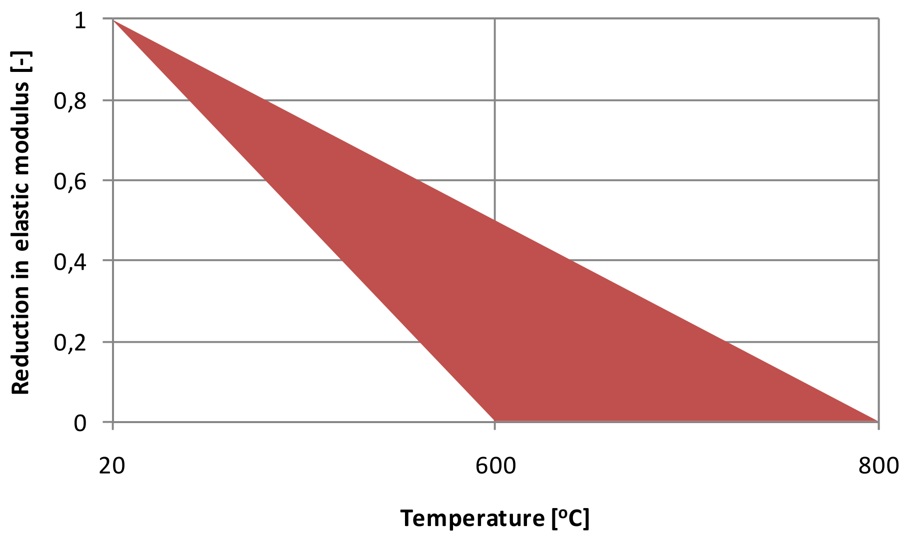

Figure 6 *Region were most of the results on the temperature dependant elastic modulus can be found.*

2.1.2 Reinforcement and pre stressing wires

In reinforced concrete structures the reinforcement cover will protect the reinforcement against heat. However, in cases with long fire exposure the reinforcement will be exposed to significant heating. Hot-rolled bars shows no strength reduction up to 400 °C, but the elastic modulus starts to decrease above 100 °C and the yield plateau will disappear above 200 °C (fib, 2008), (Schneider et al, 1990). At higher temperatures the loss of strength is more serious, e.g. only 20 % of the original strength is left at 650 °C. Cold-drawn bars, wires and strands are more sensitive than hot-rolled bars to elevated temperatures. A 50 % reduction of the strength occurs at 400 °C and only 10 % of the original strength remains at 650 °C.

As long as the temperature is less than 450 °C the original yield strength of cold worked steel will be restored after cooling down. The equivalent temperature for hot-rolled steels is 650 °C. Above these temperatures the residual yield strength will decrease. Figure 7 shows conservative values of the strength degradation for typical reinforcement.

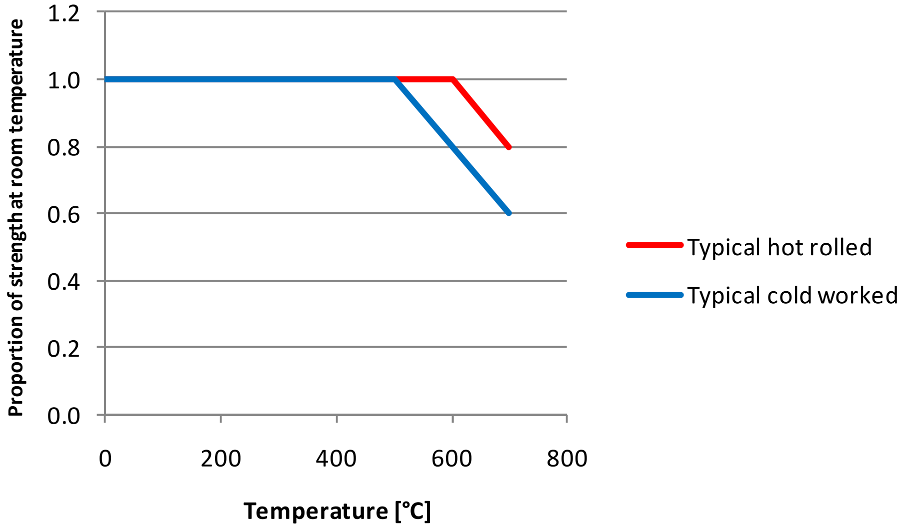

Figure 7 *Residual strength reduction for typical hot-rolled and cold worked reinforcement (fib, 2008), (Schneider et al, 1990), (Concrete Society, 1978).*

At high temperatures the ductility of the material may decrease. One indirect method of strength measurement is to measure the surface hardness of the reinforcement. However, the surface hardness and the centre hardness may differ due to quenching during fire fighting. Buckling of reinforcing bars may occur as a consequence of compressive stresses induced by thermal expansion. In case of buckling, the reinforcing bars may loss their bound to the concrete. The loss of strength at high temperatures is usually responsible for significant residual deflection. Figure 8 shows the proportion of yield strength and ultimate tensile strength for hot rolled- and cold worked reinforcing steel, respectively at room temperature (Eurocode 2, 2004).

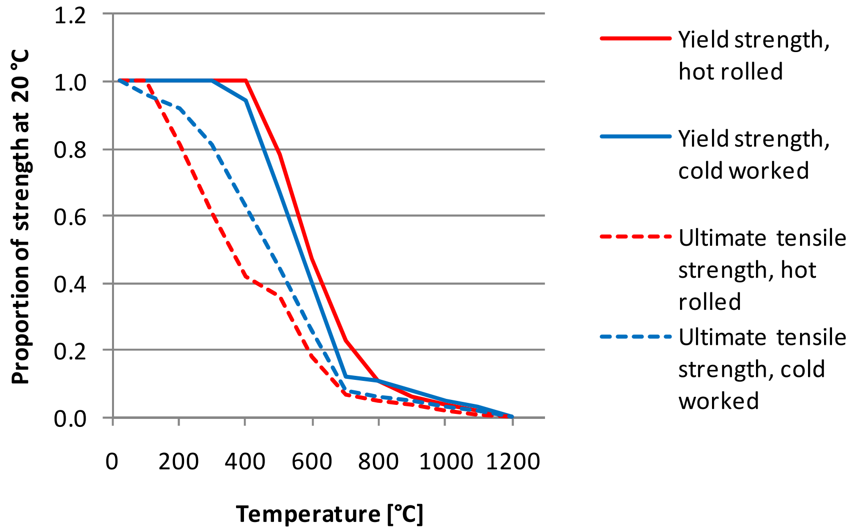

Figure 8 *Proportion of yield strength and ultimate tensile strength at 20 °C.*

2.2 Damage assessment

2.2.1 Initial assessment

When arriving to a fire damaged concrete structure it is important to start the investigation by conducting a general inspection and making observations of the extent of the fire, e.g. size and spread pattern of the fire, visible damage, etc. Useful information can often be found concerning the fire development and intensity from the incident report which can be obtained from the Fire and Rescue Services. When preparing for this general inspection, it is advantageous if relevant technical drawings for the structure are available (either from the owners or the local county authorities).

In Table 1 some useful temperature indicators that can be used during the general inspection are summarised. An example of a temperature indicator from a real assessment can be seen in Figure 9 where the state of PVC indicates the temperature. When doing this first inspection it is very useful to bring a hammer and a chisel and use them to obtain a rough overview of the situation. Differences in sound can indicate fire damage in the surface layer and delaminated areas can be identified by their typical low frequency sound response.

Table 1 *Effect of temperature on common materials (Concrete Society, 2008).*

Substance	Typical example	Conditions	Approximate temperature °C
Paints		Deteriorates Destroyed	100 150
Polystyrene	Thin-wall food container foam, light shades, handles, curtain hooks, radio casings	Collapse Softens Melts and flows	120 120-140 150-180
Polyethylene	Bags, films, bottles, buckets, pipes	Shrivels Softens and melts	120 120-140
Polymethylmeth acrylate	Handles, covers, skylights, glazing	Softens Bubbles	130-200 250
PVC	Cables, pipes, ducts, linings, profiles, handles, knobs, house ware, toys, bottles (Values depend on length of exposure to temperature)	Degrades Fumes Browns Charring	100 150 200 400-500
Cellulose	Wood, paper, cotton	Darkens	200-300
Wood		Ignites	240
Solder lead	Plumber joints, plumbing, sanitary installations, toys	Melts Melts, sharp edges rounded Drop formation	250 300-350 350-400
Zinc	Sanitary installations, gutters, down pipes	Drop formation Melts	400 420
Aluminum and alloys	Fixtures, brackets, small mechanical parts	Softens Melts Drop formation	400 600 650
Glass	Glazing, bottles	Softens, sharp edges rounded Flowing easily, viscous	500-600 800
Silver	Jewellery, spoons, cutlery	Melts Drop formation	900 950
Brass	Locks, traps, door handles, clasps	Melts (particularly edges) Drop formation	900-1000 950-1050
Bronze	Windows, fittings, doorbells, ornamentation	Edges rounded Drop formation	900 900-1000
Copper	Wiring, cables, ornaments	Melts	1000-1100
Cast iron	Radiators, pipes	Melts Drop formation	1100-1200 1150-1250

Figure 9 *A partly charred PVC pipe found embedded in the cross section. (Photograph: Robert Jansson)*

In many instances, the assessment of fire exposed concrete stops after this general inspection. Knowledge of the fire intensity, together with mapping with hammer and chisel and close study of the drawings of the concrete cross-sections, often provides sufficient information for an assessment of the damage to the concrete structure. In cases where more detailed information is needed, a variety of more sophisticated test methods are available, which are outlined below.

2.2.2 Test methods for assessment

Concrete is an incombustible material with low thermal diffusivity and will therefore usually exhibit a good behaviour at high temperatures. However, the low diffusivity causes a high thermal gradient close to the fire exposed surface, i.e. the reinforcement cover, and the thermal damage will consequently rapidly decrease at a short distance from the fire exposed surface. Only fires with long duration will affect deeper regions of a concrete structure. Therefore, it is of great interest to assess reinforced concrete structures exposed to fire in order to plan necessary strengthening action after the fire. Calculated temperature profiles in a concrete specimen exposed to a temperature increase as described in the ISO 834-1:1999 are shown in Figure 10 and Figure 11. Temperature dependent material data as described in EN 1992-1-2 was used to calculate the temperature profiles.

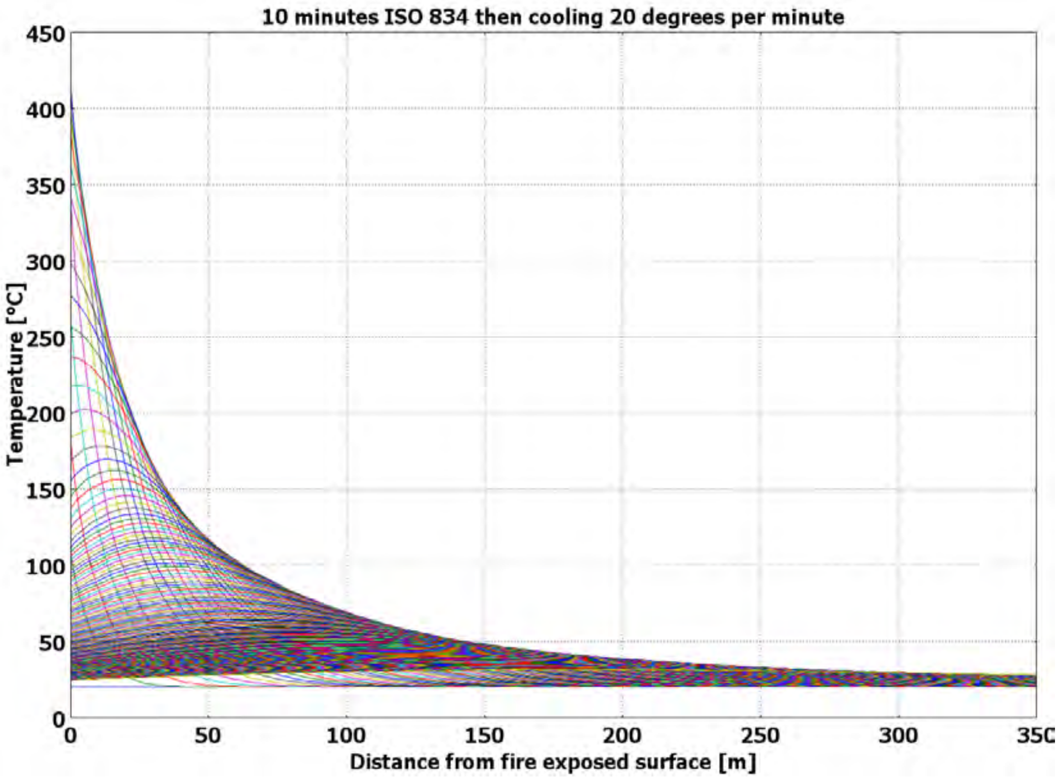

Figure 10 *Calculated temperature in a concrete specimen exposed to elevated temperature. Material properties in accordance with EN 1992-1-2. Cooling phase included.*

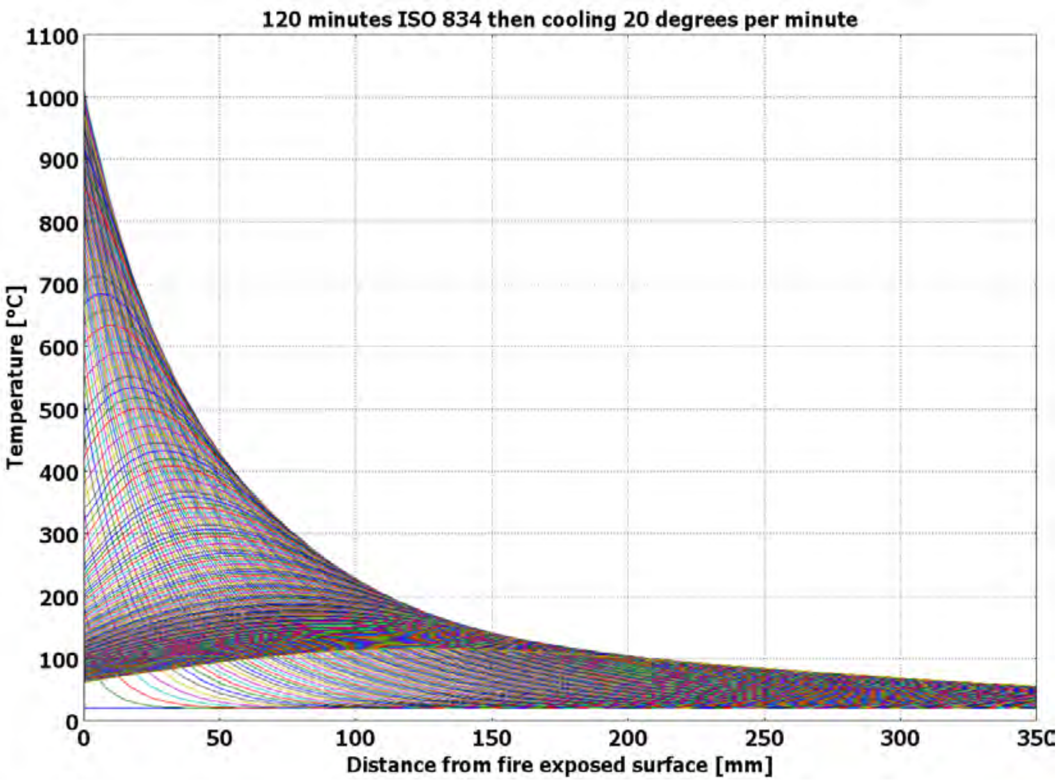

Figure 11 *Calculated temperature in a concrete specimen exposed to elevated temperature. Material properties in accordance with EN 1992-1-2. Cooling phase included.*

Numerous test methods suitable for assessing the properties of undamaged concrete have been developed internationally. Assessment of fire damage concrete, i.e. a highly heterogeneous layered-material, is quiet difficult. One approach for such an assessment that relies on non-destructive test methods is inspection of the average response of the concrete cover, i.e. a point by point analysis of small samples taken at different depths using some special techniques is conducted aimed to interpreting the overall response of the concrete member after a fire, see Table 2.

Table 2 *Possible approaches to Non-Destructive assessment of fire-damaged concrete structures (fib, 2008).*

Average response of the concrete cover	Point by point response of small samples	Special interpretation techniques
Schmidt rebound hammer Windsor probe Capo test BRE internal fracture Ultrasonic pulse velocity	Small-scale mechanical tests Differential Thermal analysis (DTA) Dilatometry (TMA) Thermoluminescence Porosimetry Colorimetry Microcrack-density analysis Chemical analysis	Ultrasonic pulse velocity, indirect method Impact echo Sonic tomography Modal Analysis of Surface Waves (MASW) Electric Resistivity

In this chapter pros and cons with these different test methods found in the literature will be discussed. The test methods discussed below have been selected due to their widespread application or use in Sweden. The list is therefore illustrative rather than exhaustive.

2.3 Test methods on site

2.3.1 Measurement of deformations

The loss of stress in pre-stressed constructions can be monitored by measurement of the deformation (sagging). When doing this it is useful to compare elements in the fire exposed area with virgin elements whenever possible. In Figure 12 an example of extreme sagging is shown.

Figure 12 *Example of extreme sagging in double T roof elements made of concrete. (Photograph: Robert Jansson)*

2.3.2 Load test

By conducting a load test on the structure the residual behaviour can be determined. There are, however, some mixed recommendations concerning whether to conduct load tests and how. Load tests are time consuming and expensive but the results form a carefully designed load test are reliable and can be useful in determining whether a structure can be repaired rather than replaced.

As a part of an investigation Reis et al. (2009) conducted a load test on a fire damaged double T element. The load deformations were measured before applying the load and at each load increment (4 levels) and after 24 hours with maximum load. The measured responses were then compared with a theoretical model accounting for the damage in the member. The main conclusion from the load test was that as the structure recovered more than 75% of the exhibited deflection upon removal of the load so the elements could return to service after some minor refurbishing. A similar load test was performed in the 1930s in Sweden when a floor structure was loaded with 80% of the service load (Schlyter, 1931). However, during this test major deformation remained after unloading.

According to the Concrete Society (1978) spurious conclusions may be drawn unless great care is taken to allow for the influence of continuity, dispersion of test load to adjoining members etc. If routine assessment and repair work is performed according to the recommendations from the Concrete Society (Concrete Society, 1978) it is unlikely that a load test will be necessary.

2.3.3 Rebound hammer

One of the most important and simple ways of assessing the condition of concrete is to listen to the sound caused by percussion from a hammer. A more consistent way of doing this is to use the Schmidt Rebound Hammer. However, when this method is used on fire damaged concrete it is not suitable as a means of measuring strength (Concrete Society, 1978). In a publication by fib (2008) the use of a Schmidt Rebound Hammer is suggested when rapid detection of areas where the surface has lost 30 – 50 % of its original strength is needed.

The Rebound Hammer consist of an outer body, a plunger, a hammer mass, a spring, a latching mechanism and a sliding rider, see Figure 13 (Malhotra V. M., 2004). When the plunger is slowly pressed against the concrete surface the spring is tensed. At the end position of the plunger the latching mechanism will release the hammer mass and the mass will strike the plunger. The rebound distance of the hammer mass is measured on an arbitrary linear scale marked 10 to 100. The reading on the scale is called the Rebound Number.

The Rebound Hammer is suitable for use in the laboratory and in the field. Test objects oriented horizontally, vertically upward or downward position or at any slope can be measured. The hammer requires calibration or correction charts for all test angles due to gravity effects.

The smoothness of the surface influences the Rebound Number, e.g. on a rough surface the plunger tip will cause excessive crushing resulting in a lower Rebound Number. A smoothed surface gives a more accurate measurement, e.g. it has been shown that concrete cast in a metal form yields a rebound number 5 to 25 % higher than concrete cast in a wooden form as the concrete cast in a wooden form has a rougher surface.

Small test specimens must be held rigidly or backed up by a heavy mass to avoid any movement of the test specimen. Movement of the test specimen during the impact will lower the Rebound Number.

Experiments have shown that a saturated concrete and a saturated surface-dried concrete yield lower readings of the Rebound Number. It is therefore recommended that field tests of concrete or test samples with unknown conditions are pre-saturated several hours before testing and that the correlation for saturated surface-dried specimens are used. However, in the case of mapping severe damages in a fire exposed structure this factor is minor.

Other factors that influence the concrete surface hardness, and consequently the Rebound Number, are the type of coarse aggregate, the aggregate source, the type of cement used and the depth of the carbonation. These factors will influence the Rebound Number even if the concrete tested has equal strength. Measurements on lightweight concrete have shown that the results varying widely, more than traditional concrete. When using Rebound Number readings to estimate the compressive strength, modulus of elasticity etc., the hammer should be corrected relative to test results obtained from cylinders tested using other laboratory methods to achieve realistic test results. In the case of testing of fire expose concrete the readings cannot reliably be related to mechanical properties as the degradation of the material often is very uneven. However, the Rebound Hammer can be used as a tool for mapping the area were the concrete has been exposed to the fire provided the Rebound Number is interpreted judiciously keeping in mind the status of the concrete after the effect of a fire.

There are several types and sizes of hammers commercially available for measurements of different types of concrete and different strength classes.

The determination of the rebound Number is standardised by the European standard EN 12504-2:2001. The standard prescribes that the concrete surface shall be smoothed with an abrasive stone to minimise variation of results. An American standard, ASTM C805/C805M, gives equivalent information.

Figure 13 *Rebound hammer, (a) spring relaxed, (b) spring tensed.*
(Photograph: Joakim Albrektsson)

2.3.4 Ultrasonic pulse velocity

This test method has been used for more than 60 years to assess the quality of the concrete (Tarun R. et al, 2004). The test equipment is easy to use in the field on structures and in the laboratory on test specimens. The ultrasonic pulse velocity through the concrete is dependent of the elastic properties and the density of the concrete. Therefore, areas with poor elasticity or low density, such as fire damaged concrete, can be detected with this method.

The test equipment consists of a pulse generator, a transmitting head, a receiving head and a measuring unit. The arrival time of the compression waves, i.e. the waves that propagate fastest in the concrete, is measured by the system at the receiving head. To avoid measurement errors the concrete surface must be smooth and the transmitting head and the receiving head must be in good contact with the concrete. Good contact is attained by maintaining a constant pressure on the heads and using a thin layer of contact gel between the heads and the concrete surface. The heads can be arranged in three different configurations, a seen in Figure 14: the direct method where the angle between the heads is 180 degrees; the semi-direct method where the angle between the heads is 90 degrees; and the indirect surface method where the angle between the heads is 0 degrees. The direct method is preferred because the maximum pulse energy is received at the receiving head, but this configuration is impossible in many cases due to the geometry of the structure. By using the semi-direct method, concentrations of reinforcement can be avoided. The indirect method does not give as good measurements as the direct and semi-direct methods, but it can be used to estimate the thickness of the poor quality layer and is suitable in cases where the other methods cannot be used.

When estimating the a poor quality layer using the indirect method, the heads are first placed close to each other and then moved further away. By plotting the arrival time as a function of the distance between the heads the thickness of the poor quality layer can be determined in cases where this layer is distinct. When the heads are placed close to each other, the waves will propagate in the upper layer of the material where the amount of fine material is high. This will cause a low velocity, when the distance between the heads is increased the waves will propagates through both the upper layer and lower layers. When evaluating fire damaged concrete, shrinkage and delamination cracks should be taken into account when interpreting the results (fib, 2008).

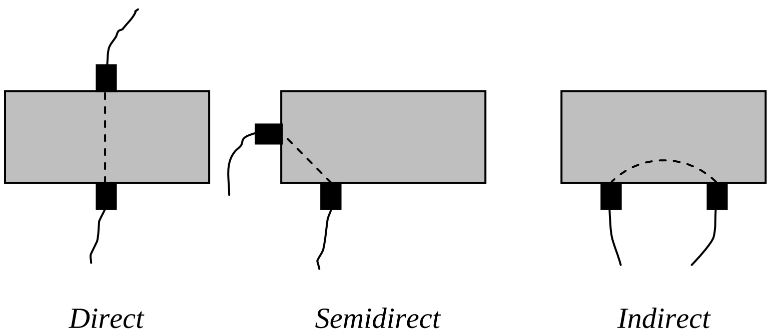

Figure 14 *Different configurations for measurements of the ultra sonic pulse velocity.*

It has been shown that the type of aggregate influences the pulse velocity and that the pulse velocity is generally lower in cement paste than in aggregate (Naik T. R. et al, 2004). A low strength concrete with a high aggregate-cement ratio will therefore show a higher pulse velocity. The cement type does not have a significant effect on the pulse velocity but when the degree of hydration increases the modulus of elasticity will increase and consequently the pulse velocity will also increase. An increase in the water-cement ratio will decrease the compressive strength and the pulse velocity. Therefore, saturated concrete yields a high pulse velocity.

When using the test method on fire damaged concrete, initial free water losses will yield a decrease of the pulse velocity even at low temperatures (fib. 2008). However, as in the case of the use of the Rebound Hammer, the Ultra Sonic Pulse Velocity measurements on site may be seen as a tool for mapping damaged areas rather than giving exact numbers on properties.

High strength concrete is less sensitive to the degree of saturation due to its lower porosity (Naik T. R. et al, 2004). The relationship between the pulse velocity and the compressive strength is not influenced by air entrainment. The pulse velocity is not normally affected by the stress level, but when a very high load is applied, over 65% of the ultimate strength, micro cracks are developed which will lower the pulse velocity. In contrast, the presence of reinforcement will increase the pulse velocity. The pulse velocity in steel is 1.4 to 1.7 times greater than in concrete. Therefore, its recommended that one should avoid measurement of the pulse velocity on heavily reinforced structures.

The main advantage of this test method is that is it easy to investigate the uniformity of the concrete, consequently fire damage areas can be readily determined. Further, the test procedure is standardized by ASTM and CEN. The main disadvantage is that a large number of factors influence the pulse velocities which may make the results difficult to interpret. It is, therefore, not recommended to use the pulse velocity to estimate the compressive strength or the flexural strength without correlation testing.

2.3.5 Drilling resistance

Continuously measurement of the work dissipated and the bore depth while drilling with an ordinary drill hammer allows detection of sizeable thermal damage concrete (Felicetti R., 2006). This method scans the material continuously from the surface to undamaged regions.

The drilling resistance in undamaged concrete not heated by the fire is used as a reference when evaluating the layers suspected of damaged. Since the measurements are relative, factors such as bit wearing, stiffness and mass of the tested object will not influence the sensitivity of the method. Correlations between compressive strength and drilling resistance are complicated to find. The drilling resistance is strongly influenced of the fracture energy of the material and the aggregate hardness. The work dissipated per unit drilling (specific work, J/mm) is found to be the most sensitively indicator of the material integrity. For example, measurements of only the drilling time result in less sensitivity. It is recommended to use a constant thrust close to the upper limit of the maximum thrust of the drill to obtain reliable results.

The method is suitable for use both in situ and in laboratories, is quick and usually provides reliable results. It is especially suitable in cases of severe fire damage. In the known reduced cross-section method sections with a temperature history above 500 °C are neglected when calculating the post-load-bearing capacity. The drilling resistance method can detect similar levels as in the known reduced cross-section model, which corresponds to a decay of 50-70 % of the virgin compressive strength. At lower temperatures the specific work is higher than in virgin concrete. The method is more sensitive in softer materials such as low-grade concrete or lightweight concrete, see Figure 15.

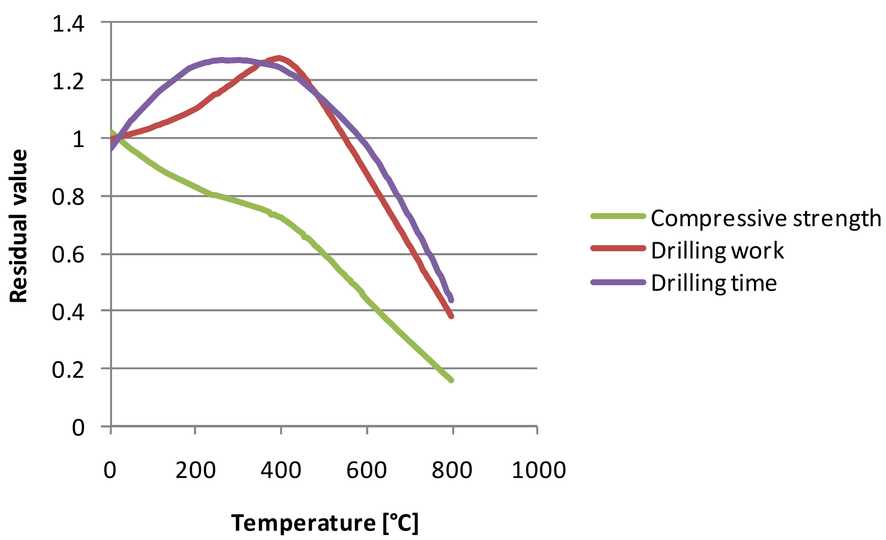

Figure 15 *Residual values of compressive strength, drilling work and drilling time vs. temperature. Redrawn from (Felicetti R., 2006).*

2.3.6 Pullout test

Pullout test methods were developed to decide when formwork removal, the application of post-tensioning and the termination of cold weather protection, can proceed (Carino N. J., 2004). By measuring the force needed to extract a metal insert from the concrete structure the compressive strength of the concrete can be estimated. Unlike other methods, the concrete is subjected to a slowly applied load and an actual strength property is measured. Initially it was necessary to pre-install inserts. The method was developed, however, to allow post-installation of inserts. In general pullout tests are not as easily applicable to the case of assessing fire damaged concrete as other tests outlined previously. A variety of methods have been developed, the two most important of which are summarised below.

BRE internal fracture test
A 6 mm hole is drilled in the concrete structure with a bore hammer. The hole is cleaned and an anchor bolt is inserted into the hole to a spit-sleeve depth of 20 mm. The reaction forces needed to pull out the insert are transmitted to the concrete surface by a circular support. An initial tension load is applied in order to expand and engage the sleeve. The load is then increased until the concrete fails. The ultimate tension load necessary to extract the anchor is recorded.

Compared to traditional pullout tests this methods gives greater test variation, probably due to the variability in the hole drilling and preparation. The aggregate particles are assumed to influence the load transfer mechanism and the failure initiation load. The static load provided by the insert allows analytical treatment of the results. Such treatment shows a non-linear relationship between the tensile force required to provoke failure and the compressive strength of the concrete.

CAPO test
The cut and pullout (CAPO) test is a further development of the traditional pullout test which require the insert to be installed in the formwork before casting. This method allows post-installing of the insert. The test is prepared by drilling an18 mm hole with a bore hammer and using a special milling tool to create an undercut with slot diameter of 25 mm at a depth of 25 mm. An expandable ring is placed into the slot and expanded using a special tool. The post-installed insert is then extracted using a bearing ring and a loading arm which is seated on the bearing ring. The reaction forces are transmitted to the concrete by the bearing ring.

Careful preparation of the surface before testing is required in order to obtain a flat bearing surface perpendicular to the insert. The variability of this method is similar to the standard pullout test. When using the pullout tests in the field, one should locate the insert in critical regions of the structure and conduct a test series which is large enough to achieve a reasonable degree of confidence in the test results. Before estimating the in-place strength of the concrete, the relationship between the ultimate pullout force and the compressive strength must be determined.

When a pullout test is conducted the concrete is subjected to a complex three-dimensional state of stress. Two circumferential crack systems are developed when the stresses rise. At 1/3 of the ultimate load a stable primary system is initiated at the insert head. These cracks propagate at a large apex angle from the insert head. Cracks in the secondary system define the shape of the conical fragment extracted from the concrete.

The failure mechanism is not really known, one theory is that the failure occurs as a consequence of fact that the ultimate compressive strength is reached along the lines from the top of the insert head and the bottom of the bearing ring. Another theory is that aggregates interlocks across the line between the top of the insert head and the bottom of the bearing ring. The ultimate load is reached when sufficient amounts of aggregates have been pulled out of the matrix. In the first case a good correlation between the pullout strength and the compressive strength is explained by the fact that both methods are dependent of the ultimate compressive strength. In the second case good correlation is due to the fact that both methods are influenced by the strength of the mortar. It has been found that both the size and type of aggregate influence the pullout force. Variability of the pullout force is lower in mortar and light weight concrete than traditional concrete.

2.3.7 Winsor probe

Firing a metal probe towards a concrete surface allows the measurement of the hardness or penetration resistance which can be used to estimate the concrete strength (Malhotra V. M., Carette G. G., 2004). This method is increasingly used for quality control and strength estimation in situ for concrete. Only one surface is needed and both vertical and horizontal surfaces can be evaluated using this method (Schneider et al, 1990), (fib, 2008). The equipment is easy to use both in situ and in a laboratory but should be handled with care due to the potential for the release of particles from the concrete surface (Malhotra V. M., Carette G. G., 2004).

The hardened alloy-steel probe is driven by a powder-actuated gun or driver. To measure the penetration depth a depth gauge is used. The length of the probe is 79.5 mm and the tip diameter is 6.3 mm. The rear of the probe is threaded and fits in the bore of the driver. Very rough surfaces need slight preparation to improve the accuracy of the test results. The kinetic energy is absorbed during the penetration, first by fracture at the surface layer and by friction between the probe and the concrete deeper in the concrete. At the surface, the probe will fracture the concrete within a cone shaped zone and cracks will propagate up to the surface. Below this zone the penetration is resisted by compression of the concrete.

The penetration depth is related to strength parameters of concrete below the surface. This relationship makes it possible to create an empirical relationship between the penetration depth and the compressive strength of the concrete. The hardness, type and size of the coarse aggregate will significantly influence the penetration depth. Other parameters such as mixture properties, moisture content, curing regime, condition of the surface, degree of carbonation and age of the concrete will also influence the penetration depth. Cracks between the cement paste and aggregates, caused by the service load, will decrease the compressive strength but not influence the penetration depth of the probe. The Windsor probe method is affected by a relatively small numbers of variables compared to other methods for in situ strength testing. The method also shows high repeatability (Schneider et al, 1990), (fib, 2008).

To achieve reliable test results the test sample must have a thickness of at least three times the expected penetration depth (Malhotra V. M., Carette G. G., 2004). Measurement points should not be placed closer than 150 – 200 mm to any edge or other measuring point. The presence of reinforcement, closer than approximately 100 mm, can also affect the penetration depth.

The method is considered a non-destructive method but causes disturbances of the concrete at the measurement points. When the probe is removed an 8 mm hole with the penetration depth of the probe is left. Using this method usually requires repair of the concrete surface afterwards.

The correlation between the penetration depth and the concrete strength is slightly better compared to other methods but requires comparison with non-fire damage areas of the structure to yield reliable results. This method is ideal for determining the strength profiles used on surfaces cut to different depths (Schneider et al, 1990), (fib, 2008).

2.3.8 Summary of pros and cons with different methods used on site

Table 3 *Summary of pros and cons with different methods used on site.*

Method	**Pros**	**Cons**
Hammer	Good as an assessment of the surface	The surface properties is dominant.
Rebound hammer	Good as an assessment of the surface	The surface properties is dominant.
Drilling resistance	Unaffected regions are used as reference.	Can only make safe assessments of the depth that correspond to a decay of 50-70 % of the virgin compressive strength. Require repair afterwards. No commercial equipment.
Pull out test	Good relation with compressive strength	Will measure an average response of the outer layer of the concrete
Ultra sonic pulse velocity	Truly non-destructive method. Three different configurations can be used.	An indirect method. Relative measurements are necessarily to achieve reliable results.
Winsor probe	Can be used to determine the strength profile of a cross section (requires step wise milling of the surface between shots)	Measure only the outer layer of the concrete

2.4 Test methods off site

2.4.1 Colour analysis

At increased concrete temperatures it is known that chemo-physical transformations take place (Felicetti R., 2004). Above 100 °C the physically bound water is released, above 300 °C the silicate hydrates decompose and above 500 °C the portlandite dehydrates. Aggregates expand when the temperature is increased and some aggregates begin to undergo crystalline changes or decompose above 600 °C. The mostly irreversible chemo-physical transformations yield a degradation of the strength of the concrete.

In addition to this strength decay the concrete may crack, spall, vitrify and change colour which can be detected visually. Concrete may change colour from its typical grey to pink or red between 300 – 600 °C, whitish grey between 600 – 900 °C and buff between 900 – 1000 °C, see Figure 16. The pink or red discolouration occurs because of the presence of iron compounds in the fine or coarse aggregate that dehydrate or oxidise at this temperature. The strength of the colour change is dependent of the type of aggregate, for example a siliceous aggregate shows a more pronounced colour change than calcareous and igneous aggregates. For concretes with aggregates showing no reliable colour changes the image analysis can be restricted to the cement paste, where the colour change is independent of type aggregates used (Short N. R. et al, 2001). The cement paste can also be discoloured due to carbonation and therefore care needs to be taken when assessing old structures. By spraying a freshly broken surface with phenolphthalein the carbonation zone can be indicated. If the visible discolouration is deeper than the carbonation zone, the discolouration is due to the fire exposure. A method that allows determination of the carbonation depth from powder obtained while drilling with an ordinary drill-hammer is described in (Felicetti, 2009).

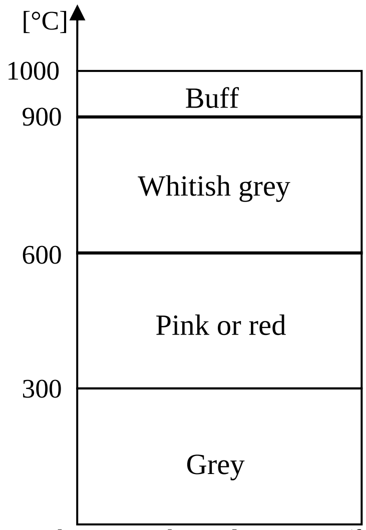

Figure 16 *Colour changes in heated concrete (fib, 2008).*

The change in colour is not directly related to a change in mechanical properties but the occurrence of colour change indicates a temperature range where the mechanical properties may start to decrease.

There are numerous systems to quantify these colours but they can largely be divided into two categories: the RGB system and the HSI system (Short N. R. et al, 2001). The RGB system is commonly used in cameras and monitor screens. A specific colour is defined as the percentage of the primary colours red, green and blue. The HSI system uses the terms: hue, saturation and intensity. Hue is the type of colour defined by the wavelength. Degree of saturation is defined as the percentage of pure colour mixed with white colour. The third property, intensity, describes the relative brightness or darkness of the colour and is defined as the extent of reflected light.

Colorimetric analysis has traditionally been performed in laboratories using an optical microscope combined with digital analysis. This allows a point by point examination of the material constituents and the outline of the colour profiles. The test specimen requires careful preparation such as impregnation with a colourless resin, after which it is cut, ground and examined in reflected light. Experiments have shown that the hue is mainly affected by elevated temperature. This methodology can provide a detailed analysis of the colour after careful sample preparation and analysis but is time consuming.

A more rapid but coarser method requires the use of simple digital images taken with a commonly available low cost digital camera which can be used to evaluate the thermal history (Felicetti R., 2004). Such images contain a considerable amount of data, allowing a separate analysis of the cement mortar and the aggregate which can be used to outline some statistical trends ascribable to the inherent heterogeneity of the test sample. This test method requires cores from the structures to be evaluated. Digital images can also be provided by a scanner (Hager I., 2010). By using a scanner the surrounding light and reflecting objects are avoided.

2.4.2 Reference sample in laboratory furnace

It can be very useful to heat reference samples in a laboratory furnace. The samples used should be from the same concrete but from a part of the structure that has not been exposed to fire. This can provide useful information when conducting colour analysis and microscopic analysis (see below 3.5.4).

2.4.3 Traditional core testing

Although it is a common test method to drill cores and conduct traditional compressive strength test on fire damaged concrete, this gives only a rough picture of the depth of damage. The part of the core closest to the fire will break first and the value of compressive strength from the test is not easy to associate with a specific depth in the cross-section.

2.5 Other methods

There are a numerous indirect methods that can be used to evaluate fire damage in concrete. The short pulse radar method uses electromagnetic waves as in the ultrasonic pulse transmission time method (Clemeña, 2004). The difference between these methods is that the short pulse radar uses a combined transmitter and receiver instead of a separate transmitter and receiver. A short pulse is transmitted followed by a dead time in which reflected signals are received. This method can be used to detect delamination caused by thermal stresses in the fire exposed concrete. Such damage can also be detected by applying a thermal pulse and study the thermal response with an infrared camera (Weritz et al., 2003). When the structure differs in thermal properties the heat flow will accelerate or slow down in these local areas. During heating of concrete it is known that the cement paste undergoes a series of dehydration reactions (Harmathy, 1993). By taking a set of small samples (500 mg) at different depths from the fire exposed side of a core and using a TGA (thermogravimetric analysis) the maximum temperature can be determined at each depth. When heating the samples almost no weight loss occurs up to the maximum temperature attained during the fire. Some of the dehydration reactions are reversible, so it is recommended to perform the TGA a short time after the fire.

2.6 Damage classification

It is especially important when doing on site damage assessments on fire damaged concrete structures of high complexity that some type of classification of the different parts is used. In Table 4 an example of a set of divisions in 5 different damage classes ranging from small cosmetic damage to major irreparable damage is shown. A similar but slightly different class division developed by the Concrete Society is shown in Table 5.

Table 4 *Classes of damage according to fib (fib, 2008).*

Class	Characterization	Description
1	Cosmetic damage, surface	Characterized by soot deposits and discolouration. In most cases sooth and colour can be washed off. Uneven distribution of soot deposit may occur. Permanent discolouration of high-quality surfaces may cause their replacements. Odours are included in the class (they can hardly be removed, but chemicals are available for their elimination)
2	Technical damage, surface	Characterized by damage on surface treatments and coatings. Limited extent of concrete spalling or corrosion of unprotected metal. Painted surfaces can be repaired. Plastic-coated surfaces need replacement of protection. Minor damages due to spalling may be left in place or may be replastered.
3	Structural damage, surface	Characterized by some concrete cracking or spalling, lightly-charred timbre surfaces, some deformation of metal surfaces or moderate corrosion. This type of damage also include type 2 damages, and can be repaired in a similar way.
4	Structural damage, cross-section	Characterized by major concrete cracking or spalling in the web of I-beams, deformed flanges and partly charred cross-sections in timber members, degraded plastics. Damages can be repaired n existing structure. Within the class are also (a) the large structural deformations that reduce the load bearing capacity, and (b) the large dimensional alterations, that prevent the proper fitting of the different substructures and systems in the building. This applies in particular to metallic constructions.
5	Structural damage to members and components	Characterized by severe damages to structural members and components, with local failures in the materials and large deformations. Concrete constructions are characterized by extensive spalling, exposed reinforcement and damaged compression zones. In steel structures extensive permanent deformations due to diminished load-bearing capacity caused by high temperatures. Timber structures may have almost fully charred cross-sections. Mechanical decay in materials may occur as a consequence of the fire. Class 5 damages usually will cause the dismissal of the structure.

Table 5 *Classes of damage according to Concrete Society (2008).*

Class of damage	**Element**	**Surface appearance of concrete**			**Structural condition**			
		Condition of plaster/finish	**Colour**	**Crazing**	**Spalling**	**Exposure and condition of main reinforcement***	**Cracks**	**Deflection/ distorsion**
0	Any	Unaffected or beyond extent of fire						
1	Column	Some peeling	Normal	Slight	Minor	None exposed	None	None
	Wall							
	Floor							
	Beam					Very minor exposure		
2	Column	Substantial loss	Pink/red **	Moderate	Localised to corners	Up to 25% exposed, none buckled.	None	None
	Wall				Localised to patches	Up to 10% exposed, all adhering		
	Floor							
	Beam				Localised to corners, minor to soffit	Up to 25% exposed, none buckled		
3	Column	Total loss	Pink/red ** Whitish grey ***	Extensive	Considerable to corners	Up to 50% exposed, not more than one bar buckled	Minor	None
	Wall				Considerable to surface	Up to 20% exposed, generally adhering	Small	Not significant
	Floor				Considerable to soffit			
	Beam				Considerable to corners, sides, soffit	Up to 50% exposed, not more than one bar buckled		
4	Column	Destroyed	Whitish grey ***	Surface lost	Almost all surface spalled	Over to 50% exposed, more than one bar buckled	Major	Any distortion
	Wall					Over 20% exposed, much separated from concrete	Severe and significant	Severe and significant
	Floor							
	Beam					Over 50% exposed, more than one bar buckled		

Notes
*In the case of beams and columns the main reinforcement should be presumed to be in the corners unless other information exists.
**Pink/red discolouration is due to oxidation of ferric salts in aggregates and is not always present and seldom in calcareous aggregate.
***White-grey discolouration due to calcinations of calcareous components of cement matrix and (where present) calcareous or flint aggregate.

2.7 Case studies of special interest

2.7.1 Shear failure by thermal expansion

During a fire in a warehouse in Ghent in 1974 a building with 3 storeys made of reinforced cast-in-situ concrete collapsed due to shear failure of the columns (fib, 2008). The size of the building was 50 m × 50 m and the construction was designed according the common design practice concerning minimum cross-sections and concrete cover. Despite this the building began its collapse after 80 minutes of fire exposure. The long beams in the fire room were heated from three sides leading to a sizable longitudinal expansion. And as one of the sides was restrained by the unheated structure the expansion was able to occur predominantly in one direction. As a consequence of this, shear failure of several columns occurred resulting in the collapse of a large part of the building. Computer simulations showed the average temperature increase of the beams was somewhere between 150 and 200°C.

A similar collapse occurred in 1996 in the city library of Linköping, Sweden (Anderberg & Bernander, 1996), (fib, 2008). The two storey high building collapsed after 30 minutes fire exposure. As a consequence of a large opening between the first and second floor of the building the floor construction was heated from two sides, which led to a large thermal expansion. In the beginning this was compensated for by a 30 mm wide expansion joint but as the expansion was greater than 30 mm, further thermal expansion was restrained and the developed compression forces deformed the columns leading to a sudden shear failure in the main stabilising walls. A theoretical calculation of the thermal expansion of the floor parts can be seen in Figure 17.

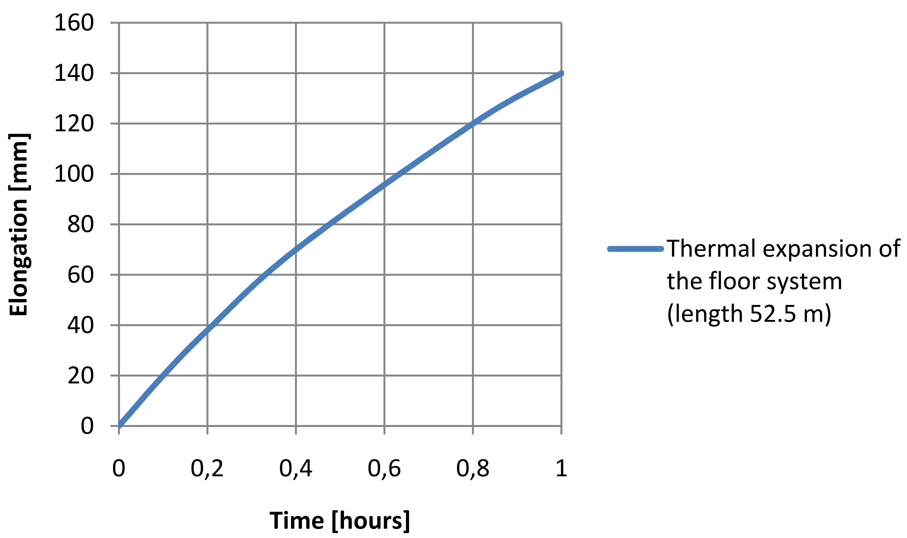

Figure 17 *Thermal expansion of the floor construction during the library fire in Linköping (redrawn from Anderberg & Bernander, 1996).*

2.7.2 Fire spalling during fires

During real fires the occurrence of different degrees of fire spalling in not an uncommon phenomenon. When the Concrete Society investigated the consequences of real fires on concrete structures one finding from the survey was that some kind of fire spalling occurred in 80% of the fires (Malhotra 1984). However, none of the investigated cases involved buildings which experiencing a collapse due to the fire spalling.

A more modern example of a fire in a construction that exhibited fire spalling without collapsing is the fire under the Swedish bridge N844 close to the town Heberg (Boström, 2006). During a traffic accident in November 2005 an intense fire developed in a tanker filled with 50 m^3 isobutyralaldehyde, a solvent used in paint. The bridge was a double bridge consisting of one arm carrying traffic in the north direction and on heading south. After the traffic accident the tank truck was suspended between the north and south arms of the bridge and the burning solvent flowed down between the arms of the bridge leading to a very rapid fire development underneath of the bridges. The bridges consisted of pre-stressed box girders where the pre-stressed members contained almost all of the load carrying capacity of the bridge. Therefore, the maximum temperature that the pre-stressing wires had been exposed to during the fire was crucial to the investigation of the structural integrity of the bridges. The wires were protected by a 100 mm concrete cover. On some positions the first visual inspection showed fire spalling depths of up to 50 mm, see Figure 18; but these positions were not close to the pre-stressing wires. During the investigation, cutting samples of the wires for laboratory analysis was possible from positions where this did not change their load bearing capacity. The aim of the investigation was to indirectly determine the maximum temperature that the wires had been exposed to in order to determine whether the bridges could be repaired or would need to be replaced. Therefore, it was necessary to assess the strength of the remaining concrete. Field tests with ultra sonic pulse velocity measurements and the Rebound Hammer were performed but the results were not deemed sufficiently definitive, so a more indepth study was necessary.

The indepth study was conducted by drilling cores from parts of the concrete structure located between the pre-stressing cables. In the laboratory, the cores were then analysed using microscopy. From the microscopy study some fixed temperature points could be determined from changes in the aggregate and the cement paste. These temperatures could then be used as input to a theoretical temperature calculation to estimate the heat penetration. From this investigation it was shown that the maximum heat in the pre-stressing wires was below 90°C witch was estimated not to be a problem for this construction. Based on these results repair of the bridges could be made rather than demolition and replacement.

Figure 18 *Fire spalled surface of bridge N844 in Heberg.*

3 Experimental study

3.1 Introduction

An experimental study has been performed in order to evaluate different methods for assessing the degradation of concrete after fire exposure. Two different fire scenarios and two concrete mixes were used. In total ten test samples were produced and eight of them were exposed to fire conditions. The remaining test samples were use as references.

As the methods described in the literature study all have their limitations, when a detailed picture of the damage to a cross-section is needed, a totally new approach has been tested. By recording the deformation field with a camera system on a drilled core from fire exposed concrete during loading a picture of the degradation in a cross-section can be monitored. In the experimental study this new method is compared with more traditional methods such as the Schmidt Rebound Hammer, Ultrasonic Pulse Velocity and Microscopy. All measurements except the Schmidt Rebound Hammer were performed on cores taken from the test samples. The study was performed the autumn of 2010.

3.2 Materials and specimens

A typical Swedish tunnel concrete was used in this study. In addition a similar concrete mix with reduced aggregate size was used. This choice of test material allows an investigation of the influence of aggregate size on the degradation of the fire exposed concrete. The concrete contained polypropylene fibres (PP-fibre) in order to avoid spalling at the fire exposed surface, as an investigation of the spalling behaviour of concrete was not in the scope of the investigation. Super plasticizer was added to obtain a good workability of the concrete. To be able to add a realistic amount of super plasticizer in the concrete with reduced aggregate size the water-cement ratio (w/c) was increased to

0.47. The concrete mixes used are shown in Table 6. The aggregate size is used to distinguish between the two mixes when the results are discussed below.

The aggregate size fraction 0-8 mm used was a natural sand composed of quartz, feldspar particles and rock fragments of granitic composition. The feldspar was often sericitic and often contained iron oxides that gave a reddish tint. Further, the biotites had a strong brown reddish colour. The granitic particles often contained strongly deformed quartz. Particles of diabase and amphibolites were present in low numbers.

The aggregate in the size fraction 8-16 mm was composed of crushed rock particles of granitic composition, mostly with equilibrium texture but also more deformed varieties. Feldspars were in some cases sericitic and contained to a lesser extent iron oxide ex-solutions. The colour of biotites was mostly green.

Table 6 *Concrete mixes used in the experimental study.*

Series	w/c	Gravel 0-8 mm [kg/m^3]	Gravel 0-16 mm [kg/m^3]	Water [kg/m^3]	Cement CEM I [kg/m^3]	Super-Plasticizer [kg/m^3]	Fibre Amount [kg/m^3]
0-16	0.45	898.5	863.3	180.9	402.8	0.16%	1.0
0-8	0.47	1637.8	-	181.1	385.5	0.72%	1.0

Ten slabs, five of each recipe, were moulded with a size of: 600 × 500 × 200 mm^3. The samples were cured indoors for approximately 6 month after moulding.

3.3 Fire exposure and external load

The fire exposure of the test samples was conducted in a small scale furnace constructed for fire resistance tests with the fire exposed area 500 × 400 mm. Detailed information concerning the construction of the furnace can be found in test standard SP Fire 119. The furnace was heated with a gas burner and the furnace temperature was measured with an Ø 1 mm shielded thermocouple. The slabs were exposed to a fire from below only. Soft thermal resistant insulation was placed on the upper edges of the furnace before the concrete slabs were mounted, see Figure 19. Approximately 50 mm of the circumference of the slabs were supported by the furnace edges and was therefore not exposed to the fire.

Figure 19 *Small scale furnace with test specimen on top.*

The two fire scenarios used were the standard time-temperature cure described in ISO 834-1 and a temperature ramp, further designated Slow heating, of 10 °C/min to a maximum temperature of 1000 °C. The choice of these two scenarios of thermal exposure allowed an investigation of how the temperature history influenced the strength decay. Five thermocouples were pre-installed at the centre of the slab and at a depth of 10, 30, 45, 80 and 120 mm, respectively. This allowed monitoring of the temperatures at different depths during the test and determination of the degradation of the strength decay as a function of temperature. The duration of the two different heating scenarios were selected to reach the same temperature level at 45 mm from the fire exposed surface. After estimation by calculation of the temperature at this level the duration of standard time-temperature curve scenario was set to 90 minutes and the duration of the slow heating scenario was set to 130 minutes. This gave a temperature of approximately 310 °C at the position 45 mm at the termination of the both fire scenarios. Examples of the furnace temperature and the measured temperature inside the test specimens are shown in Figure 20 and Figure 21.

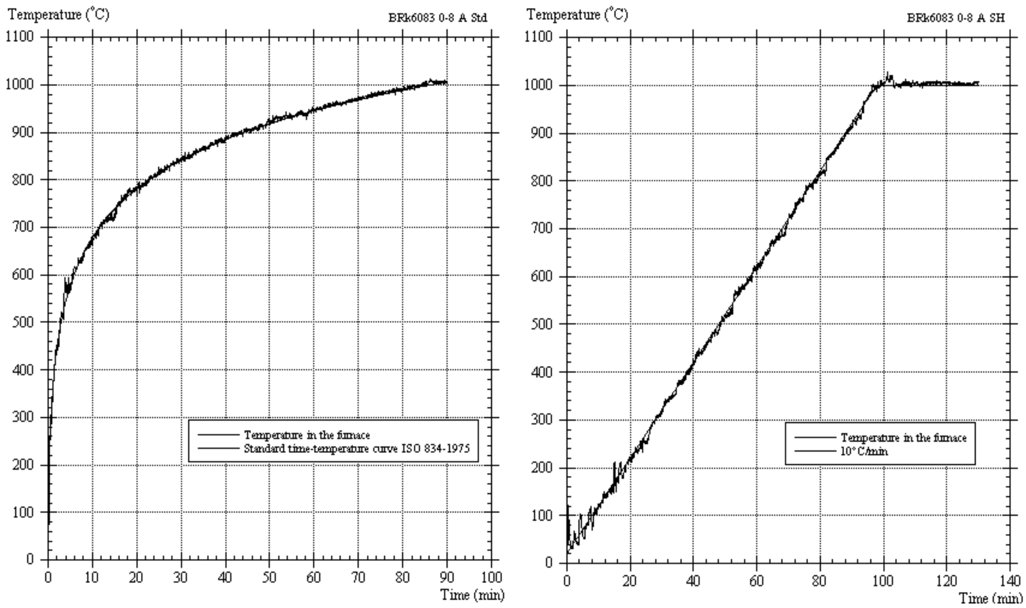

Figure 20 *A) Standard time- temperature curve and actual furnace temperature, 0-8 A Std B) Slow heating curve and actual furnace temperature, 0-8 Sh.*

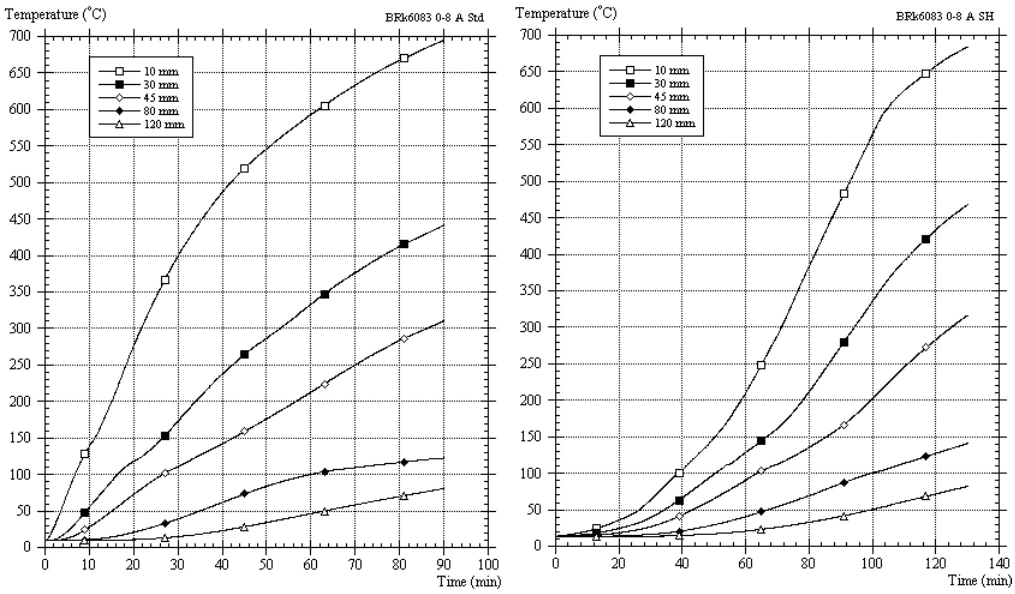

Figure 21 A) *Temperature inside test specimen, 0-8 A Std B) Temperature inside test specimen, 0-8 A Sh.*

A one dimensional compressive load was applied in the longitudinal direction of the slabs. Two rigid beams were placed at the short sides of the slabs and were pressed against the slab by two bolts to a load level of 2 MPa.

Directly after the termination of the fire tests the slabs were removed from the furnace and were cool down in room temperature.

3.4 Sampling

Approximately 2 weeks after the fire test the hardness of the surfaces of the test specimens was evaluated with the Schmidt Rebound Hammer. Subsequently 8 cores (nominally with a diameter of 60 mm) were drilled from each slab, see Figure 22. By drilling from the fire exposed side of the test specimens the damage of the weak surface was minimized. The cores were then further used in the experimental study of different evaluation methods as shown in Table A 1. The surface layer, 10 mm, on the fire exposed side of the cores was cut off on cores intended for mechanical testing. These cores were then cut to a length of approximately 127 mm. The fire exposed side of the cores were then planed in a milling machine. To obtain a core length of 122.5 mm the unexposed side of the core was adjusted and planned in the milling machine.

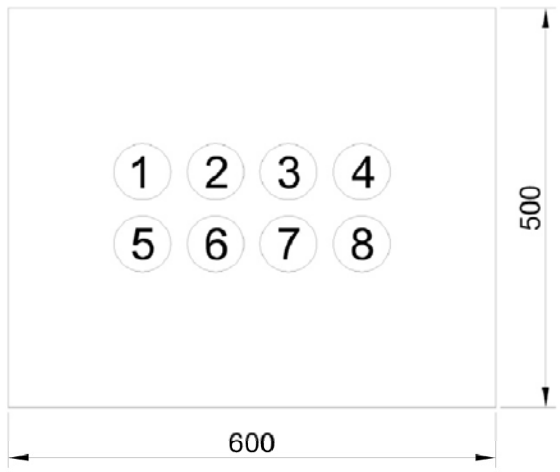

Figure 22 *Location and numbering of cores.*

3.5 Test methods

3.5.1 Rebound hammer

Before the fire test, and approximately 2 week after, the test specimens were examined with the Schmidt Rebound Hammer. To avoid disturbance during the measurement the test samples were fixed to a rigid construction. On the vertically orientated fire exposed surface a grid with 50 mm between the vertical and horizontal lines was drawn. The rebound number was recorded at each point, in total 99 measurement points per test specimen. When compared the readings taken before and after the fire exposure the readings taken 50 mm from the edges were neglected in order to avoid boundary effects.

3.5.2 Ultrasonic pulse transmission time measurement

The ultrasonic transmission time was measured through cores taken from the unexposed test specimens and the fire exposed test specimens. The ultrasonic pulse transmition times were measured in the radial direction of the cores at a distance of 20, 30, 40, 50, 60, 70, 80, 100, 140 and 180 mm from the fire exposed surface as shown in Figure 23. Measurements were not performed closer than 20 mm from the edges to avoid boundary effects. Before sending the pulses through the cores a layer of contact jelly was placed at each measuring point. During the measurement the transmitting head and the receiving head were pressed against the cores by hand.

The ultrasonic pulse velocity was not calculated in this study, instead the ultrasonic pulse transmission times were compared for different scenarios. The measurements were made with AU2000 Ultrasonic Tester.

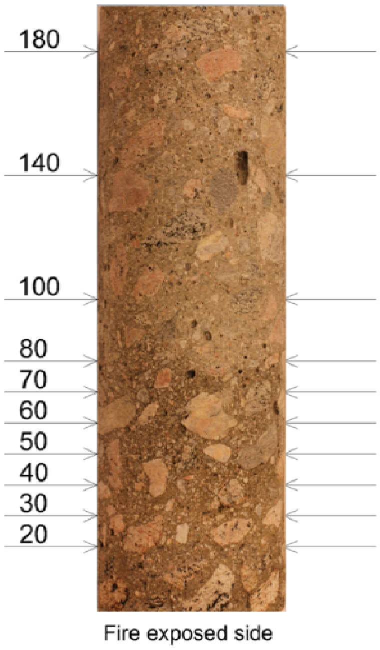

Figure 23 *Placement of measuring points of the ultrasonic pulse transmission time measurment.*

Figure 24 *Measurement of ultrasonic pulse transmission time.*

3.5.3 Mechanical testing

3.5.3.1 Test set-up and performance

The uniaxial compression tests of the drilled concrete cores were carried out in a GCTS servo hydraulic testing machine with a maximum load capacity of 1.5 MN, see Figure 25. The load frame is characterized by a high stiffness and is supplied with a fast responding actuator. The tests were carried out under load control with a stress rate of 12 MPa/min. The axial load was recorded by a load cell and the axial displacement of the axial actuator was recorded by an LVDT, connected to a high-speed data logger. The uncertainty of the load measurement is less than 1 %.

For each of the fire exposed slabs three cores were loaded to failure and one core was loaded to 20 MPa and then unloaded. The latter core was then further analyzed by means of ultra sonic pulse. For the unexposed slabs four cores were loaded to failure. The core diameters were between 59.8 and 60.6 mm and the core heights were between 122.2 and 122.7 mm. The first 10 mm of the drilled cores was removed due to severe damage from the fire exposure. The core end surface closest to the fire exposure, or corresponding surface of the unexposed cores, was placed against the lower loading plate. During the loading the strain-field was monitored at the surface of the cores by means of full-field strain measurement, see chapter 3.5.3.2.

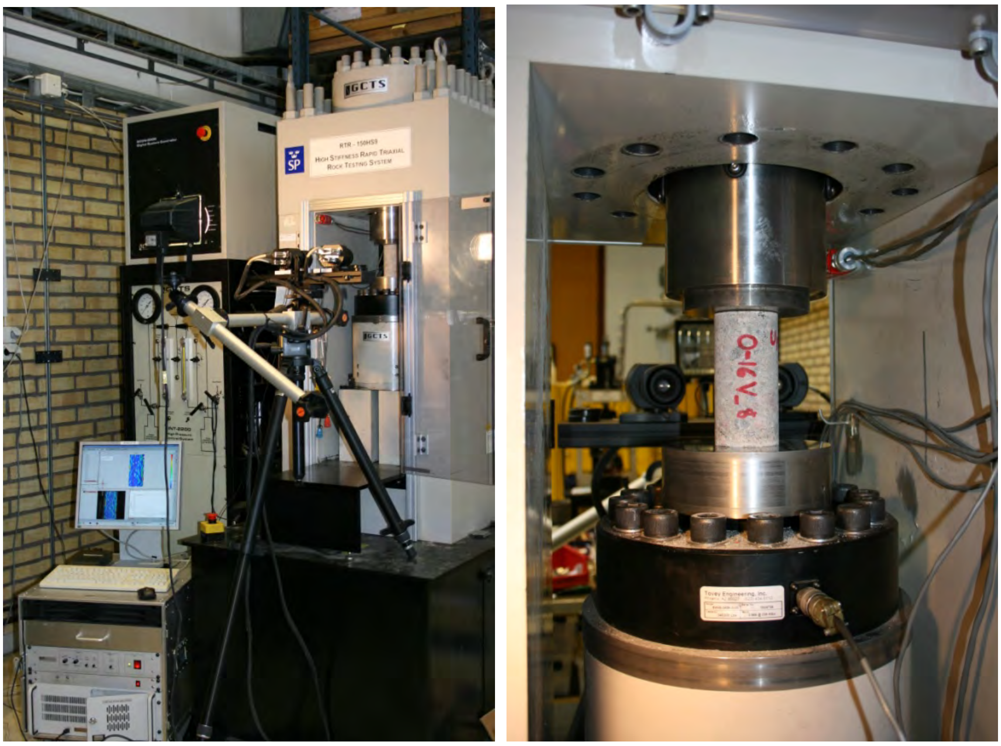

Figure 25 *Experimental test set-up with optical measuring system (the two cameras).*

3.5.3.2 Optical full-field strain measurement

Full-field strain measurement was performed on all concrete cores tested in this study. The optical full-field deformation measurement system ARAMIS™ 4M (v6.2.0-6) by GOM was used. The system uses a measurement technique based on Digital Image Correlation (DIC) with a stereoscopic camera setup, consisting of two CCD-cameras with 4.0 Mega pixel resolutions.

Essentially, DIC measures the displacement of the specimen under testing by tracking the deformation of a naturally occurring, or applied surface speckle pattern in a series of digital images acquired during the loading. This is done by analysing the displacement of the pattern within discretized pixel subsets or facet elements of the image. In combination with correlation based stereovision techniques the measurement of 3D shapes as well as the measurement of 3D displacements fields and surface strain field, is possible.

The experimental setup of the system can be seen in Figure 25. The cameras, which are mounted on a rigid bar to avoid motion relative to each other, are placed in front of the specimen at angles and a distance, both of which depend on the desired measuring volume and the lenses used. In this study 50 mm Schneider Macro lenses were used and the system was calibrated (Panel 100 × 80 mm, ID: C04235) for a measurement volume of approximately 100 × 100 × 100 mm^3. Hence, the measuring area covered a length of approximately 100 mm from the fire exposed end of the core.

The natural pattern at the surface of the drilled cores was used as the speckle pattern. To obtain high contrast levels the specimen was illuminated by a white light. In the tests an image pair was captured with a frequency of 1 Hz; at the same time the load and displacement, obtained from the testing machine, were recorded in the ARAMIS system. In this study a facet size of 25 × 25 pixels and a three-pixel overlap along the circumference of each facet were chosen. This gave a spatial resolution of 22 pixels in the displacement measurement, which for the system setup employed corresponds to a division of approximately 1.1 × 1.1 mm^2. The accuracy of coordinate measurements was approximately 2 µm.

3.5.4 Microscopy

The analysis was performed using thin sections with the approximate size of 50 × 65 mm^2. The samples were impregnated with epoxy glue with fluorescent dye, Struers Epodye. Light optical microscopy with bright field, polarization and fluorescence technique was applied. The thin sections covered an area about 65 mm in from the fire exposed surface.

Thermal alterations in fire exposed concrete

Microscopy is often used for the assessment of the temperature history of a fire damaged concrete structure. A comprehensive discussion of useful and potentially useful reactions is presented by Njland and Larbi, 2001. A summary is given in Table 7.

Table 7 *The table gives a summary of changes caused by heating. Based on Nijland and Larbi 2001.*

Temperature	
70-80 ^oC	Dissociation of ettringite
120-160 ^oC	Dehydration of gypsum to hemihydrate and anhydrite
<250 ^oC	Small changes
200-500 ^oC	Loss of bound water in the cement paste
250-300 ^oC	Reddish discolouration of the cement paste
375 ^oC	Hemihydrate to anhydite
500-600 ^oC	The colour of the cement paste turns grey
500 ^oC	Changed colour of the cement paste viewed in polarized light
510-550 ^oC	Dehydroxylation of portlandite
500-650 ^oC	Fracturing of quartz bearing rocks
573 ^oC	Quartz changes from α to β
600-850 ^oC	Decarbonation of carbonate minerals
800-1200 ^oC	Complete disintegration of the structure, cement paste whitish

In the temperature range 120 to 200 ^oC gypsum is successively dehydrated. A transition to anhydrite occurs at 375 ^oC. Portlandite decomposes to calcium oxide and water according to the reaction:

$$Ca(OH)_2 \rightarrow CaO + H_2O$$

The temperature estimates for this reaction ranges from 510 to 547 ^oC (Boynton 1980). As the partial pressure of water in the concrete is higher than in air at ambient conditions the dissociation temperature will be slightly higher. Calcium carbonate dissociates to calcium oxide and carbon dioxide at a temperature of approximately 840 ^oC. Magnesium calcium carbonate dissociates in a temperature range from about 600 ^oC to 800 ^oC (Boynton, 1980). The crystal structural change from the α-quartz to the β-quartz occurs at 572 ^oC. This transformation is reversible and rapid and independent of pressure differences in the concrete.

The temperatures for the colour changes differ between different concretes and possibly also between different heating scenarios.

Crack counting method

The analysis was conducted in a light microscope at 50 times magnification. The analysed thin section was attached to a motorized table. The motorized table was initially set in zero position, thereafter the sample was moved to predefined levels. The first level was chosen at approximately 5 mm in from the side which had been exposed to fire. Cracks were counted along lines at 6 levels, the distance between these levels was 1 cm. At each level five fields were analysed. The distance between these fields varied, as a function of damage to the sample or whether the field to >50 percent was covered by one aggregate grain. In each field micro-cracks (<10 micron) and thin cracks (10 – 100 micron) in the cement paste and adhesion cracks in the ITZ were counted. To be able to assess orientation of the cracks the analysis was performed as a linear traverse analysis along lines perpendicular and parallel to the exposed surface respectively. In each observation field cracks were counted along three perpendicular and three parallel traverse lines, each line 2 mm long. This gave 30 mm traverse lines horizontally and vertically respectively per level. If an adhesion crack with origin from one and same aggregate crossed more than one traverse line it was counted only once, see Figure 26.

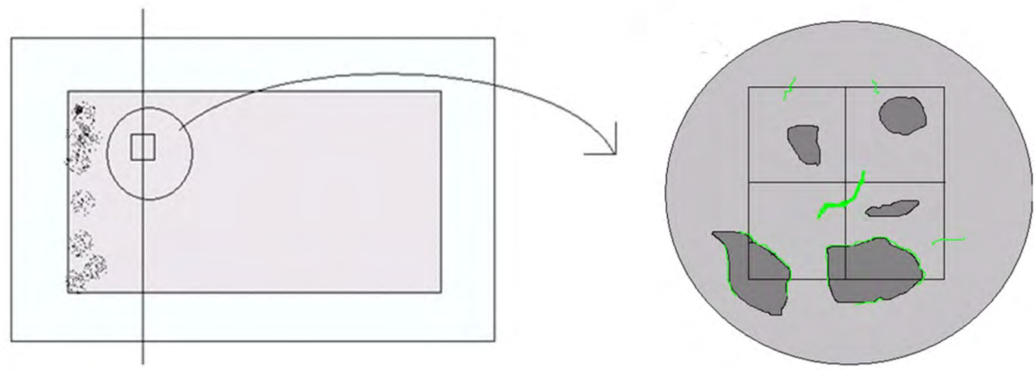

Figure 26 *The left hand figure shows the prepared fire exposed concrete sample with blue glass and grey concrete sample. The fire exposed side is shown to the left. The figure also shows a line for the first level and an observation field with four traverse lines visibly. The right hand figure shows a magnification of an observation field (the square) and cracks marked in green.*

Of course counting implies an objective evaluation of which cracks are micro-cracks and which are thin cracks. Pursuant to the picture above the results would be as shown in Table 8.

Table 8 *Example of crack count based on Figure 26.*

	Level	**x=10000**
	Field	1, y=2000
Micro cracks crossing	Perpendicular traversline	1
	Parallel traversline	2
Thin cracks crossing	Perpendicular traversline	1
	Parallel traversline	1
	Adhesion cracks	2

3.6 Test results

3.6.1 Rebound hammer

Measured Rebound Numbers before and after fire exposure are shown in Figure 27 and Figure 28. As shown in the diagram the reduction in Rebound Numbers is approximately 30% for the concrete with an aggregate size of 0-16 mm and approximately 25 % for the concrete with an aggregate size of 0-8 mm. Less variation is found between the different heating scenarios and the Rebound Number decay is found to be more influenced by the aggregate size than the thermal history.

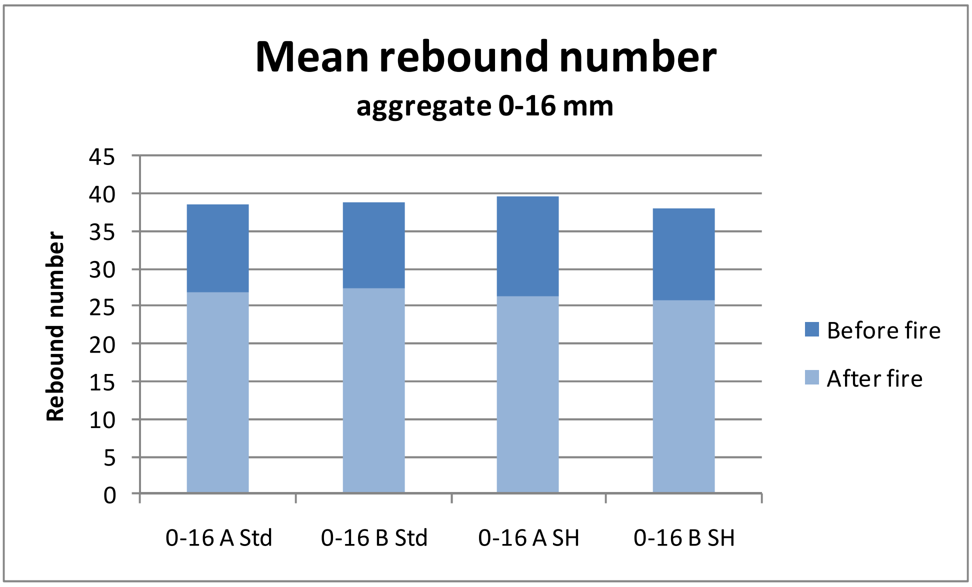

Figure 27 *Mean rebound number before and after fire exposure for the concrete mix containing aggregate of size 0-16 mm.*

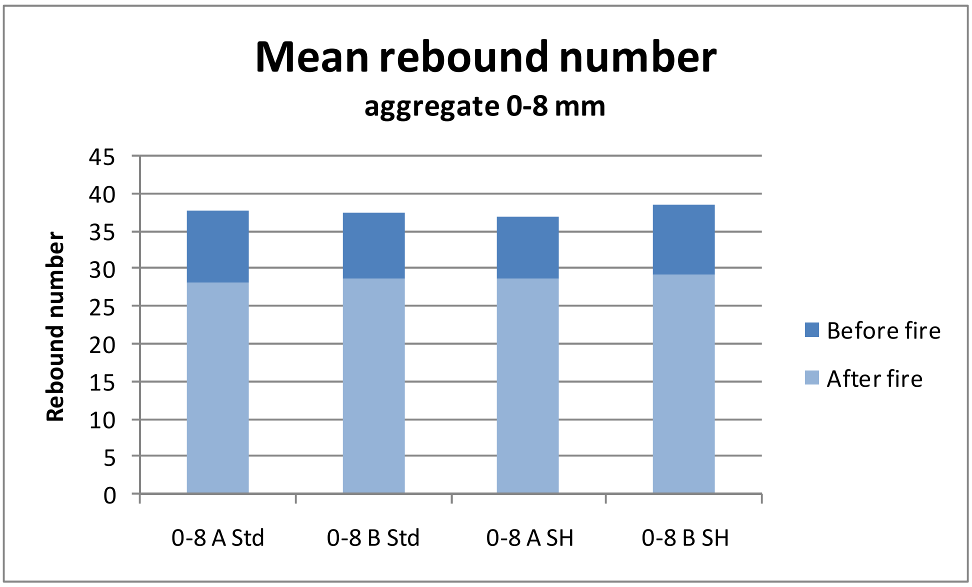

Figure 28 *Mean rebound number before and after fire exposure for the concrete mix containing aggregate of size 0-8 mm.*

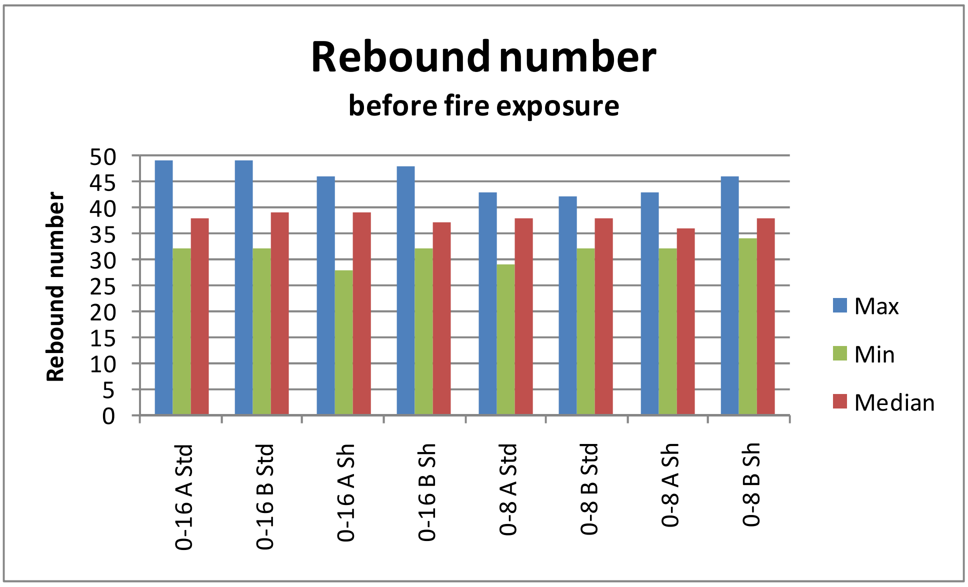

Figure 29 *Maximum, minimum and calculated median before fire exposure.*

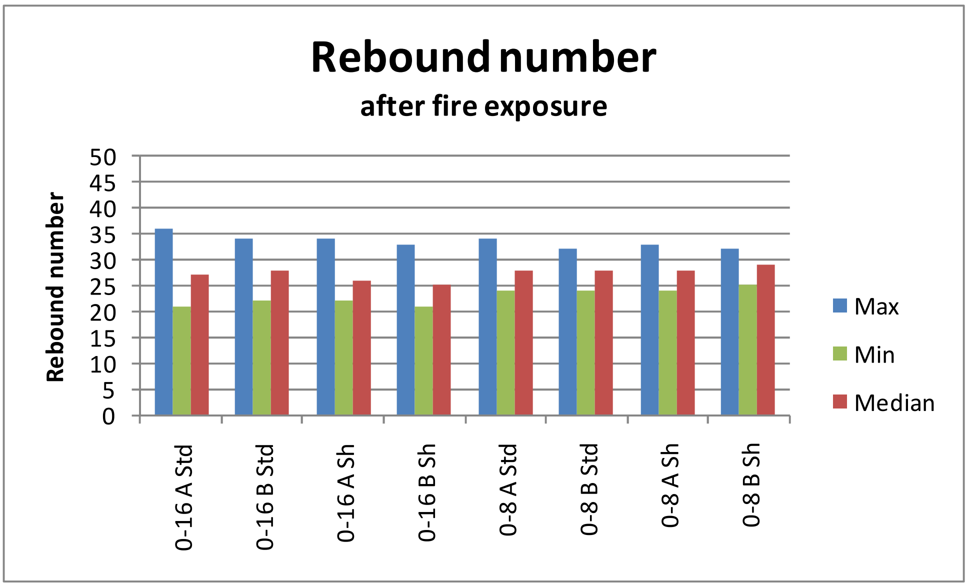

Figure 30 *Maximum, minimum and calculated median after fire exposure.*

3.6.2 Ultrasonic pulse transmission time measurement

Test results obtained when measuring the ultrasonic pulse transmission time through cores taken from the slabs are shown in Figure 31 - Figure 34. The ultrasonic pulse transmission time was measured in the radial direction in the cores at different depths from the exposed side. In case of surface voids at the measuring depth the measuring angle (counted from the core axis) was chosen to avoid these voids. Sometimes the reading fluctuated, in which case the measurement was then continued until stable readings were achieved. In general the values descend away from the fire exposed side of the samples. At the unexposed side of the virgin core and the exposed cores the readings are almost the same. Generally, the degradation of the transmission times through the cores exposed to the standard time-temperature curve is slightly higher.

Measurements of a calibrated sample for AU2000 Ultrasonic Tester were made before the measurement of the cores. The result of the measurements can be seen in Table 9 below.

Table 9 *Result of ultrasound measurement for calibrated reference.*

Sample label	AU2000 [µs]
Calibrated value according to marking	26.6
Measured value	27.6

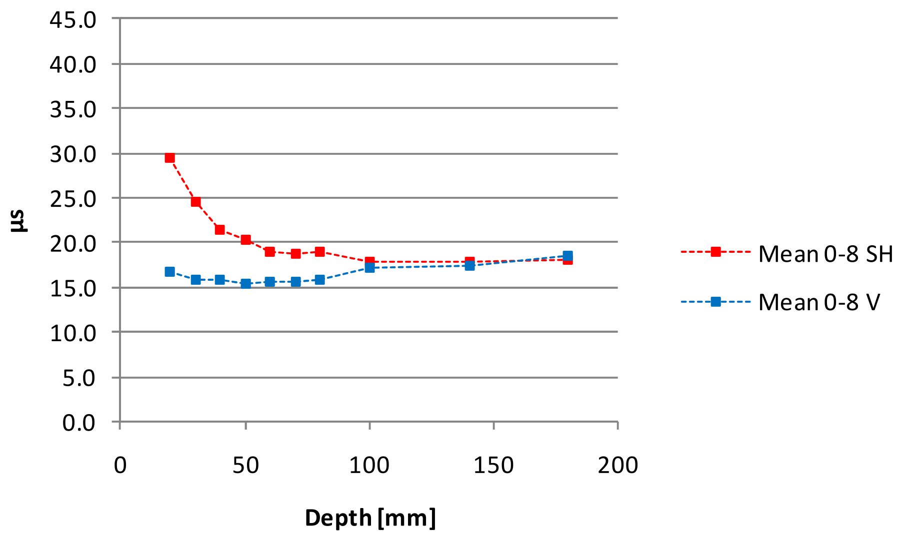

Figure 31 *Ultrasonic pulse transmission time for 0-8 Sh mean and 0-8 Sh unexposed mean.*

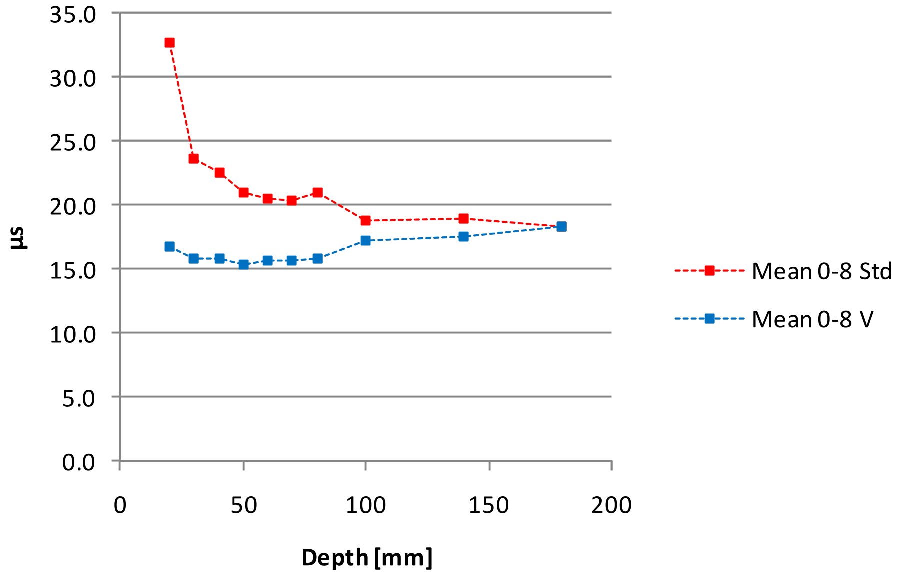

Figure 32 *Ultrasonic pulse transmission time for 0-8 Std mean and 0-8 Std unexposed mean.*

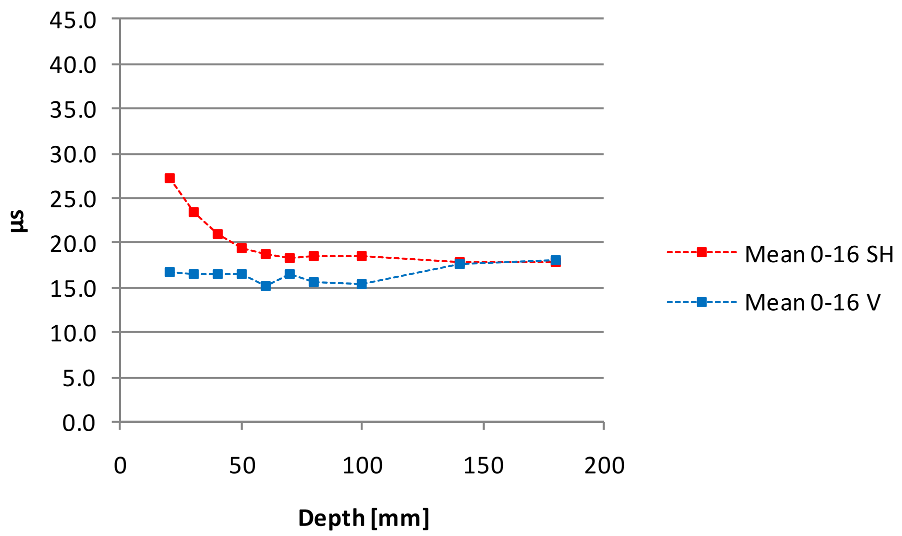

Figure 33 *Ultrasonic pulse transmission time for 0-16 Sh mean and 0-16 Sh unexposed mean.*

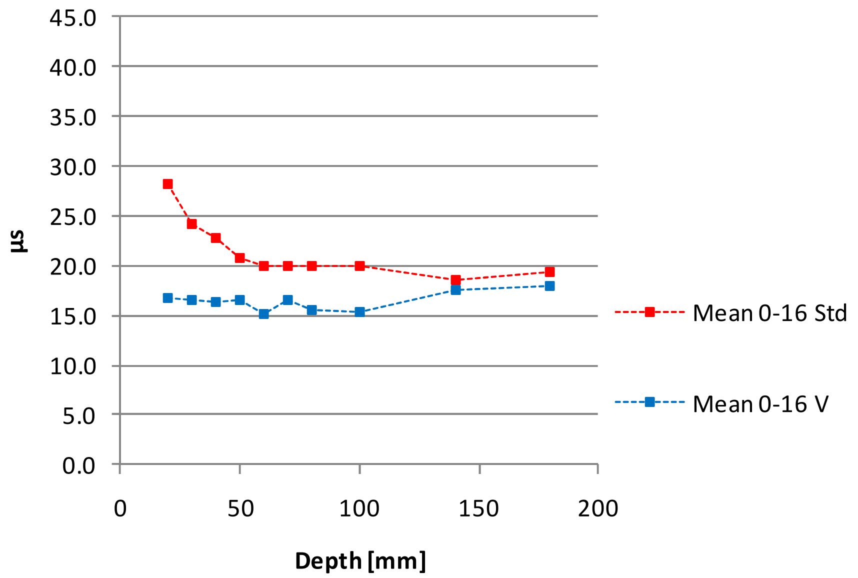

Figure 34 *Ultrasonic pulse transmission time for 0-16 Std mean and 0-16 Std unexposed mean.*

3.6.3 Mechanical testing

Figure 35 and Figure 36 show the compression test results in the form of axial compressive stress verses displacement of the axial actuator. As expected, the fire exposed specimens exhibit a lower stiffness and lower ultimate compressive strength compared to the unexposed reference specimens. For the concrete with an aggregate size of 0-16 mm the compressive strength of the slabs exposed to a standard fire (Std) was reduced by 47 % while that for the slabs exposed to a slow heating fire (Sh) was reduced by 40 %. Corresponding reductions for the concrete with an aggregate size of 0-8 mm were 34 % and 26 %. This indicates that the maximum aggregate size and the heating scenario affect the strength degradation of the concrete. A summary of the compression tests is reported in Table 10. The stress-deformation relations of the individual specimens can be found in Appendix F.

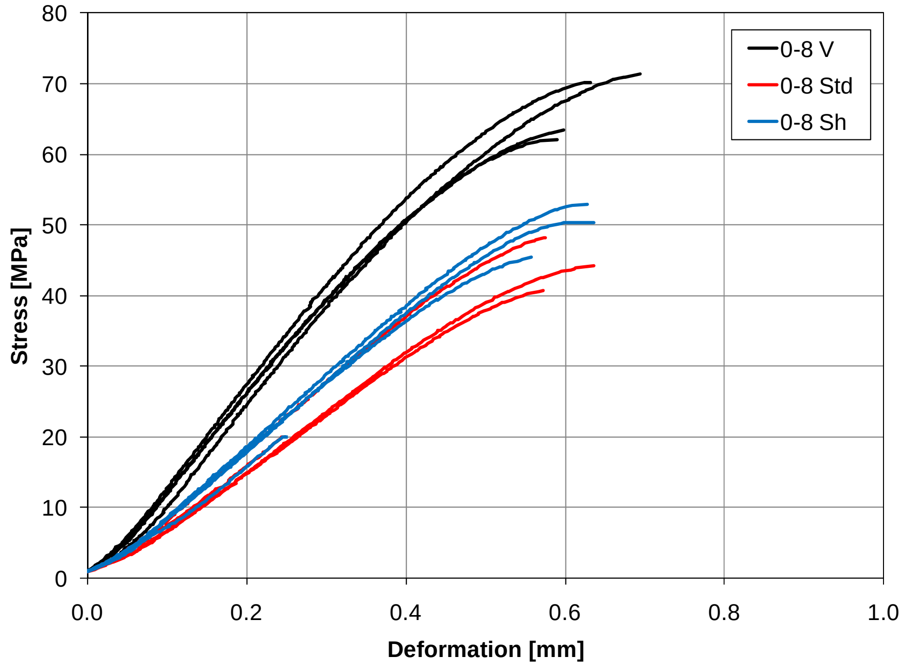

Figure 35 *Comparison of compressive stress vs. axial deformation for specimens 0-8 V, 0-8 Std and 0-8 Sh.*

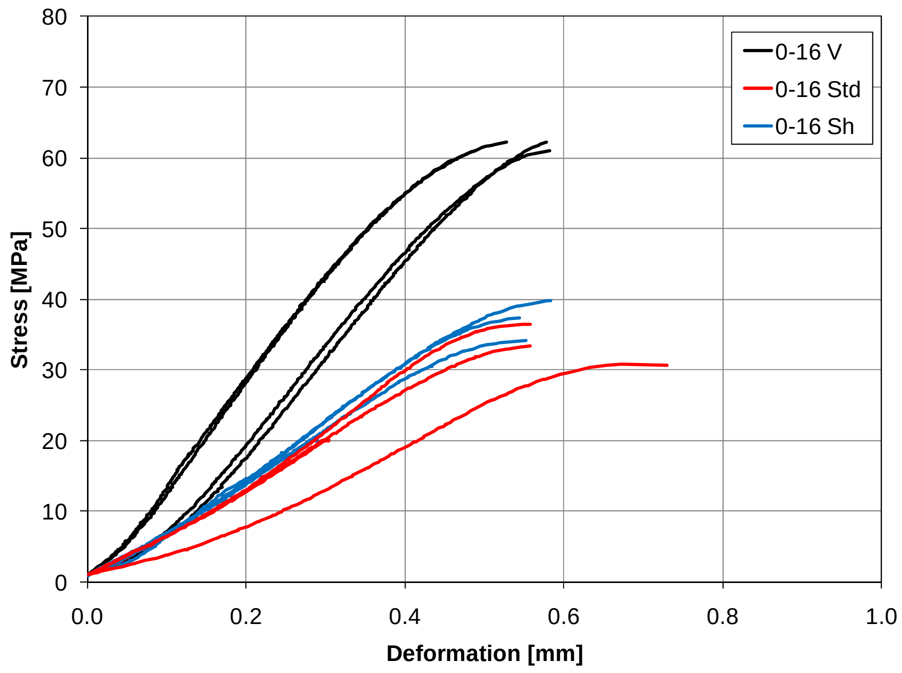

Figure 36 *Comparison of compressive stress vs. axial deformation for specimens 0-16 V, 0-16 Std and 0-16 Sh.*

Table 10 *Summary of results for the compression tests.*

Specimen	**Diameter [mm]**	**Height [mm]**	**Fire** [1)]	**Strength [MPa]**	**Strength Mean [MPa]**	**Strength CV [%]**
0-16V_3	60.3	122.4	-	62.2	61.6	1.2
0-16V_4	60.3	123.2	-	62.2		
0-16V_5	60.3	123.2	-	61.2		
0-16V_8	60.3	122.6	-	60.7		
0-16Std_4	59.8	122.7	std	33.0	32.9	7.3
0-16Std_5	59.8	122.5	std	35.3		
0-16Std_6	59.8	122.3	std	30.5		
0-16Std_7	59.8	122.3	std	- [2)]		
0-16Sh_2	59.8	122.4	sh	33.7	36.8	8.2
0-16Sh_3	59.8	122.4	sh	37.1		
0-16Sh_4	59.8	122.2	sh	- [2)]		
0-16Sh_7	59.8	122.5	sh	39.7		
0-8V_4	60.3	122.4	-	71.1	66.8	7.1
0-8V_5	60.3	122.6	-	61.9		
0-8V_6	60.3	122.5	-	63.5		
0-8V_8	60.3	122.5	-	70.5		
0-8Std_1	60.3	122.2	std	43.1	44.0	8.6
0-8Std_2	60.3	122.4	std	40.8		
0-8Std_5	60.3	122.4	std	48.2		
0-8Std_7	60.3	122.5	std	- [2)]		
0-8Sh_1	60.3	122.5	sh	52.9	49.6	7.5
0-8Sh_3	60.3	122.4	sh	50.4		
0-8Sh_6	60.3	122.4	sh	- [2)]		
0-8Sh_7	60.3	122.5	sh	45.6		

[1)] std = standard fire curve and sh = slow heating curve.
[2)] Loaded to 20 MPa and then unloaded.

A stiffness degradation of the concrete can be seen as a measure of the level of damage caused by an elevated temperature. With modern optical measuring systems, it is possible to obtain a complete picture of the strain field at the surface of a specimen and thus to study local effects. In this study an optical measurement technique was used to quantify how the damage to the concrete changes with distance from the fire exposed surface by analyzing the stiffness degradation along cored concrete cylinders. In an assessment of an actual concrete structure exposed to fire it is often more important to determine how far into the structure the concrete can be assumed to be affected than to determine actual values of the stiffness.

Figure 37 shows an example of results obtained from the optical measurements presented as an overlay of continuous field at the surface of specimen 0-8 Sh-1. The reported results are the strain and the deformation in the axial direction of the specimen at a compressive stress of 20 MPa. In Figure 5 the axial compressive strain distribution along three sections (Section 11, 12 and 13) is shown. The strain field of the individual specimens can be found in Appendix D.

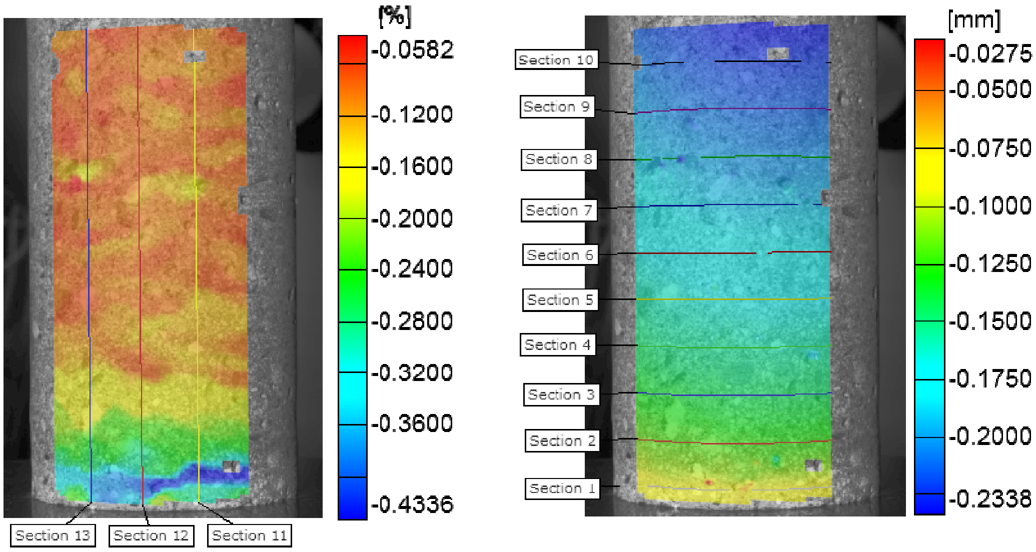

Figure 37 *Results from specimen 0-8Sh-1 at an axial compressive stress of 20 MPa. The fire exposed end of the core is located at the bottom of the photo. Left figure: Overlay of axial strain field together with the location of the vertical section lines. Right figure: Overlay of axial deformation field together with location of the horizontal section lines. The nominal strain is -0.13 % over a measuring length of 90 mm.*

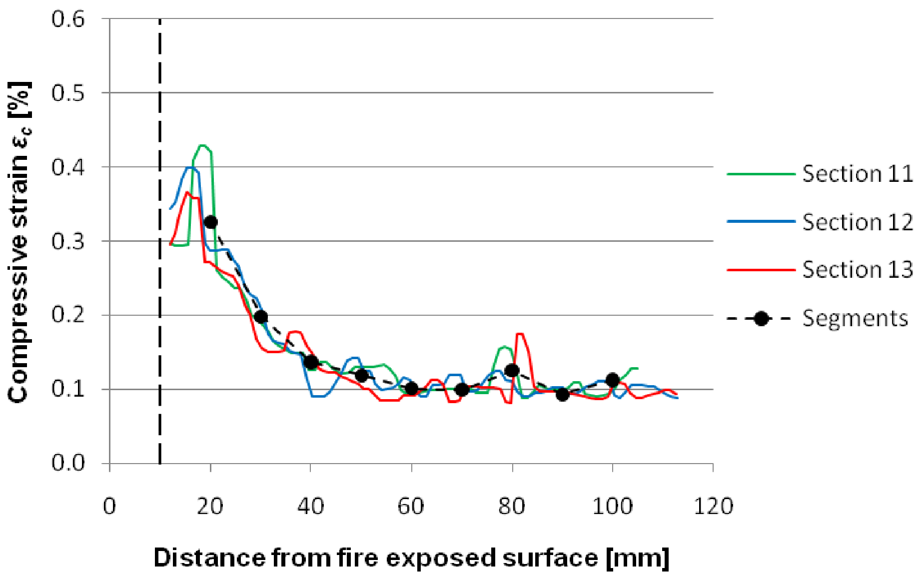

Figure 38 *Axial compressive strain vs. distance from fire exposed surface for specimen 0-8Sh-1 at an axial compressive stress of 20 MPa. Comparison of strain distribution obtained directly from vertical sections and evaluated from segments. The black dashed line at 10 mm indicate the bottom end of the tested core. The position of the sections is shown in the left hand image in Figure 37.*

From the strain distribution, it is obvious that there are large local variations in the strain values. These are mostly natural variations caused by local variations in stiffness of the cement paste and aggregates. Some parts of the variations are also due to measuring noise. These local variations can be reduced by filtering the results. Studying the strain distribution is a very effective way to analyze individual specimens, e.g. to find local weak zones. However, this becomes a little bit blunt when it comes to compare the stiffness degradation of different specimens, since this depends on where the sections are placed and how much the results are filtered. To avoid these disadvantages and to obtain a more straightforward and reliable method the strain distribution was evaluated by discretizing the core in the axial direction as illustrated in Figure 39.

The DIC measuring area was divided into nine 10 mm thick segments defined by ten equally spaced sections. The first section was located approximately 5 mm from the bottom surface of the core, which should be compared to 20 mm from the fire exposed surface to the centre of the first segment. The axial displacement of each facet element along the sections was exported from the ARAMIS system. The strain in each segment $\varepsilon_{c,s}^{m-n}$ was then calculated as the difference between the mean values of the axial displacement δ_m^n and δ_m^m of the corresponding sections *n* and *m*, respectively, divided by the initial distance l_0 between the sections as:

$$\varepsilon_{c,s}^{m-n} = \frac{\delta_m^n - \delta_m^m}{l_0} \tag{1}$$

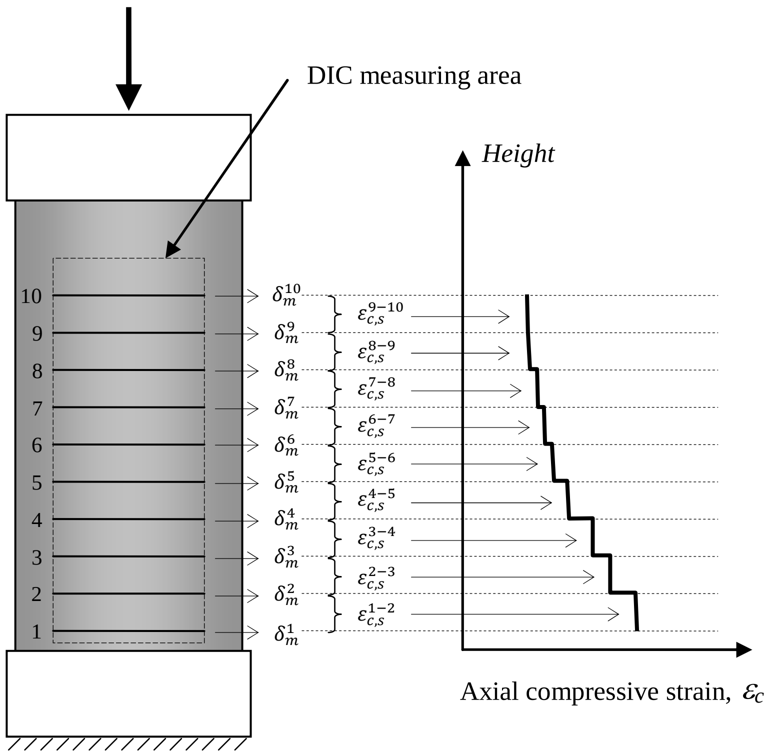

Figure 39 *Illustration of the evaluation of the compressive strain by dividing the core into segments.*

A comparison of the strain distribution along specimen 0-8 Sh-1, obtained directly from the vertical sections (Section 11, 12 and 13) and evaluated from segments as described above can be seen in Figure 38. There is good correspondence in the overall strain distribution while the main local variations are suppressed without any results filtering.

The distribution of the axial compressive segment strain ($\varepsilon_{c,s}$) evaluated according to this method is presented for all tested specimens at a stress level of 20 MPa in Figure 40 to Figure 43. The stress level was chosen so that all specimens were within elastic response. The strain distribution of the individual specimens can be found in Appendix E. As can be seen there is some scatter between the segment values within the same group of specimens. This might be an effect of variations within the concrete slabs. To obtain more representative values for the entire concrete slabs a mean axial compressive section strain, $\varepsilon_{c,sm}$, were calculated as the mean values of the segments at corresponding locations of the specimens originating from the same slab, see Figure 44 and Figure 45.

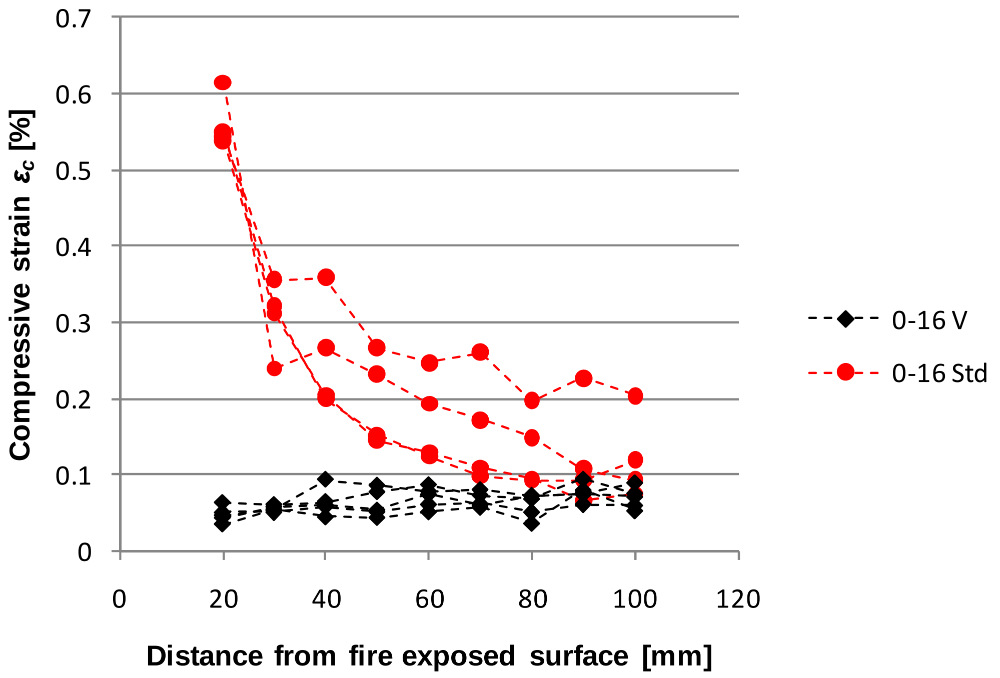

Figure 40 *Axial compressive section strain $\varepsilon_{c,s}$ vs. distance from fire exposed surface for specimens in group 0-16 V and 0-16 Std. The axial compressive stress was 20 MPa.*

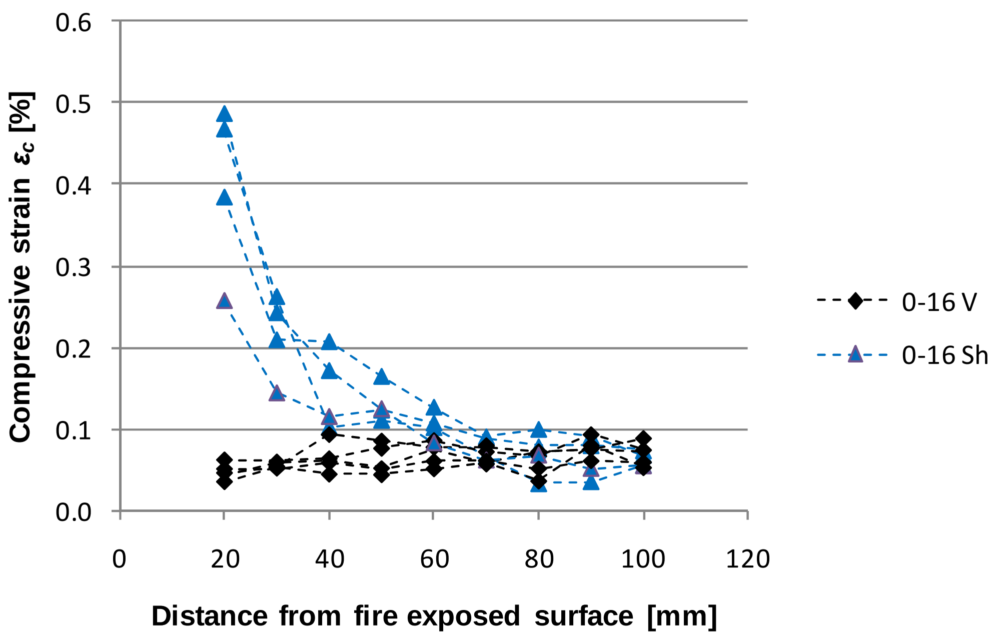

Figure 41 *Axial compressive section strain $\varepsilon_{c,s}$ vs. distance from fire exposed surface for specimens in group 0-16 V and 0-16 Sh. The axial compressive stress was 20 MPa.*

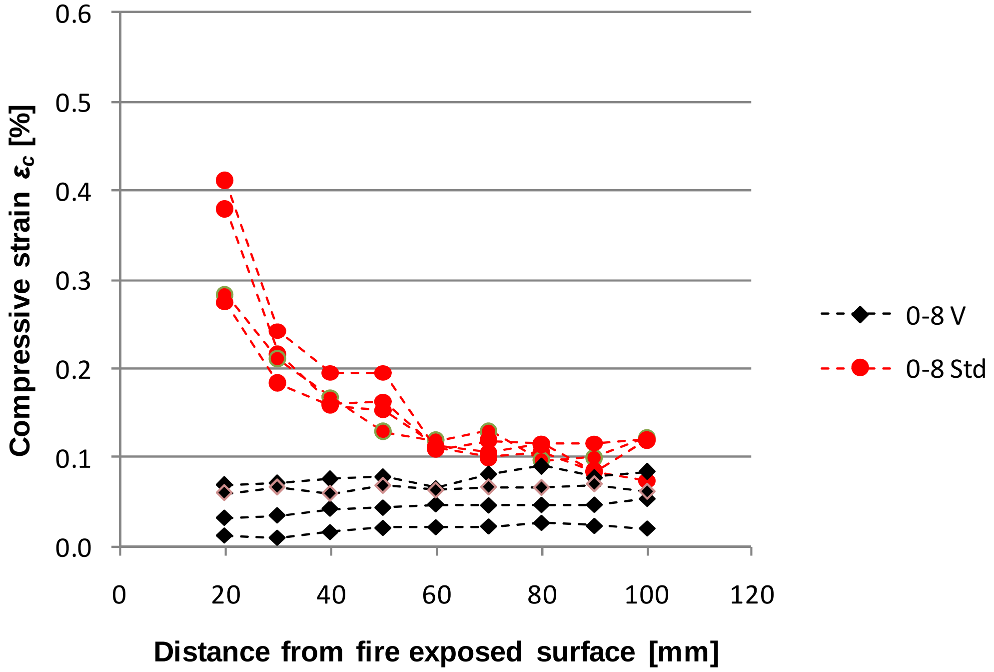

Figure 42 *Axial compressive section strain $\varepsilon_{c,s}$ vs. distance from fire exposed surface for specimens in group 0-8 V and 0-8 Std. The axial compressive stress was 20 MPa.*

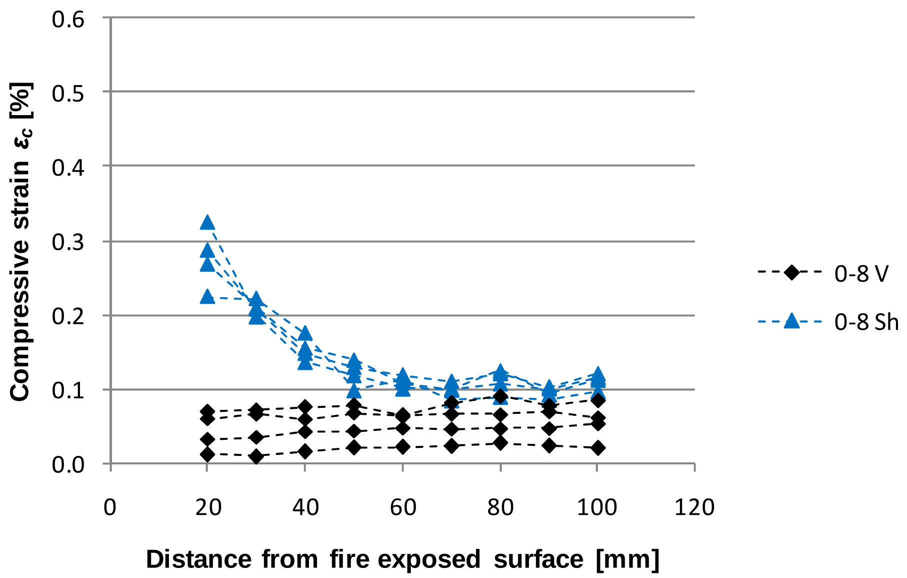

Figure 43 *Axial compressive section strain $\varepsilon_{c,s}$ vs. distance from fire exposed surface for specimens in group 0-8 V and 0-8 Sh. The axial compressive stress was 20 MPa.*

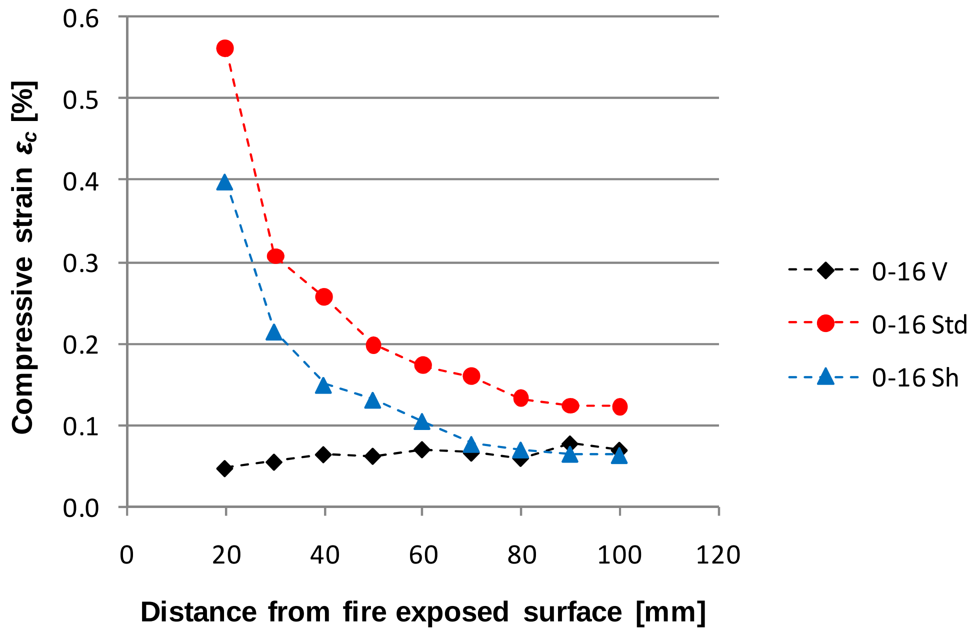

Figure 44 *Mean axial compressive section strain $\varepsilon_{c,sm}$ vs. distance from fire exposed surface. The strain values were calculated as the mean values of the segments at corresponding location of the specimens within the same group 0-16 V, 0-16 Std and 0-16 Sh, respectively. The axial compression stress was 20 MPa.*

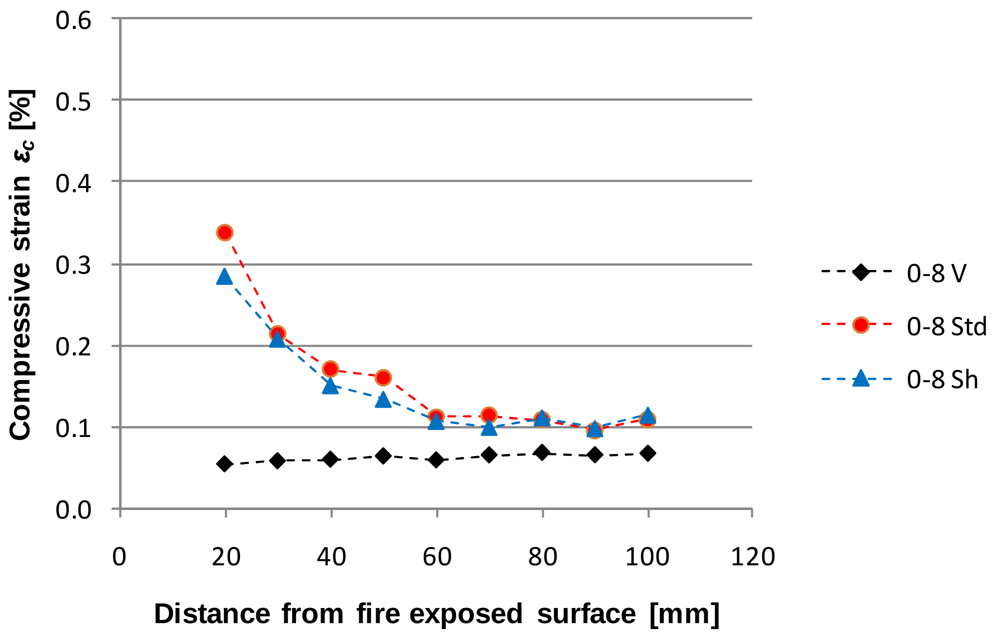

Figure 45 *Mean axial compressive section strain $\varepsilon_{c,sm}$ vs. distance from fire exposed surface. The strain values were calculated as the mean values of the segments at corresponding location of the specimens within the same group 0-8 V, 0-8 Std and 0-8 Sh, respectively. The axial compressive stress was 20 MPa.*

For the specimens from the unexposed reference slabs the strain distributions are relatively uniform along the specimen. Possibly one can identify that the strain values are smaller closest to the surface and then gradually increases inwards in the slab. This might be an effect of a better concrete compaction near the mould. For the fire exposed slabs there is a general trend that the specimens exhibit high strain values close to the fire exposed surface and that the values decreases towards the strains of the unexposed specimens with increasing distance from the fire exposed surface. From the highly non-uniform strain distribution for the fire exposed specimens it becomes very clear that the global stiffness of the core is a result of the stiffness reduction along the core. For instance, specimen 0-16 Std-6 both exhibit noticeably larger strain values along the core and lower stiffness compared to the other specimens within group 0-16 Std, see Appendices E and F.

To relate the residual stiffness of the fire exposed slabs to the unexposed plates a stiffness reduction factor was introduced. As the mean axial stress level is the same in all specimens, the stiffness reduction factor of each segment can directly be related to the segment strain as:

$$k_{c,s} = \frac{\varepsilon_{c,sm}^{unexposed}}{\varepsilon_{c,sm}^{exposed}} \tag{2}$$

where $\varepsilon_{c,sm}^{unexposed}$ and $\varepsilon_{c,sm}^{exposed}$ are the mean values of the segment section strain of the specimens from the unexposed and fire exposed plates, respectively. The stiffness reduction factors for the fire exposed slabs are presented in Figure 46 and Figure 47.

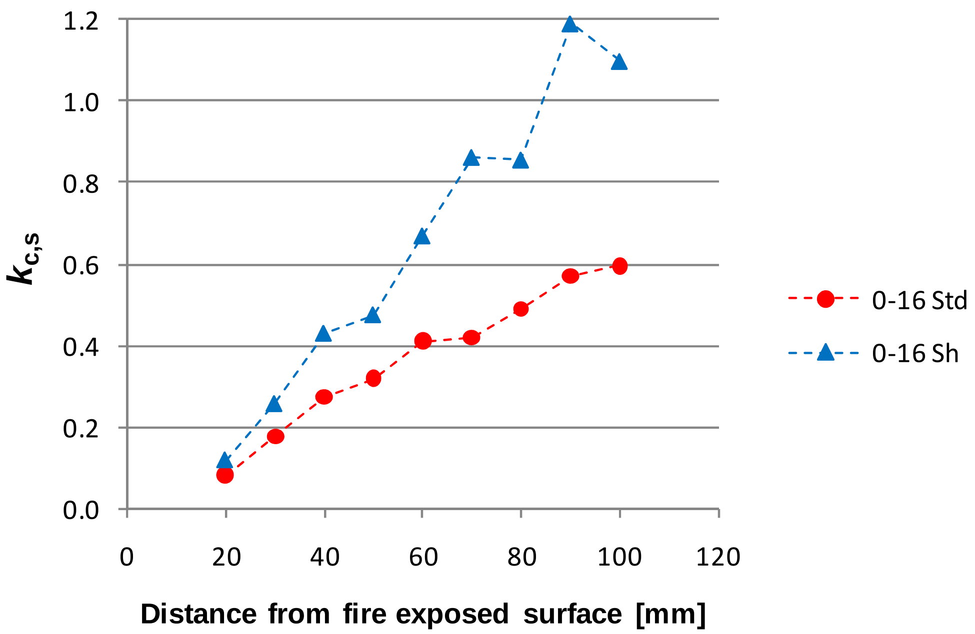

Figure 46 *Stiffness reduction factor $k_{c,s}$ vs. distance from fire exposed surface for specimen group 0-16 Std and 0-16 Sh. The axial compressive stress was 20 MPa.*

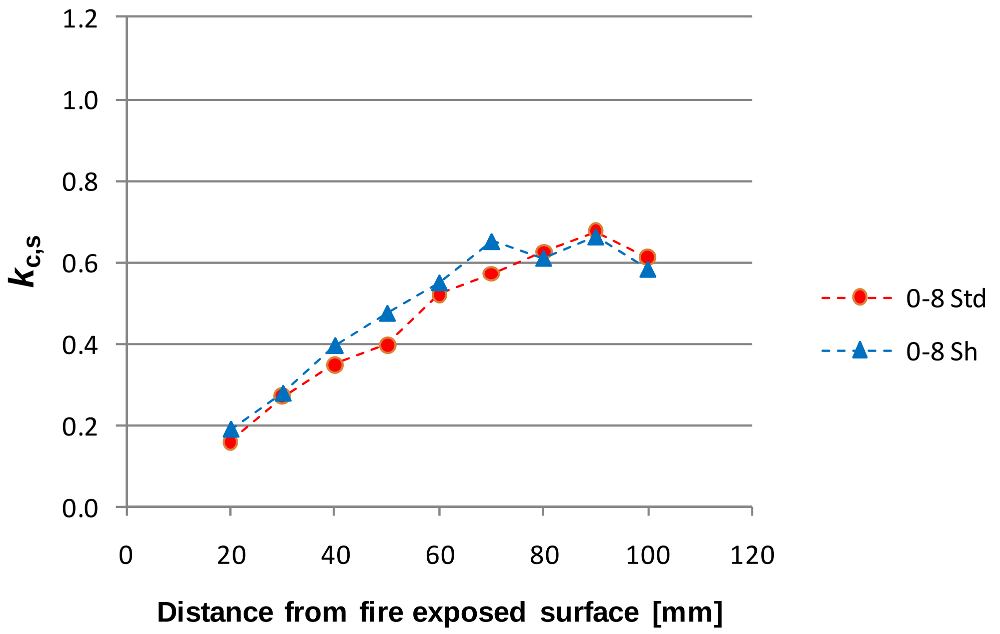

Figure 47 *Stiffness reduction factor k $_{c,s}$ vs. distance from fire exposed surface for specimen group 0-8 Std and 0-8 Sh. The axial compressive stress was 20 MPa.*

The stiffness reduction factor gives a picture of the damage level within the concrete slabs as a result of a temperature profile caused by the fire heating scenario. The stiffness degradation of 0-8 Std and 0-8 Sh coincides well, while there is a rather big difference between 0-16 Std and 0-16 Sh with increased distance to the fire exposed surface. The explanation for the latter difference has not yet been found, but one explanation could be that the scatter in strain values for each segment is larger for the 0-16 specimens than for the 0-8 specimens, see Figure 40 to Figure 43. The slabs with 0-16 mm aggregates exhibit lager stiffness reduction close to the surface for both fire scenarios, compared to the slabs with 0-8 mm aggregates. At a depth of 100 mm the reduction factor is around 0.6 to 0.7 for 0-16 Std, 0-8 Std and 0-8 Sh, while it is above 1.0 for 0-16 Sh. Values above 1.0 should not be physically possible and are probably explained by natural scatter and measurement uncertainties.

3.6.4 Microscopy

The microscopic analysis shows that thermal alterations in samples from the slow heating and the standard fire are rather similar. The sample 0-8 SH-4 show thermal alterations at larger depth compared to the other samples. For the 8 mm and 16 mm samples, respectively, there is also a difference in the relationship between the depth to the portlandite and quartz transitions. In samples with 8 mm aggregate this occurs at nearly the same depth while there is a clear difference in the 16 mm samples. The portlandite reaction is dependent on both temperature and water pressure. Results from the quantitative analysis of cracks indicate that thermally induced cracks are more frequent in the samples with coarser aggregate.

Table 11 The estimated depth in mm from the fire exposed surface to different changes.

	0-8 SH-4	0-8 Std-1	0-16 SH-1	0-16 Std-1	0-16 Std-8
Portlandite ($Ca(OH)_2$)	19-20 mm	11-14 mm	15-18 mm	14-17 mm	13-15 mm
Quartz α to β transition	21 mm	13-16 mm	26 mm	25 mm	25 mm
Reddish cement paste	4-12 mm	0.5-12 mm	3-12 mm	2-13 mm	1-14 mm

Cement paste

The type of changes in colour, mineralogy and micro-texture with depth from the fire exposed surface were similar in the different samples but the specific values were different, see Table 11. The colour of the paste, seen in plain light in the microscope, is brown to dark brown in the outermost 0.5 to 4 millimetres. From this level and into about 12 to 14 mm the colour of the paste is rust red and appears to have a less accentuated micro-structure in the microscope. The reddish colour comes to some extent from iron oxide exsolutions in the paste. Further in, to approximately 50 mm, the colour gradually turns towards a greyish brown and the micro-structure has a more accentuated cement paste structure (see Figure 48). In polarized light the colour is brownish down to a depth of about 10 mm. The brownish colour in polarized light and the change from reddish in normal light at 12 to 14 mm corresponds to the depth of the portlandite dehydroxylation (Figure 49, Table 11). It should be noted, however, that the colour changes seen by the naked eye on these samples were mainly different shades of grey although they are comparable to those discerned using microscopy concerning the depth in from the fire exposed surface.

Cracks in the cement paste and the ITZ

Cracks in the cement paste and in the contact between aggregate and paste, and the inter-transitional zone (ITZ), were quantified. There was a significant increase in both micro-cracks (< 10 micrometer) and thin cracks (10-100 micrometer) in the fire exposed samples (Table 12). The crack frequency was 0 to 0.07 cracks/mm in the reference samples. The quantitative analysis of micro and thin cracks show that the samples with finer 0-8 mm aggregate showed less cracks in the cement paste and that the cracks identified were more superficial, see Figure 51 and Figure 52. Near the surface in the samples containing 0-16 mm aggregate the crack frequency was about 0.5 cracks/mm and in the 0-8 mm aggregate samples the crack frequency was about 0.3 cracks/mm. It should be noted that there was a lower crack frequency at 15 mm in all the analysed samples. This level coincides with a change in colour and micro structure of the paste at the same level. The increased crack frequency goes to a greater depth in the 0-16 mm aggregate samples compared to the 0-8 aggregate samples. The crack frequency is determined as cracks intersecting traverse lines parallel and perpendicular to the exposed surface. This provides a possibility to assess the degree of orientation in the different samples. The cracks are mainly oriented sub-parallel and sub-perpendicular in relation to the fire exposed surface. There is an indication that perpendicular cracks are slightly more frequent in the samples.

Fine cracks were found extending away from and perpendicular to the exposed surface. These cracks can be traced as discontinuous cracks through the whole thin section. On the micro scale the shape of these cracks was very irregular. Cracks parallel to the fire exposed surface were relatively frequent down to a depth of approximately 1 cm. These parallel cracks were not concentrated to a few fine fractures but disseminated to several small micro-cracks.

Most cracks passed round the aggregate as adhesion cracks. Adhesion cracks often leave the aggregate particle ITZ at a point where the surface has a high curvature. Some of the cracks pass thorough the aggregate particles, especially although not always, in the severely cracked aggregate particles. The coarse cracks perpendicular to the fire exposed surface typically passed around the aggregate particles. That was often the case for those particles that were badly damaged by internal thermal grain boundary delamination implying that the external cracks were developed before the internal cracks. Intense internal fracturing gives fractures that can be traced out in the surrounding paste as short micro cracks. This may result in fringes of micro-cracks extending from some of the larger aggregate particles (Figure 50). Indeed, this was the general fracture pattern for the small surface parallel fractures mentioned above. The cracks passed through these aggregate particles mostly as intra- or inter-granular cracks rather than grain boundary cracks.

Considering the severe fire exposure of the samples from both the slow heating and the standard fire test the number of micro cracks was low in all samples. The crack pattern and frequency is probably strongly dependent on the presence of fibres and the heating scenario. The situation would therefore be different for other concretes and other heating scenarios.

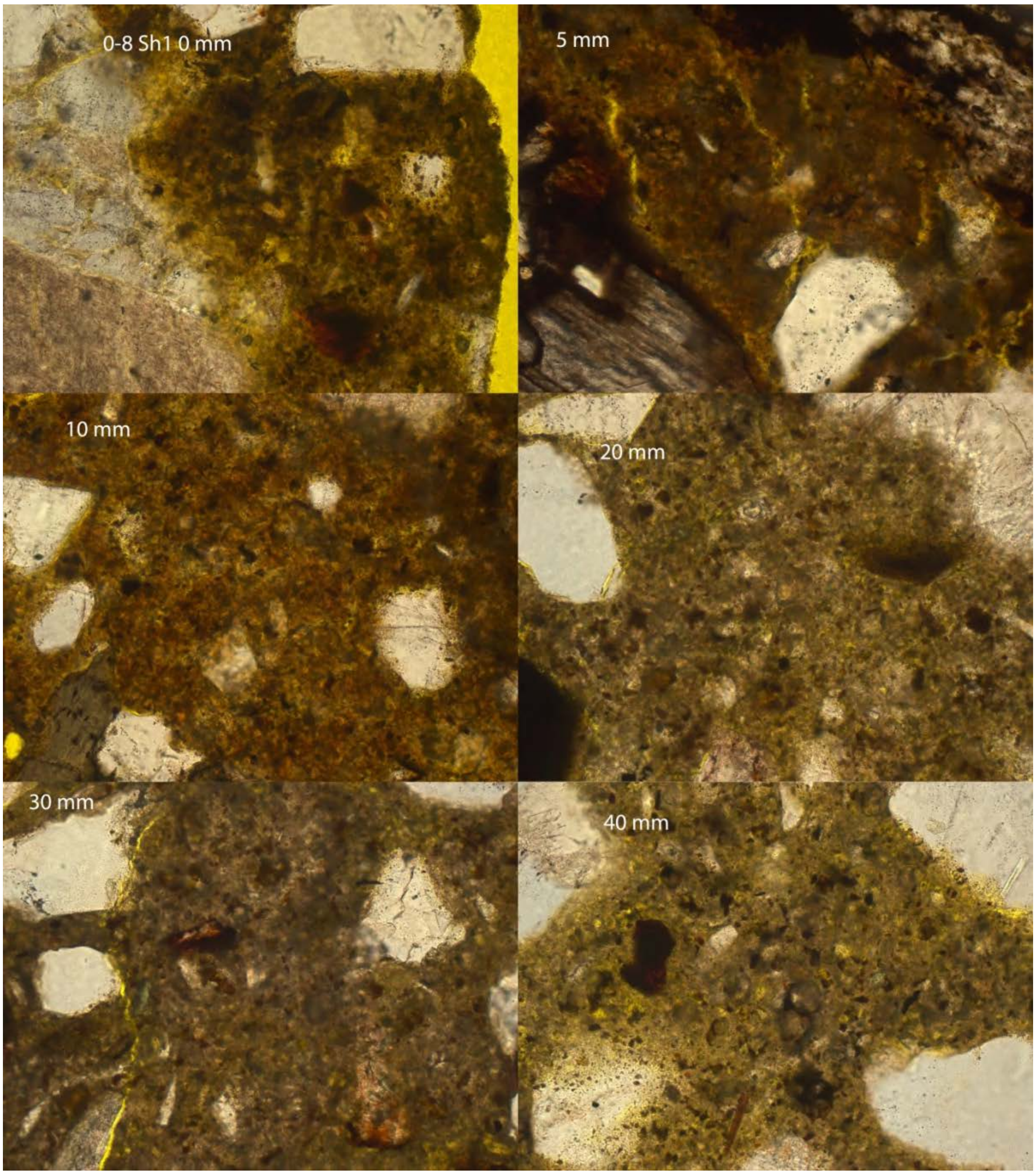

Figure 48 *The images illustrates the variation on colour and microstructure from the fire exposed surface and in to 40 mm below the surface in the sample SH-4. Plain light, the size of the individual images is 0.7x0.5 mm*^{2}.

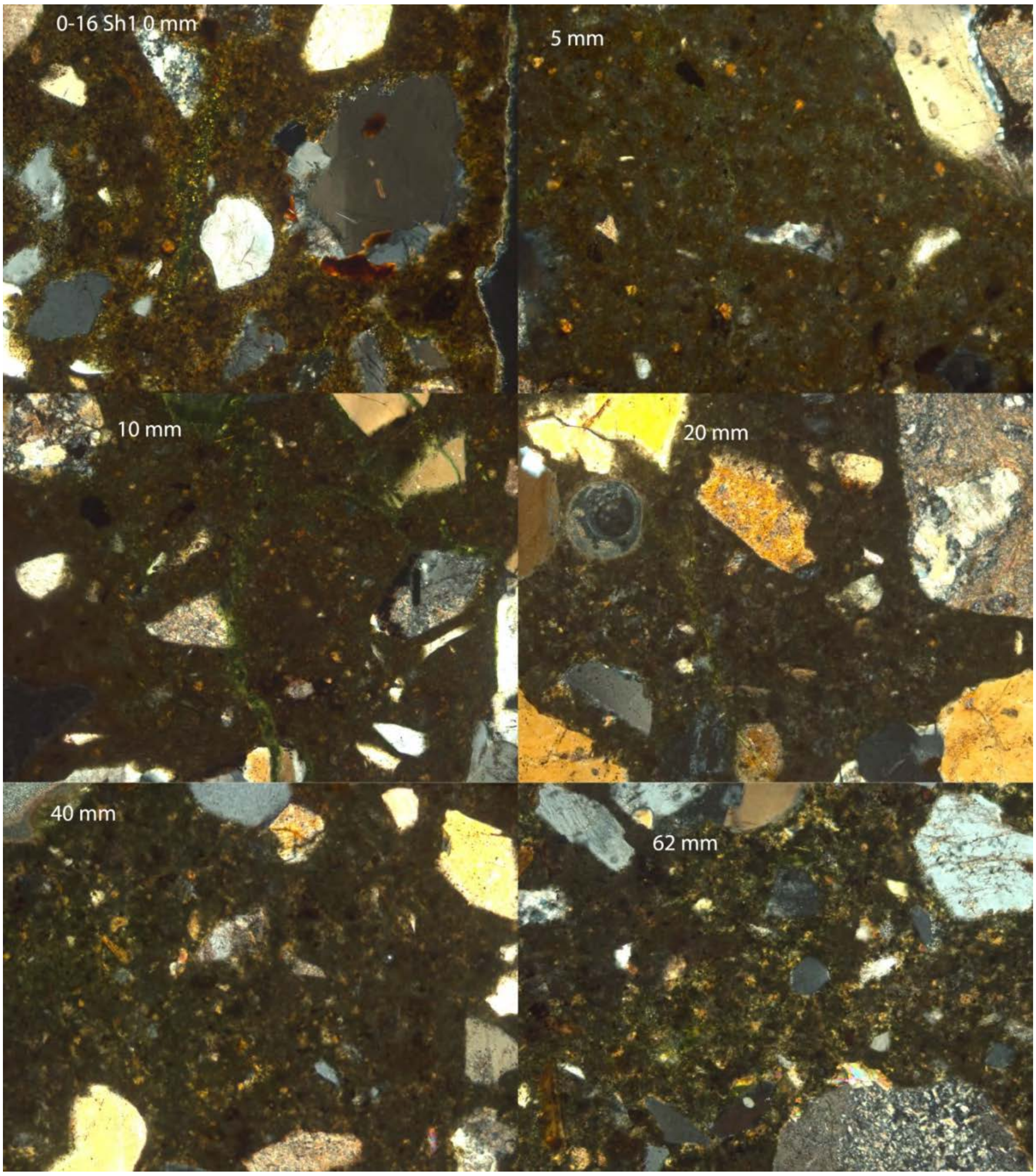

Figure 49 *The micro graphs show the change in micro structure and in polarization colour. Down to 10 mm the colour is slightly brownish and the structure of the cement paste is less pronounced and portlandite is lacking. The size of the individual images is 1.4x1mm^2.*

Aggregate

Fluorescence microscopy shows that the quartz bearing aggregate had severe internal fracturing down to 13 to 25 mm from the fire exposed surface. The thermal fractures in the quartz bearing rocks were dominated by grain boundary cracks and in pure quartz grain domains almost exclusively located at grain boundaries. This led to a thermal de-cohesion of the aggregate particles. The micro-texture determines how prone to fracturing though thermal decohesion the different quartz bearing aggregate particles are. The worst case being equigranular quartz grains in an equilibrium texture. Very fine grained quartz and deformed quartz grains with dislocations and formation sub-grain boundaries have a lesser tendency to exhibit thermal fracturing. In aggregate particles with mixed quartz and feldspar, grains may exhibit radial cracks extending away from the quartz grains towards the feldspar grains. Feldspars often display fractures along internal crystallographic slip planes. Although Feldspar crystals that are sericitic or contain exsolutions of iron oxide do not develop fractures along slip planes. Further, aggregate particles that have a high content of mica exhibit fewer thermal fractures. In particles with high frequency of grain boundary cracks these cracks may cause delamination of the particle surface.

Some of the feldspar and biotite aggregate particles were reddish, in particular close to the fire exposed surface. The higher abundance of reddish particles close to the exposed surface was thermally induced. However, reddish aggregate was preset to some extent at all levels, even in the non-fire exposed samples. It is therefore difficult to use as a temperature indicator in this case. As a consequence it was difficult to assess the thermal influence on the exsolution. In sample SH-4 no cracks were found in aggregate particles in the outermost 1 to 2 mm of the fire exposed surface. Further, the paste had a lesser micro-porosity in this zone. This is change was interpreted as being caused by sintering.

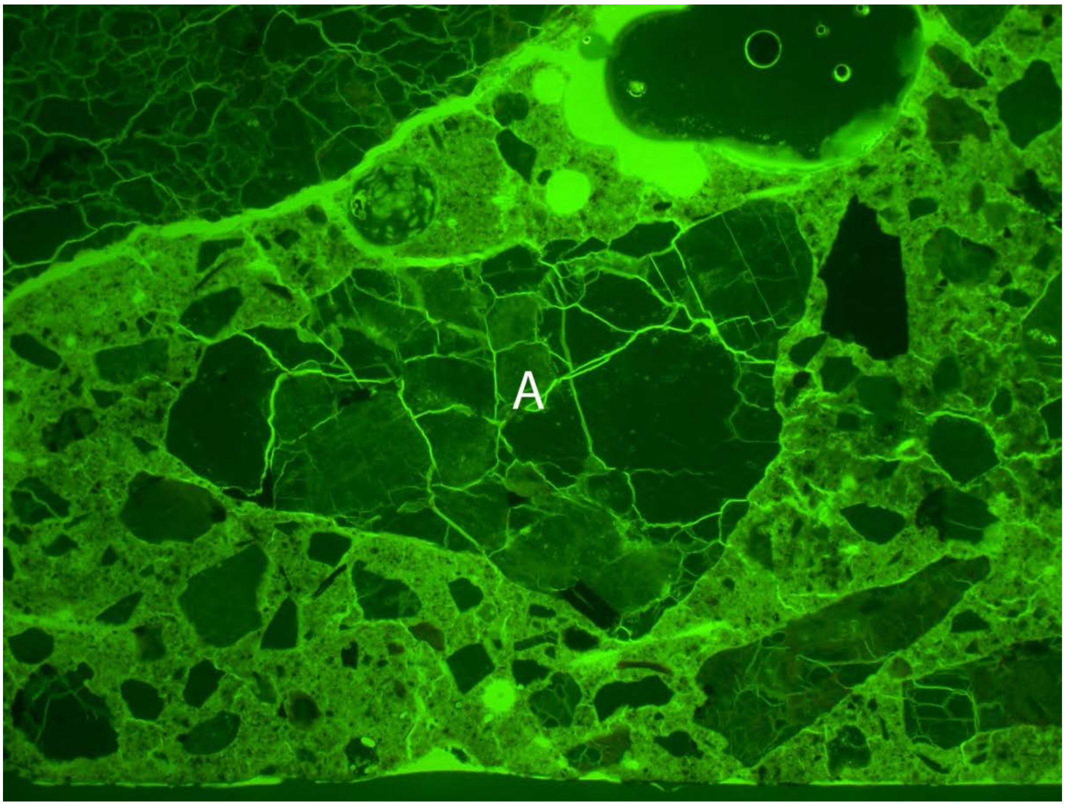

Figure 50 *Shows an aggregate particle where grain boundary and inter-granular cracks passes out into the paste as a fringe parallel to the exposed surface. Cracks and pores are seen in light green. The exposed surface is seen in the lower part of the image. The image surface is 5.5x4.2 mm^2.*

Table 12 *Crack width in the analyzed samples.*

Sample	Parallel	Perpendicular
0-8 Std-1	50 micrometer	100 micrometer
0-8 SH-4	20 micrometer	50 micrometer
0-16 mm Std-1	100 micrometer	150 micrometer
0-16 mm Std-8	100 micrometer	20 micrometer
0-16 mm SH	30 micrometer	50 micrometer

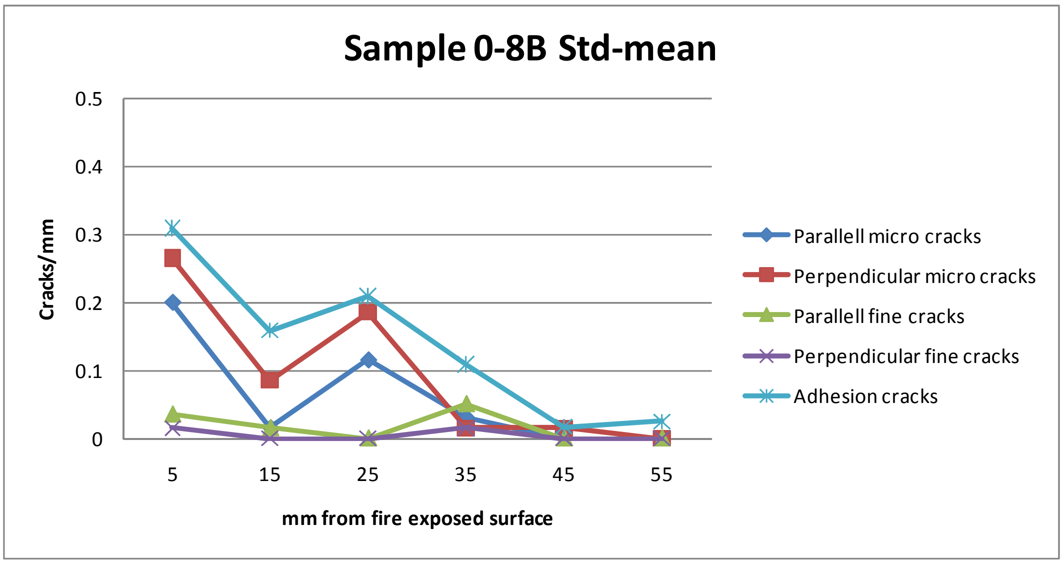

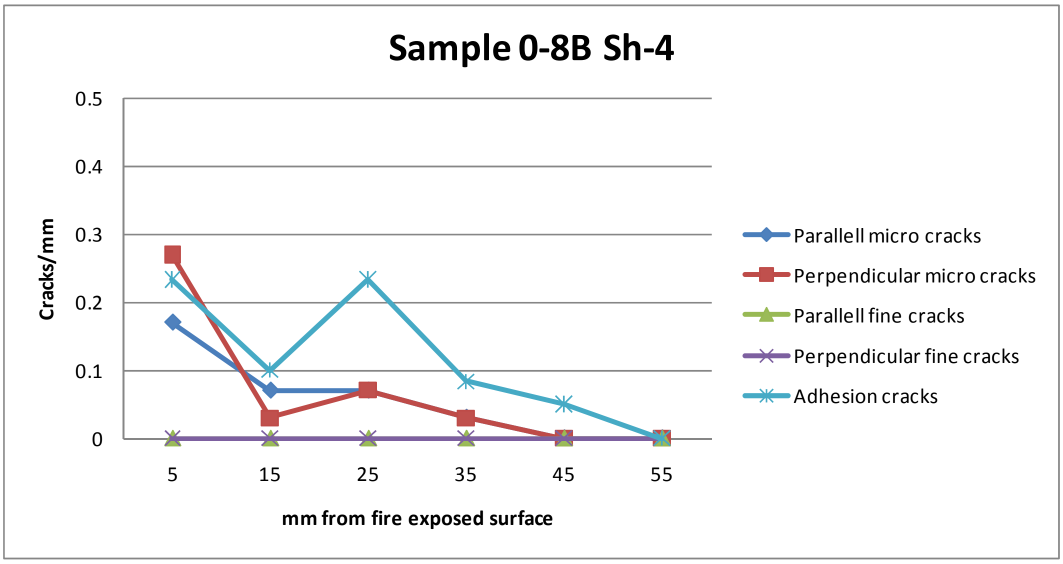

Figure 51 *Crack frequency from the fire exposed surface and inwards. The levels given in mm compares with those given in the Aramis analysis. The crack frequency is 0 to 0.07 crack/mm in the reference samples.*

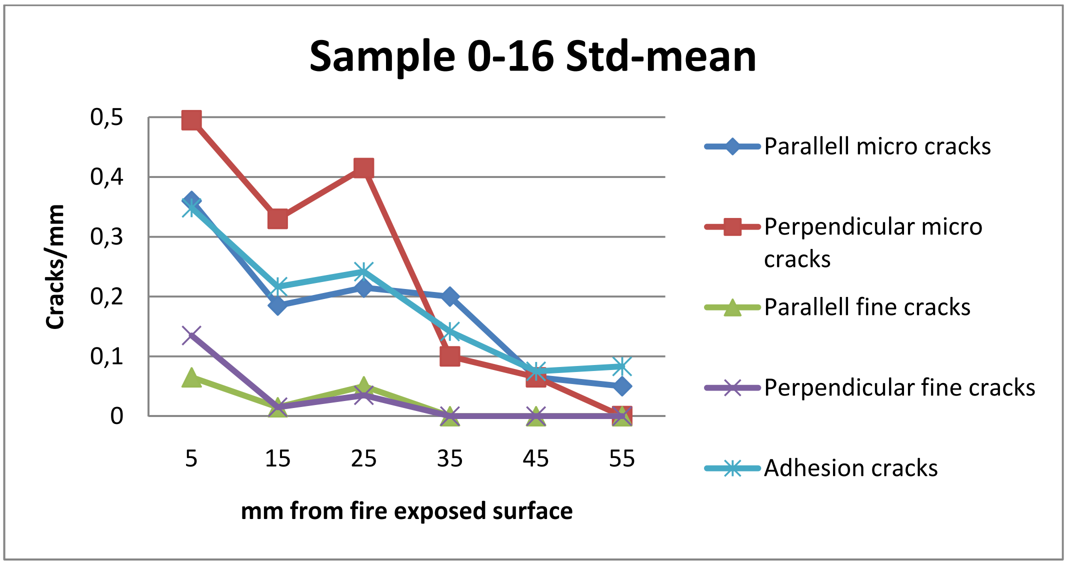

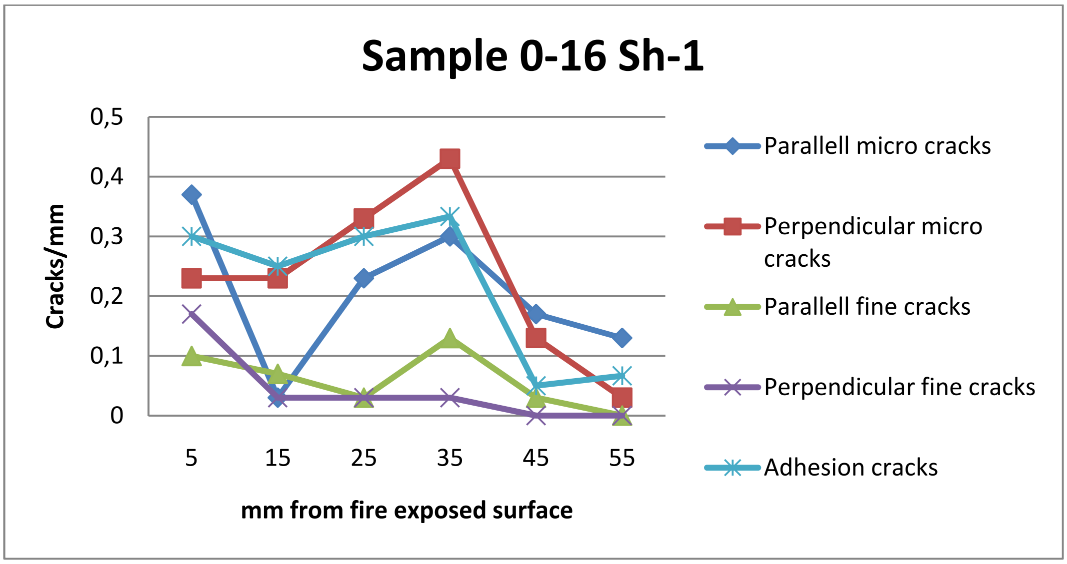

Figure 52 *Crack frequency from the fire exposed surface and inwards. The levels given in mm compares with those given in the Aramis analysis. The crack frequency is 0 to 0.07 crack/mm in the reference samples.*

Polypropylene fibres
There are a large number of traces from polypropylene fibres (pp-fibres) in the form of empty micro- channels in the cement paste. In the reference samples the fibres were identified through the interference colour of the polypropylene. The pp-fibres were unevenly dispersed in the mm scale. There were domains of a few square mm in size with a number of fibres while other domains lacked fibres. In the thin sections studied the pp-fibres were less frequent near the surface in both the fire exposed samples and the reference samples.

4 Discussion

The change in ultrasonic velocity is sensitive to changes in stiffness, which decreases at an early stage in a fire scenario. The relative change in ultrasonic velocity is more important than the absolute value. The absolute value for the ultrasonic velocity is dependent on several factors and is as a consequence difficult to relate to the condition of the concrete. It is therefore useful if concrete of the same type in a part of the structure that is unaffected by fire can be used as a reference value. The decrease in velocity can be used as an indicator of the degree of damage. The measurement can be performed on a surface or through a structural element such as a concrete beam.

The ultrasonic pulse transmission time (USPTT) measurement, as described in section3.6.2, shows that the transmission times of the ultrasonic pulse through the unexposed cores and fire exposed cores are equivalent close to the unexposed side of the core. When approaching the fire exposed side of the core the readings increase. By introducing an ultrasonic pulse transmission reduction factor the test results can be compared to the stiffness reduction obtained from the mechanical tests, i.e.:

$$Ku = \frac{USPTT_{unexposed}}{USPTT_{exposed}}$$

As shown in Figure 53 and Figure 54 the stiffness reduction and the USPTT reduction is significant close to the fire exposed surface. Further away from the fire exposed surface, deeper into the structure the stiffness reduction is still of significant. The USPTT readings in these regions are reduced as well. As shown in this study, regions with significantly reduced stiffness can be detected with this method.

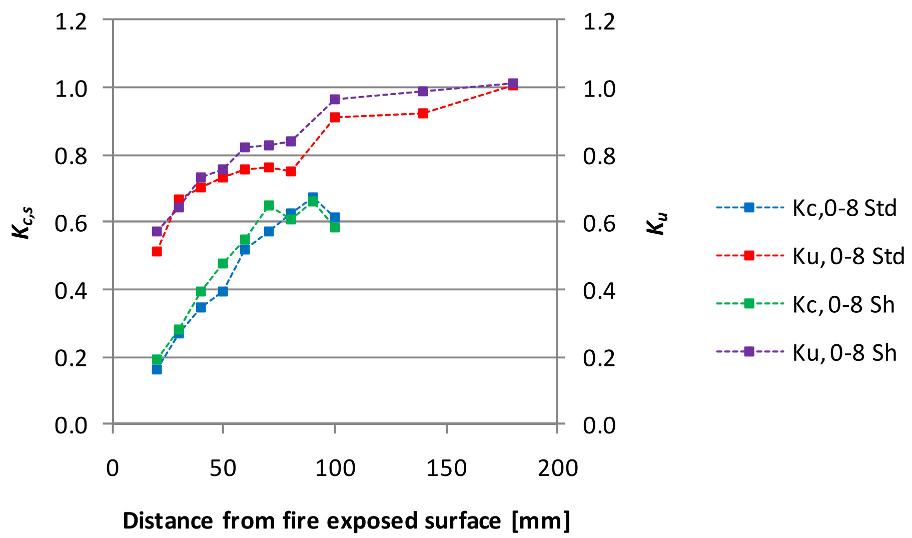

Figure 53 *Stiffness reduction factor $K_{c,s}$ and ultrasonic pulse transmission time reduction factor Ku for 0-8 Std and 0-8 Sh.*

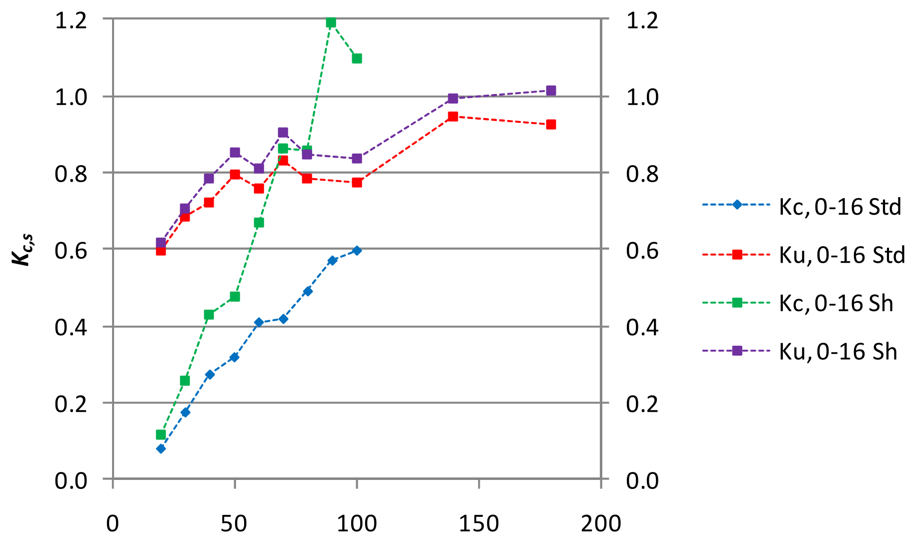

Figure 54 *Stiffness reduction factor $K_{c,\,s}$ and ultrasonic pulse transmission time reduction factor Ku for 0-16 Std and 0-16 Sh.*

As presented in section 3.6.1, the residual stiffness reduction factor evaluated according to the proposed method based on DIC measurements gives a picture of the level of damage within the concrete cross-section as a result of a temperature profile caused by the fire heating scenario. In this study it was possible to compare the fire exposed concrete with unexposed reference concrete from the same batch in a straightforward way. In a real assessment situation this is often more complicated. One way is to identify unexposed concrete members in the immediate proximity where the same concrete could be expected and to take core samples to be used as references. For example, the lower part of a fire exposed column may be regarded as unexposed. Another method is to use the inner part of the cored cylinder as the reference. When the strain distribution becomes constant over a longer part of the core it is likely that one has found unaffected concrete. At this point one can use the stiffness of this unaffected part as the reference in the evaluation of the stiffness reduction factor in the area closer to fire exposed surface. If none of these methods are possible one could compare the segment stiffness of the fire exposed concrete with a theoretical value of the stiffness of the original concrete.

With an understanding of the relationship between the residual stiffness degradation and the temperature, it would also be possible to establish a rough estimation of the temperature profile based on the residual stiffness degradation measurements. This estimation might be a use as an indication of the maximum temperature in the reinforcement. Since the temperature profile is known in these tests it is possible to plot the stiffness reduction factor versus the maximum temperature for each segment as shown in see Figure 55. This gives a relationship between the stiffness reduction factor and the maximum temperature which can be compared to theoretical models for the residual stiffness degradation. In this report, the test results are compared with two simple linear models where the stiffness reduction factor goes from 1 to 0 in the temperature range of 20 – 600°C and 20 – 800°C, respectively. In this case there is a better agreement between the test results and the former model. However, at lower temperatures the model seems to underestimate the stiffness degradation for 0-16 Std, 0-16 Sh and 0-8 Sh. The reason for this might be the development of a crack system in the virgin part of the cross-section caused by extensive thermal expansion closer to the surface. This leads to a bowing of the structure with associated crack formation. In general during fire tests on slabs, cracks open up on the non-fire exposed side of the specimen, often followed by water pouring out in the cracks. During tests of E-modulus at high temperatures the test specimens are heated slowly to reduce effects from high thermal gradients (RILEM TC 129 MHT, 2004).

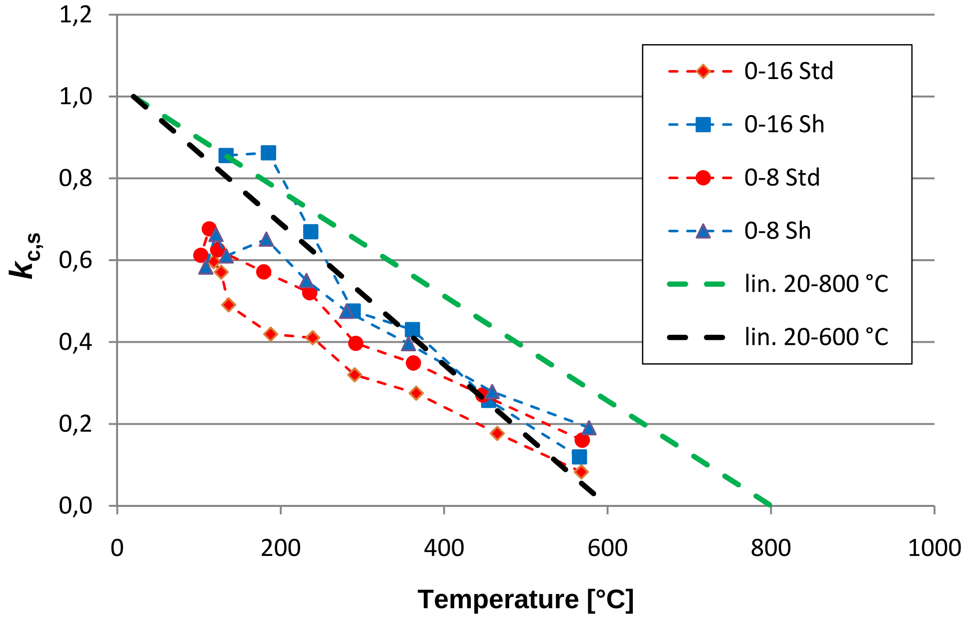

Figure 55 *Stiffness reduction factor* $k_{c,s}$ *vs. temperature.*

Together with other temperature indicators, an understanding of the residual stiffness degradation could form the basis for determining the maximum temperature profile within a fire exposed structure. Further, the extent and duration of a fire could be inferred from this information when this is not a known fact. For instance, often the most important factor to be determined in an assessment of a fire exposed concrete structure is the maximum temperature at the location of the reinforcement. However, this requires reliable models for the relationship between the temperature and the residual stiffness degradation. Figure 56 and Figure 57 show a comparison of the temperature profile based on the temperature measurements in the cross section during fire exposure and that evaluated from the stiffness degradation test method based on DIC measurements. In this case the linear stiffness reduction factor model for 20 – 600 °C was used.
Rather good agreement was found for the higher temperatures close to the fire exposed surface, while the temperatures deeper in the slab were overestimated, which is acceptable as it corresponds to an assessment of fire impact that errs on the safe side.

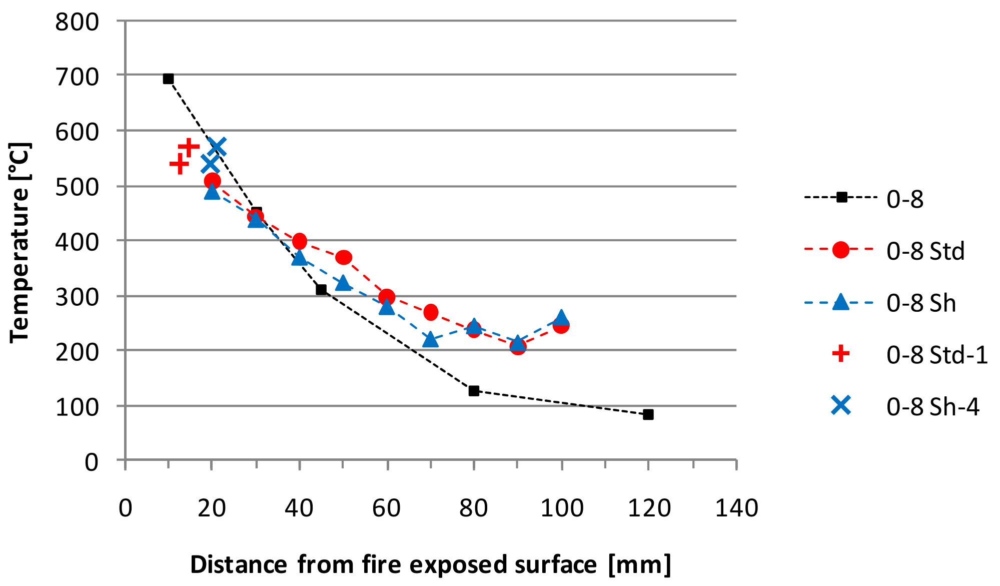

Figure 56 *Comparison of measured temperature profile and evaluated by the stiffness degradation for specimen group 0-8 Std and 0-8 Sh by using the linear stiffness reduction factor model 20- 600°C. In addition, the decomposition of portlandite and the quartz α β transition are marked for 0-8 Std-1 and 0-8 Sh-4.*

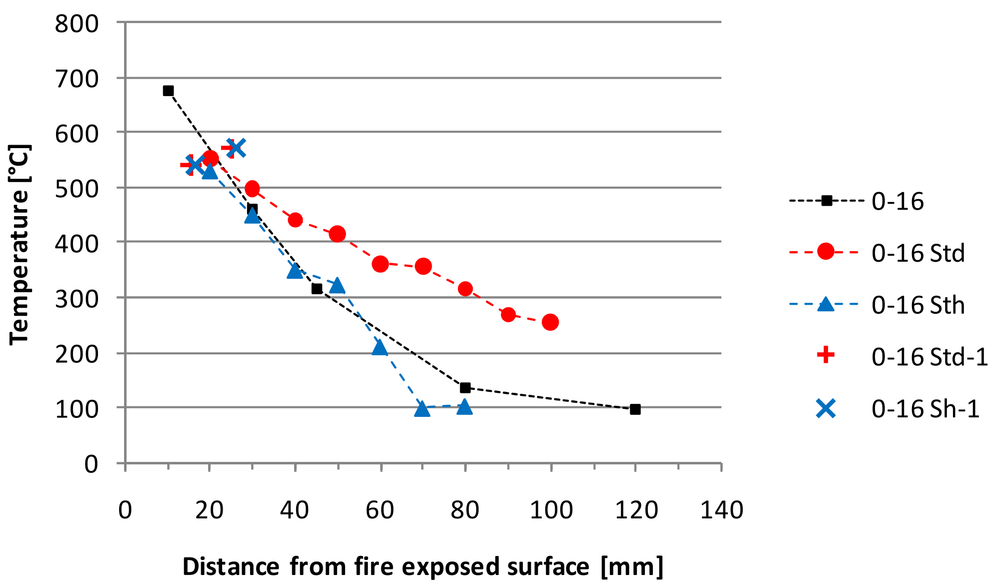

Figure 57 *Comparison of measured temperature profile and evaluated by the stiffness degradation for specimen group 0-16 Std and 0-16 Sh by using the linear stiffness reduction factor model 20- 600°C. In addition, the decomposition of portlandite and the quartz α β transition are marked for 0-16 Std-1 and 0-16 Sh-1.*

The quantification of crack frequencies gives a similar pattern in all samples. There is a high crack frequency near the surface, a minimum at about 15 mm depth and a maximum again at about 25 mm. This pattern is specific for the combination of material and fire scenario and cannot be transferred to a different situation.

The depth away from the fire exposed surface where the crack frequency decreases agrees with a strong change in mechanical properties shown by the Aramis measurements. The change in mechanical properties cannot be explained only by the formation of cracks. This is shown by the crack distribution in the 0-8 mm samples where the crack frequency at 55 mm depth is comparable to the background values for samples that have not been exposed to a fire while the Aramis results indicate a reduction in stiffness of about 50 % at this level.

The rebound number after fire exposure is slightly higher in the samples with 0-8 mm aggregate compared to the samples with 0-16 mm aggregate. This is in agreement with the higher density of surface parallel cracks at 5 mm depth from the fire exposed surface in the 0-16 mm samples.

Decomposition of portlandite occurs closer to the surface and therefore at higher temperature than the quartz α β transition which is reversed to the actual reaction temperatures. Furthermore, the portlandite decomposition occurs further away from the exposed surface in the slow heated samples. This may be due either to the kinetics of the reaction or its water pressure dependence, i.e. if the water vapour pressure is higher this decomposition reaction will occur at a higher temperature. The quartz α β transition on the other hand is pressure independent and is a rapid transition that takes place as soon as the reaction temperature is reached. In the present study the level for the portlandite decomposition given is where the portlandite is entirely consumed. The results imply that it may be more appropriate to identify the level for the onset of the reaction.

5 Recommendations

When arriving at a concrete building after a fire, the first priority is always to evaluate whether it is safe to enter the fire exposed area. Temporary false work may in some cases be necessary to add as a safety precaution during the assessment.

When this first issue of safety has been dealt with the following assessment procedure is recommended:

- Try to obtain an understanding of the development and spread pattern left by the fire. Information from the Rescue Service can be a great help together with temperature indications from different materials found at the location. In Table 1 the effect of temperature on common materials is shown. If possible, one should also obtain drawings of the construction.
- Develop an overview of the concrete structure by mapping the visible damage, such as spalling, cracks, delaminations, deformations and other influences from the fire. When doing this it is useful to have a hammer and chisel at hand to be able to identify highly affected parts and delamitations. If the fire scene is complex it is also helpful to use a damage classification system. Two different examples of damage classification schemes that can be used are shown in Table 4 and Table 5.
- Determine remaining deformations in beams and other pre-stressed elements. A loss of pre-stress can be suspected if beams close to the fire are more deformed then virgin beams in the surrounding structure not affected by the fire. In this context, special attention should be given to support structures for floors and beams and other critical parts of the structure.
- More detailed information can be obtained using the Schmidt Rebound Hammer and ultrasonic pulse transmission time measurements. The Rebound Hammer measures only the surface properties but will with a simple measurement identify significantly damaged areas. It is recommended to take a series of measurements in a small area and to use the mean value because the test variation is sometimes high. When measuring the ultra sonic pulse transmission time it is important to remember that the damage in the cross-section usually changes from severe damage close to the surface to undamaged further into the material. Therefore this measure is recommended as a relative measurement, i.e. when comparing damaged and undamaged parts of the structure to facilitate mapping of the damaged area.

In many cases the above recommended strategy provides sufficient information on which to base a recommendation concerning how to restore a construction after a fire. However, sometimes a more in detail picture of the degradation is needed to assess the conditions of a construction. A reliable assessment is important both from a safety point of view and an economic point of view. When making an assessment from an economic point of view, the influence of the fire on properties that have an impact on the durability must be considered, e.g. at high temperatures a momentary carbonation occurs and extensive micro-cracking and melted polypropylene may result in a much more permeable micro-structure. In such cases the surface must be refurbished to restore the durability of the material although the structural function has not been affected by the fire.

To make a more detailed picture of the degradation in the cross-section of concrete elements some more advanced methods can be used. There are, as shown in the literature study, a variety of different methods available for more detailed studies of the degradation both on site and in the laboratory on drilled cores but based on the present study the following approach is recommended.

- When planning the core drilling of an area suspected of damage, make sure that the study itself does not cause damage to the structure, i.e. avoid cutting pre-stressed reinforcement or taking samples from critical parts of the structure. If possible take long enough cores to be able to determined the depth of the damaged layer and/or complement the fire damaged cores with similar (same concrete) cores that are from regions that were not exposed to the fire. This will enhance the quality of the analysis. The undamaged regions are used as references for the determination of the extent of damage.

- Ultrasonic pulse velocity measurements on cores at different depth from the fire exposed surface, as shown in chapter 3.5.2, provide information concerning the depth of damage. This method requires no preparation of the cores and is possible to do directly on site after core drilling. On site measurements allow the operator to increase the number of core samples or cancel planed drilling depending on the from previous cores results. The relative change in transmission time or velocity compared to the unaffected reference sample is more important than absolute values. This method is a fast but is an indirect method for determining the degradation in the cross-section.

- Further evaluation on the drilled cores in the laboratory:
    - Microscopy studies of cracks and colour change will give certain temperature indications that can be used to assess the maximum temperature that the reinforcement has been exposed to, as shown in chapter 3.5.4. An indication of the size of the fire damaged zone can be obtained despite the fact that the direct coupling to exact values of degradation of the mechanical properties is difficult. Further, the microscopy studied provides information concerning the residual durability as a high intensity of cracks amplifies the sensitivity to reinforcement corrosion. When conducting microscopy studies it is recommended to heat similar virgin concrete in a furnace of to obtain a better reference for the reaction and crack patterns in the specific concrete that was used in the construction.
    - To obtain a direct coupling to mechanical properties, optical full-field strain measurements during a compressive load cycle can be performed as shown in chapter 3.5.3.2.
    - Using such information, a true mechanical response of the material in the cross-section can be monitored as the most damaged parts will deform more under load as the stiffness will be reduced. This will give a picture on the degree of damage at different depths.

After assessment of the residual properties of the material, i.e. the concrete and the reinforcement, an assessment of the structural capacity can be made by a structural engineer. Other parameters such as corrosion resistance, frost resistance and fire resistance in case of a second fire should be taken into account when evaluating the potential to restore the structure rather than demolish. Note that when repairing a reinforced construction, the damaged or weakened concrete and the weakened reinforcement must be replaced.

The following functional requirements should be fulfilled for any repair (Schneider et al., 1990).

- The repair shall prevent the reinforcement from being attacked by corrosion throughout the intended service life of the repaired structure.
- The repair material shall have the same durability as the repaired material
- The repair shall restore required load bearing capacity and ensure acceptable deformations
- The repair should ensure the fire resistance of the structure as required.

Alternatively to restore the structure to the conditions before the impact of a fire one could conduct a completely new structural evaluation based on the regulations that are valid today.

6 References

Anderberg Y, Bernander K, (1996) *"Biblioteksbranden I Lindköping den 21 september 1996: stadium av orsak till tidigt ras"* Fire Safety Design AB, Lund

Bazant Z. P., Kaplan M. F. (1996) *"Concrete at High Temperatures- Material properties and mathematical models"* Book published by Longman Group Limited 1996

Bengtson S. (1969) *"Bestämning av Resthållfastheten hos Brandutsatta Betongpelare"* Thesis at KTH conducted at SP Fire Technology, 1969

Bessey G. E. (1950) *"The Visible Change in Concrete or Mortar Exposed to High Temperature"* National Building Studies, Technical Paper No. 4, London, 1950

Boström L. (2006) *"Investigation of damage to a bridge caused by a road tanker fire"* Brandposten No.34 2006: 28-29

Boynton RS (1980) "Chemistry and Technology of Lime and Limestone" John Wiley & Sons

Carino N. J. (2004) "*Pull out test"* Chapter 3 in Handbook on Nondestructive Testing of Concrete, Second edition, CRC Press, 2004

Clemeña (2004) "*Short-Pulse Radar Methods"* Chapter 13 in Handbook on Nondestructive Testing of Concrete, Second edition, CRC Press, 2004

Concrete Society Technical Report No 15 (1978) *"Assessment of Fire-Damaged Concrete Structures and Repair by Gunite"* Report of a Concrete Society Working Party, Unite Kingdom, May 1978

Concrete Society Technical Report No 68 (2008) *"Assessment, Design and Repair of Fire-Damaged Concrete Structures"* Report of a Concrete Society Working Group, Unite Kingdom, December 2008

Eurocode 2 (2004) ENV 1992-1-2: *Design of Concrete Structures – Part 1-2: General Rules- Structural fire design*, 2004

Felicetti R. (2004)*"Digital Camera Colorimetry for the Assessment of Fire Damaged Concrete"* Fib Task Group 4.3 Workshop Fire Design of Concrete Structures: What now? What next? - Milan, Dec. 2-4, 2004

Felicetti R. (2006)*"The drilling resistance test for the assessment of fire damaged concrete"* Cement & Concrete Composites 28 321-329, Elsevier, 2006

Felicetti R. (2009) *"Combined while-drilling techniques for the assessment of deteriorated concrete cover"* Proceedings of the Conference on Non-Destructive Testing in Civil Engineering, Nantes, France, 2009

fib (2008) "Fire design of concrete structures – structural behaviour and assessment" State of the art report, fib bulletin 46, 2008

Hager I. (2010) *"The Application of RGB Histogram Analysis of Colour Images as a Method of Assessing the Condition of Concrete in Structures after Fire"* Proceedings of the Sixth International Conference on Structures in Fire held at Michigan State University, Michigan, U.S.A., 2010

Harmathy T. Z. (1993) *"Fire Safety Design & Concrete"* Book published by Longman Group UK Limited 1993

Jones C. D. (1986) *"Repair of fire damaged structures"* Proceedings of the International conference on Design of Structures Against Fire held at Aston University, Birmingham, UK 1986

Lindblad Å., Pettersson O., Schmidt B. and Ödeen K. (1966) *"Fire in storehouse 6 in the free port of Stockholm"* (in Swedish), Väg- och vattenbyggaren nr 12, 1966

Malhotra V. M. (2004) "*Handbook on Nondestructive Testing of Concrete"* Chapter 1, Second edition, CRC Press, 2004

Malhotra H. L (1984) "*Spalling of Concrete in Fire"s*, Construction Industry Research and Information Association, Technical Report No. 118, London 1984

Malhotra V. M., Carette G. G. (2004) "*Handbook on Nondestructive Testing of Concrete"* Chapter 2, Second edition, CRC Press, 2004

Naik T. R. et al (2004) "*Handbook on Nondestructive Testing of Concrete"* Chapter 8, Second edition, CRC Press, 2004

Nijland and Larbi (2001) "*Unraveling the temperature distribution in fire-damaged concrete by means of PFM microscopy: Outline of the approach and review of potentially useful reactions"*, Heron vol 46, no 4, 253-26.

Pettersson O. (1975) *"Post-Behaviour of Concrete Structures Subjected to Fire"*, Lund Institute of Technology, Bulletin 40, 1975

RILEM TC 129 MHT (2004) "Test methods for mechanical properties of concrete at high temperatures - Part 5: Modulus of elasticity for service and accident conditions", Materials and Structures, Vol. 37, March 2004, pp. 139-144

Schneider et al (1990) *"Reparability of Fire Damaged Structures"* by the committee CIB W14, Fire Safety Journal, Vol. 16 No.4, 1990

Short N. R. et al (2001) *"Assessment of fire damage concrete using colour image analysis"*, Construction and Building Materials 15, 9-15, 2001

Sundius N. (1931) *"Investigation of Fire Exposed Concrete by Microscopy"* (in Swedish) Betong Häfte 2, 1931

Swedish Tariff Association (1959) *"Concrete and Fire"* (in Swedish), A book published by the Swedish Tariff Association, 1959

Thelandersson S. (1974) *"Concrete Constructions at High Temperatures- An overview"* (in Swedish), VAST, September 1974

Weritz F. et al (2003) *"Investigation of concrete structures with Pulse Phase Thermography"* Proceedings of the International symposium Non-Destructive Methods in Civil Engineering, Berlin, Germany, 2003

Appendix

A. Test matrix

Table A 1 Test Matrix

Core	Ultrasonic pulse transmission time	Mechanical testing	Microscopy
0-8 A Sh-2	x		
0-8 A Sh-5	x		
0-8 A Sh-8	x		
0-8 B Sh-1		x	
0-8 B Sh-2	x		
0-8 B Sh-3		x	
0-8 B Sh-4	x		x
0-8 B Sh-5	x		
0-8 B Sh-6		x	
0-8 B Sh-7		x	
0-8 B Sh-8		x	
0-8 A Std-2	x		
0-8 A Std-6	x		
0-8 A Std-8	x		
0-8 B Std-1		x	x
0-8 B Std-2		x	
0-8 B Std-3		x	
0-8 B Std-4	x		
0-8 B Std-5		x	
0-8 B Std-6	x		
0-8 B Std-7		x	
0-8 B Std-8	x		
0-16 A Sh-1			x
0-16 A Sh-2	x		
0-16 A Sh-3	x		
0-16 A Sh-6	x		
0-16 B Sh-1	x		
0-16 B Sh-2		x	
0-16 B Sh-3		x	
0-16 B Sh-4		x	
0-16 B Sh-5	x		
0-16 B Sh-6	x		
0-16 B Sh-7		x	
0-16 B Sh-8		x	
0-16 A Std-1	x		
0-16 A Std-2	x		
0-16 A Std-3		x	
0-16 A Std-4		x	
0-16 A Std-5		x	
0-16 A Std-6		x	
0-16 A Std-7		x	
0-16 A Std-8	x		x
0-16 B Std-2	x		
0-16 B Std-3	x		
0-16 B Std-7	x		
0-8 V-2	x		
0-8 V-3		x	
0-8 V-4		x	
0-8 V-5		x	
0-8 V-6		x	
0-8 V-8		x	
0-16 V-2	x	x	
0-16 V-3		x	
0-16 V-4		x	
0-16 V-5		x	
0-16 V-8		x	

B. Furnace temperature

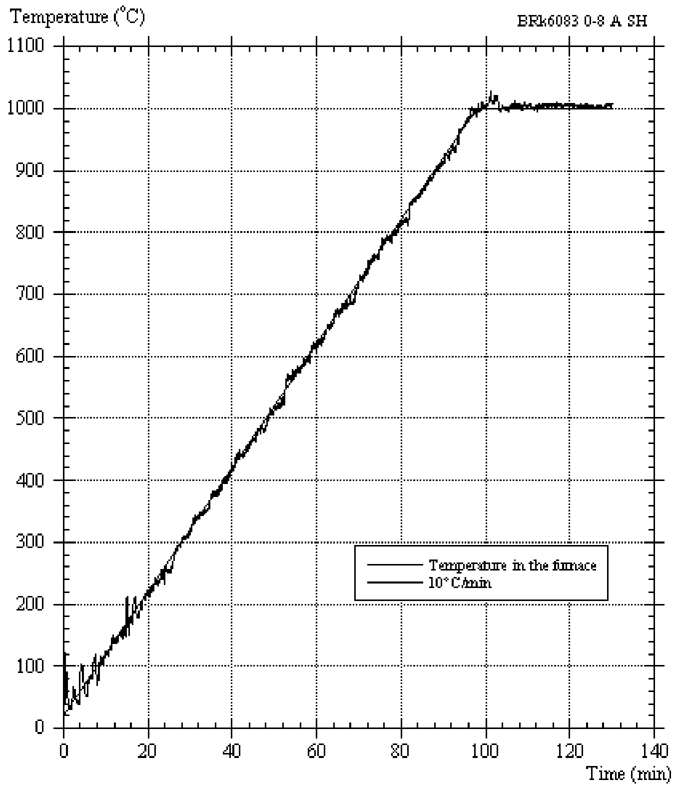

Figure B 1 *Specified temperature and actual furnace temperature 0-8 A Sh.*

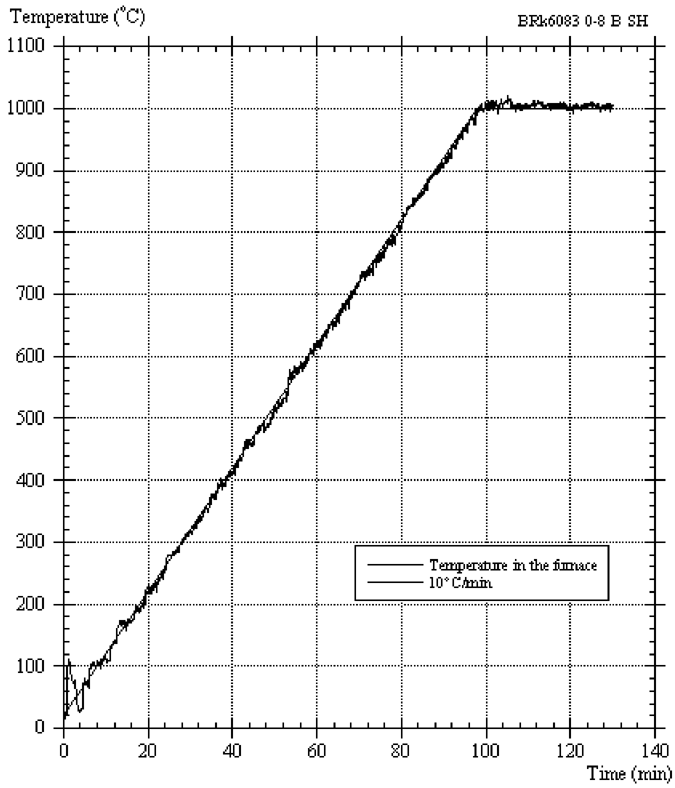

Figure B 2 *Specified temperature and actual furnace temperature 0-8 B Sh.*

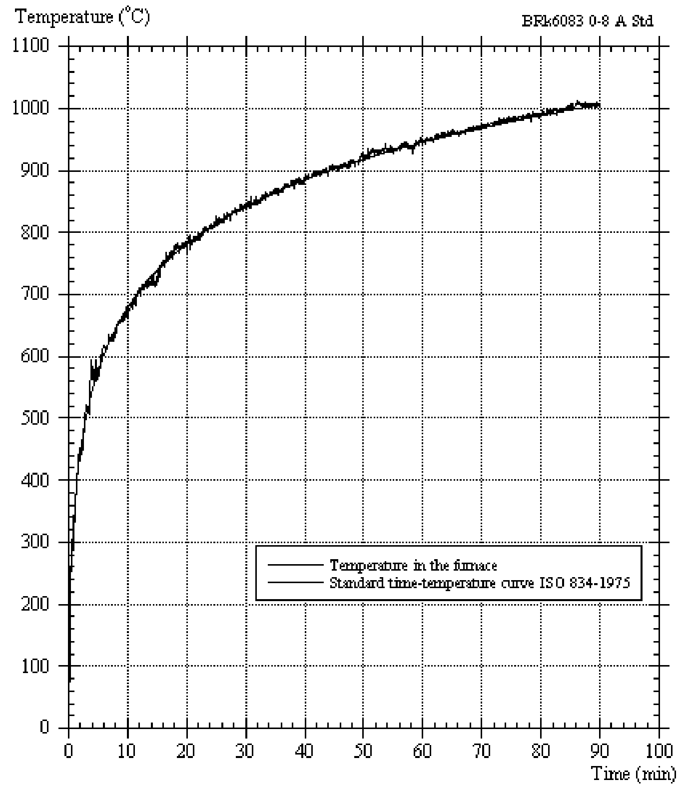

Figure B 3 *Specified temperature and actual furnace temperature 0-8 A Std.*

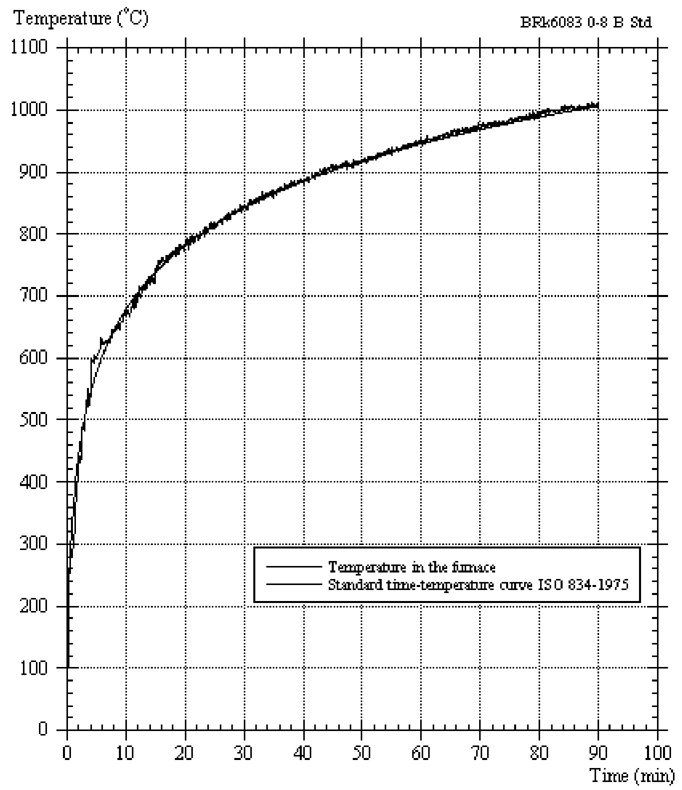

Figure B 4 *Specified temperature and actual furnace temperature 0-8 B Std.*

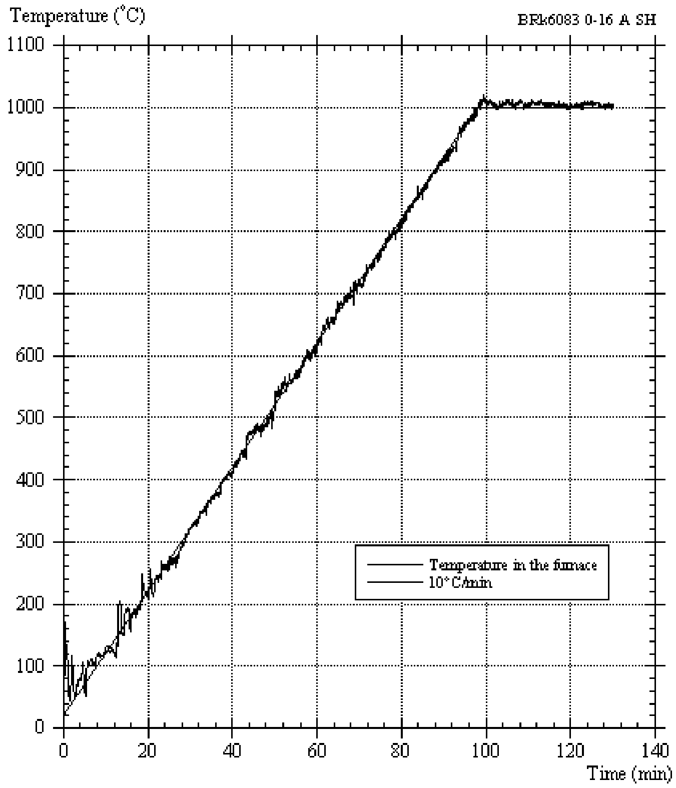

Figure B 5 *Specified temperature and actual furnace temperature 0-16 A Sh.*

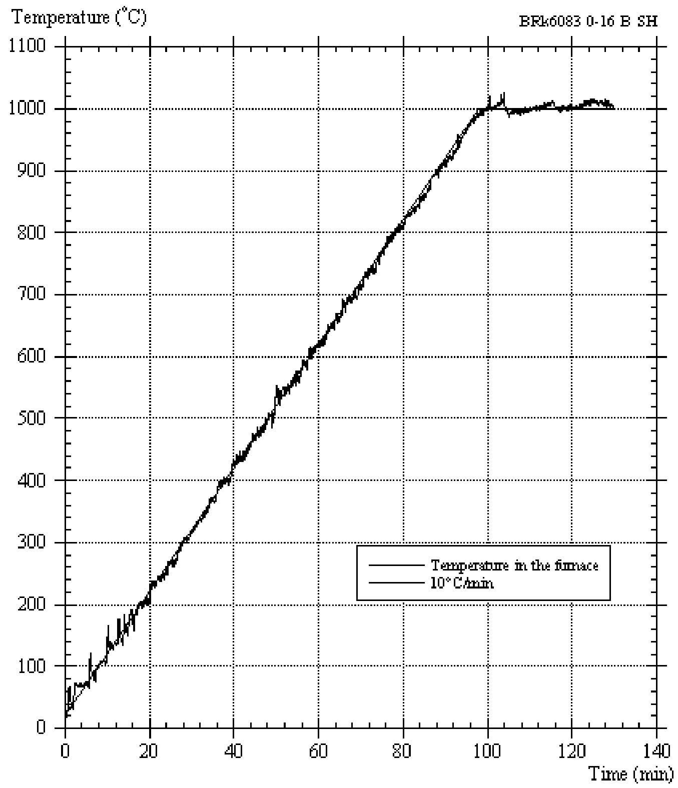

Figure B 6 *Specified temperature and actual furnace temperature 0-16 B Sh.*

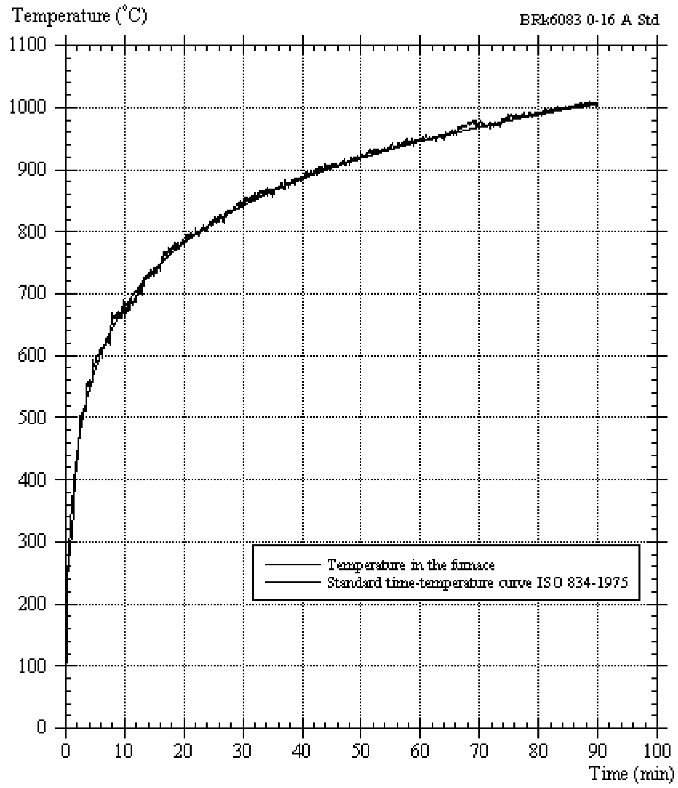

Figure B 7 *Specified temperature and actual furnace temperature 0-16 A Std.*

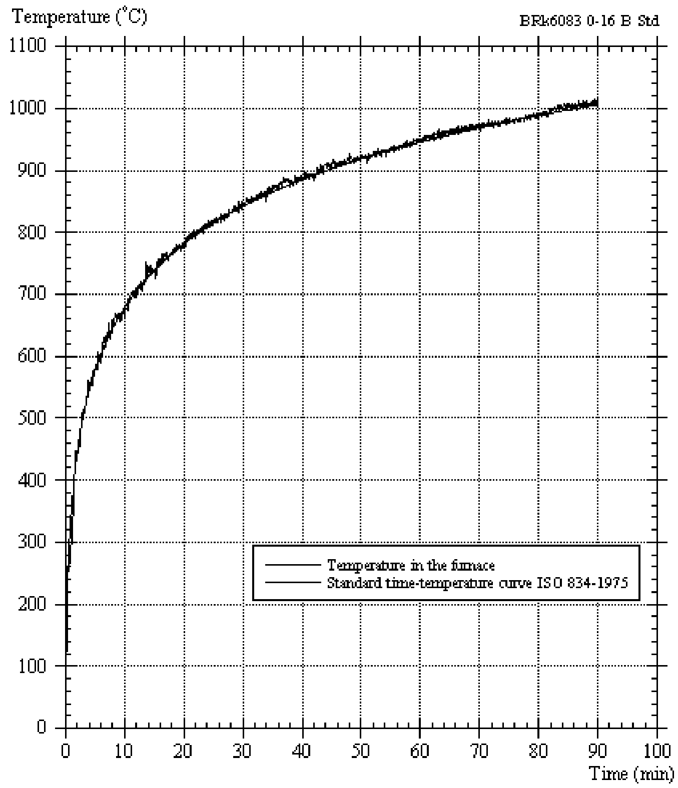

Figure B 8 *Specified temperature and actual furnace temperature 0-16 A Std.*

C. Measured temperature inside the concrete slabs

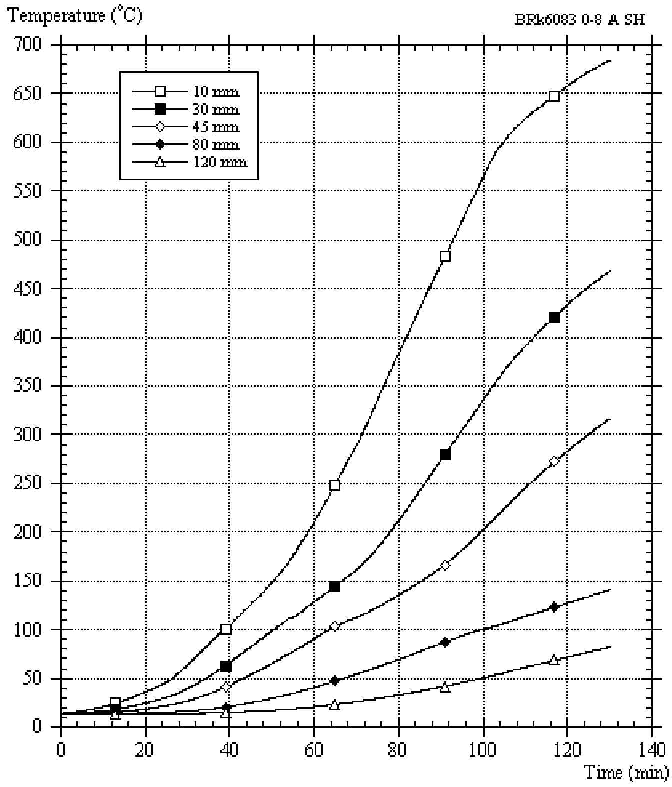

Figure C 1 *Measured temperature inside 0-8 A Sh.*

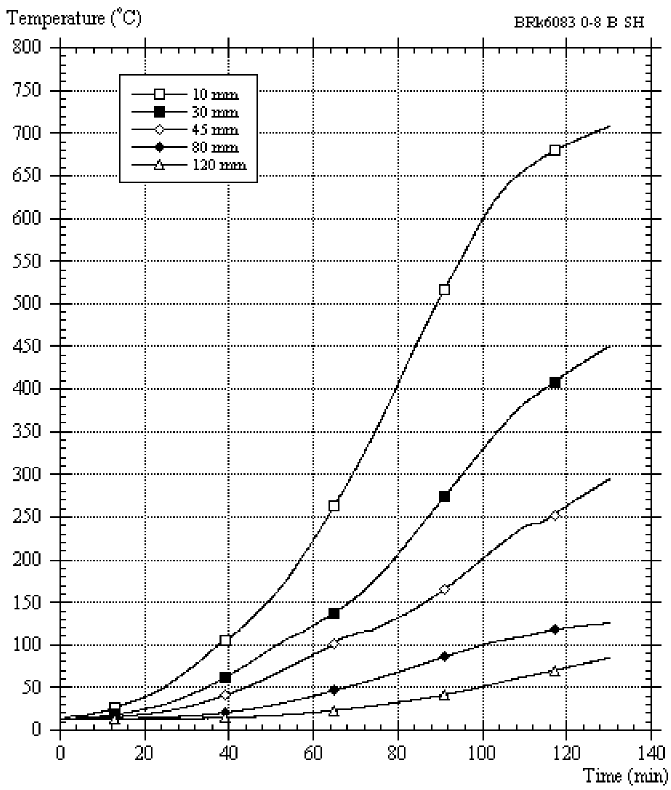

Figure C 2 *Measured temperature inside 0-8 B Sh.*

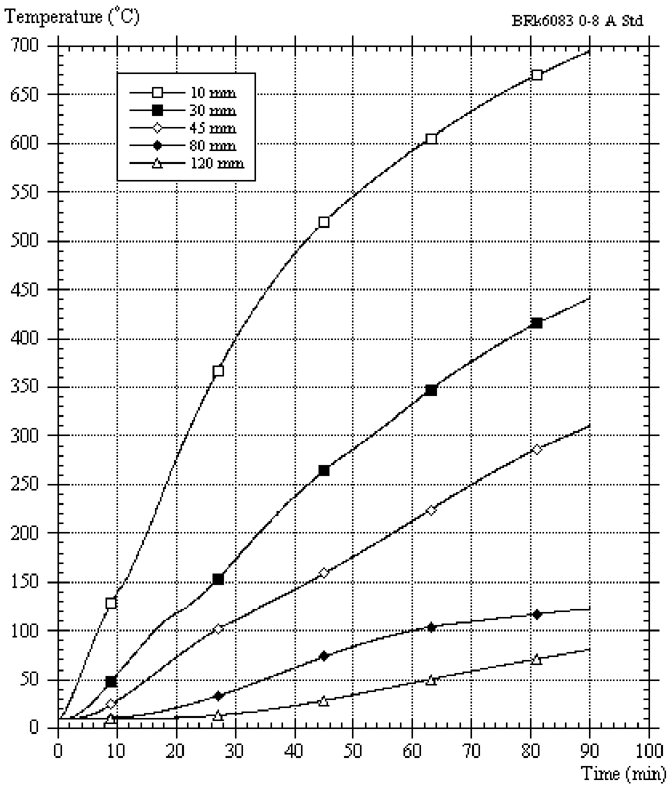

Figure C 3 *Measured temperature inside 0-8 A Std.*

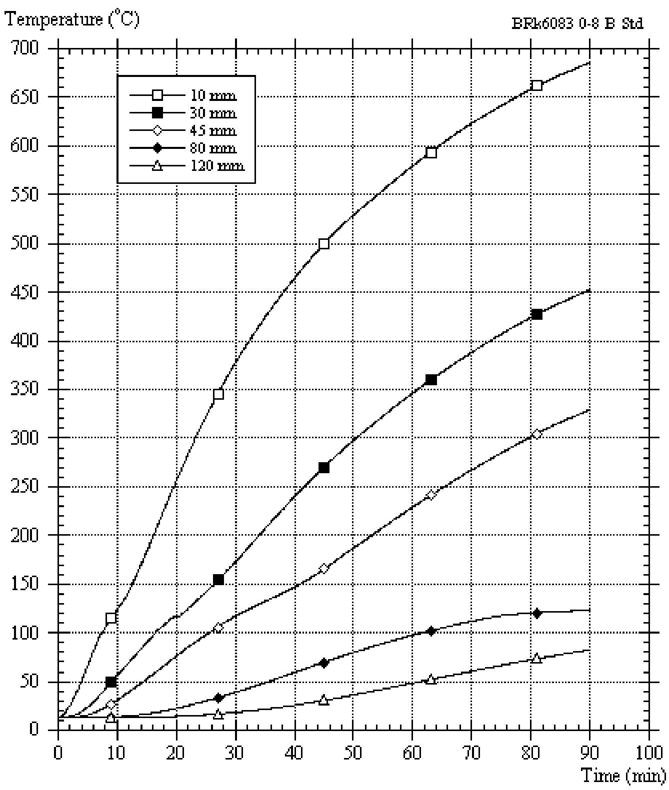

Figure C 4 *Measured temperature inside 0-8 B Std.*

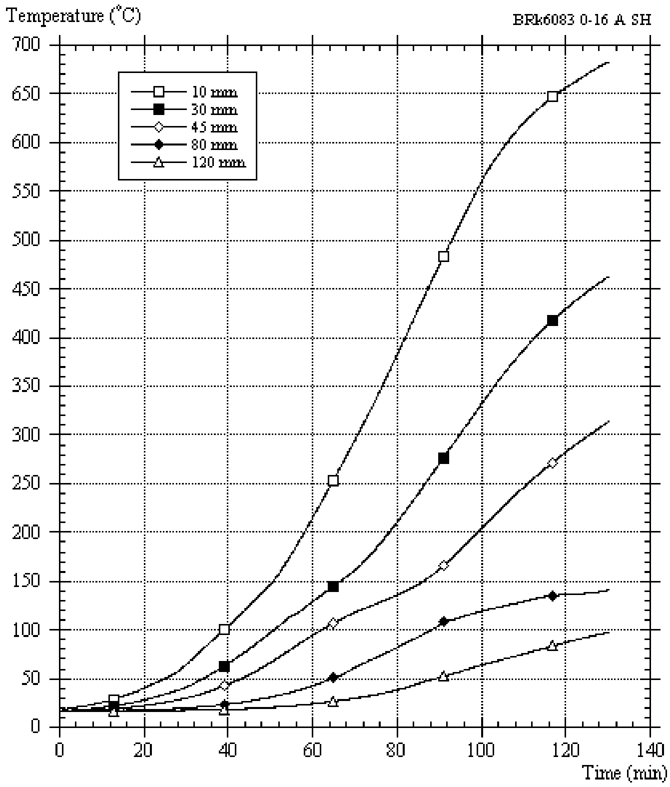

Figure C 5 *Measured temperature inside 0-16 A Sh.*

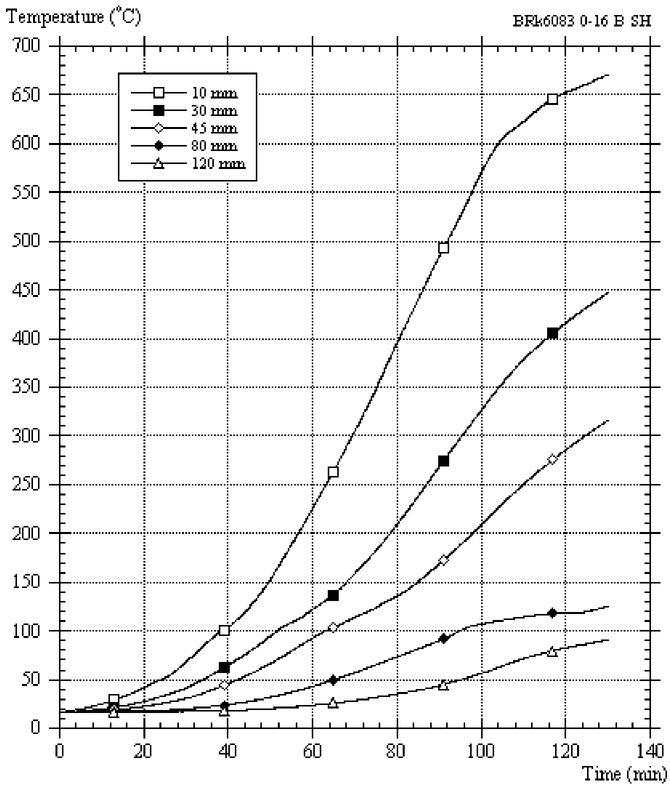

Figure C 6 *Measured temperature inside 0-16 B Sh.*

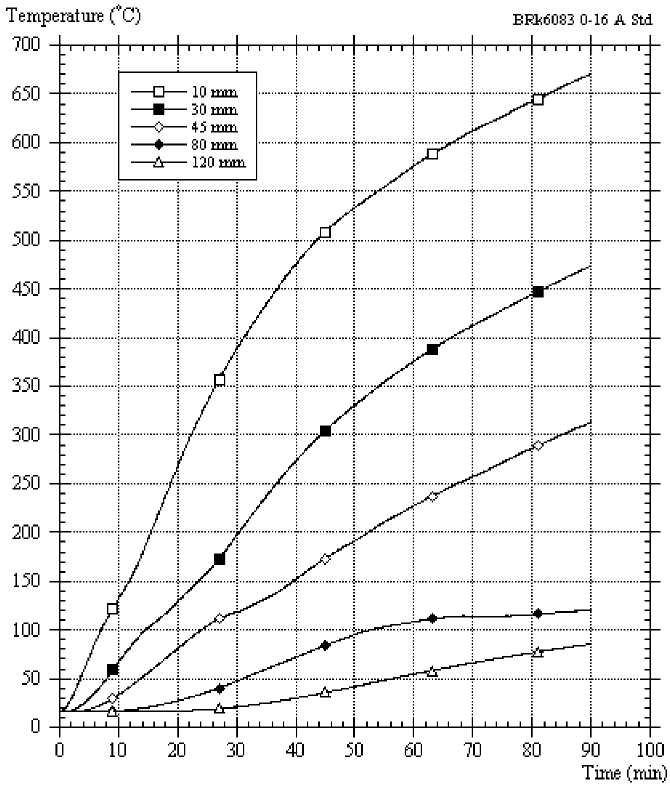

Figure C 7 *Measured temperature inside 0-16 A Std.*

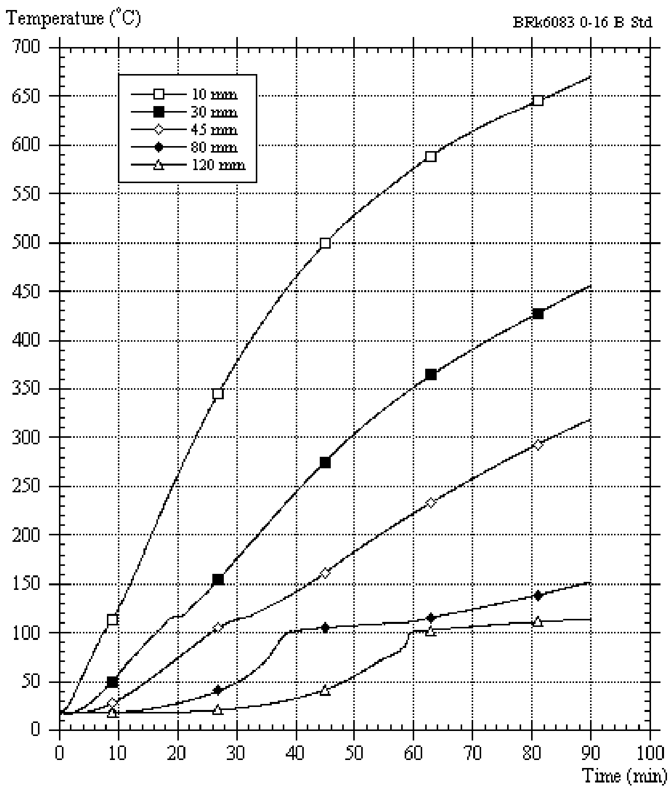

Figure C 8 *Measured temperature inside 0-16 B Std.*

D. Strain field

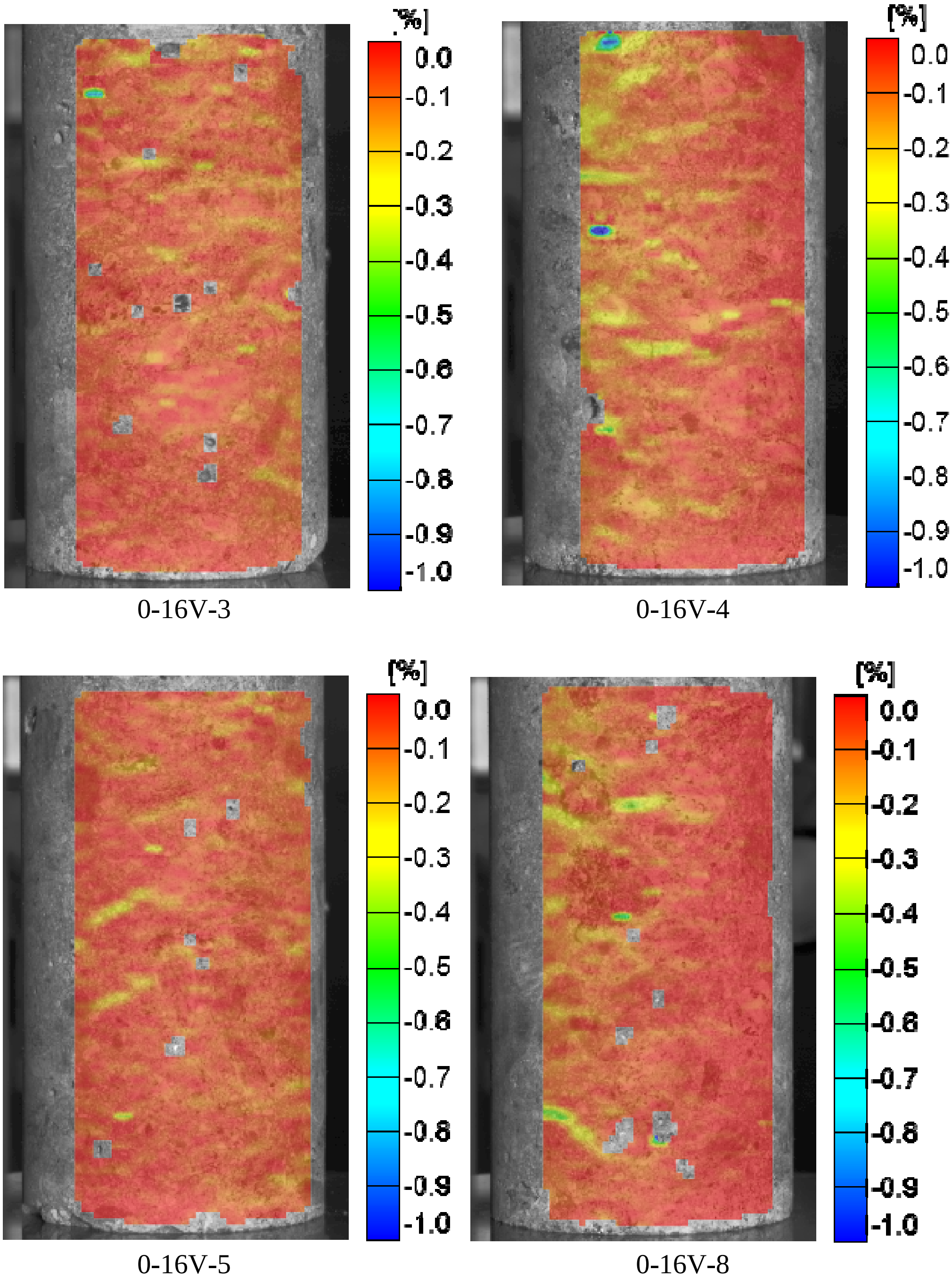

Figure D 1 *Axial compressive strain field for specimens in group 0-16 V.*

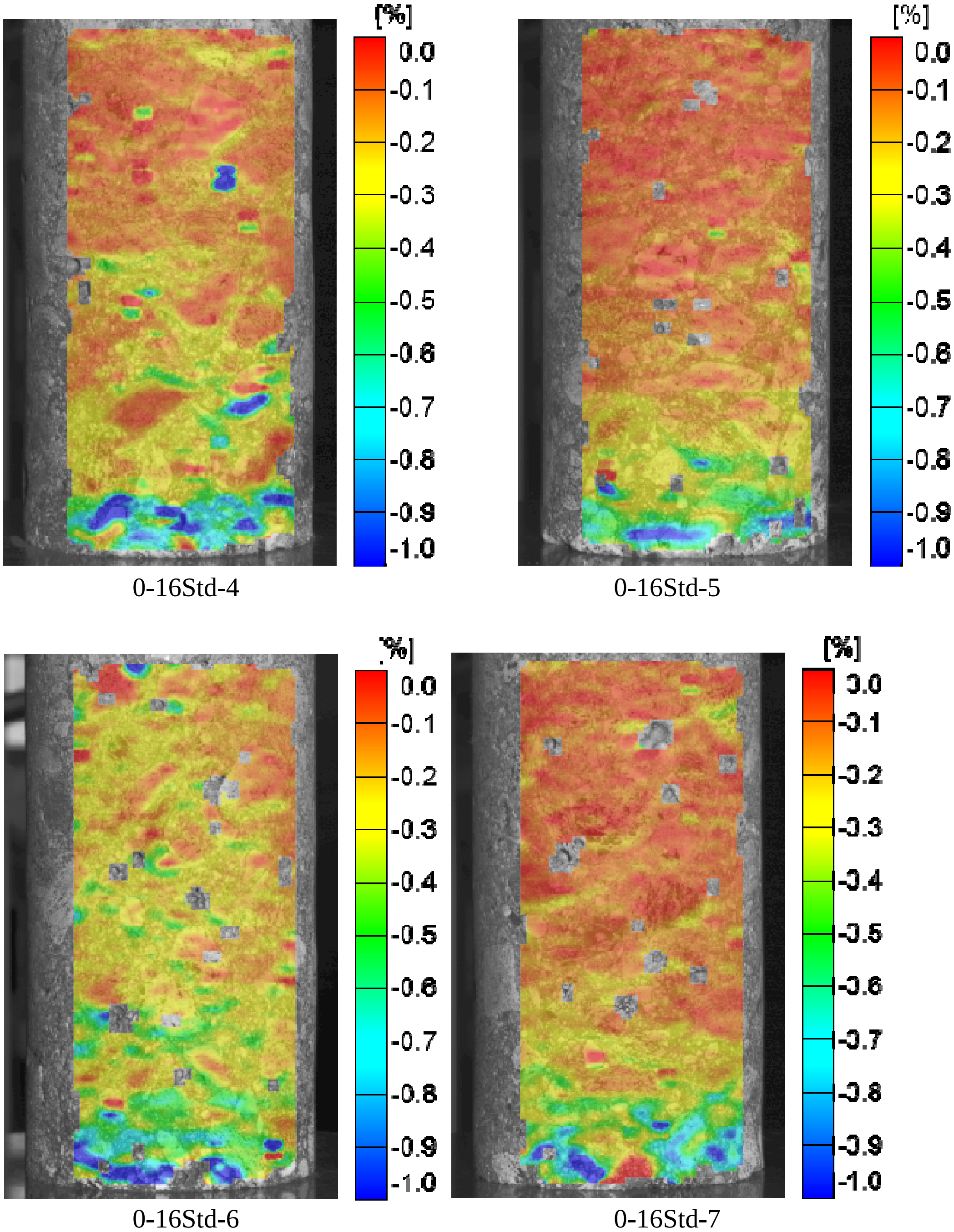

Figure D 2 *Axial compressive strain field for specimens in group 0-16 Std.*

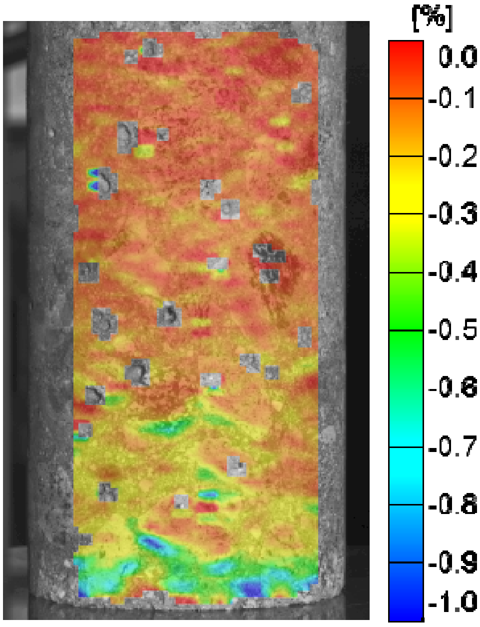

0-16Sh-2

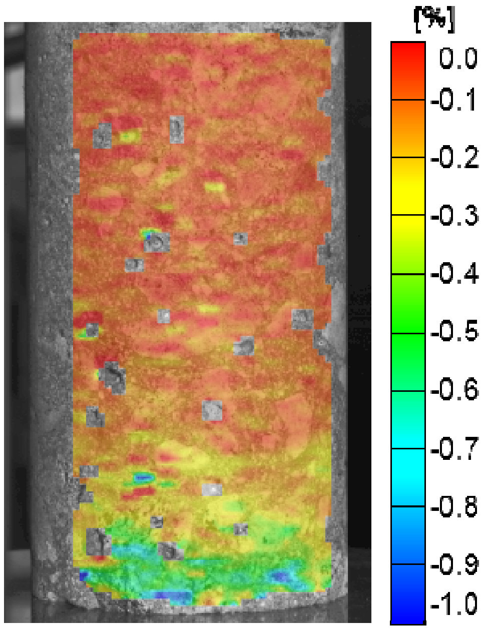

0-16Sh-3

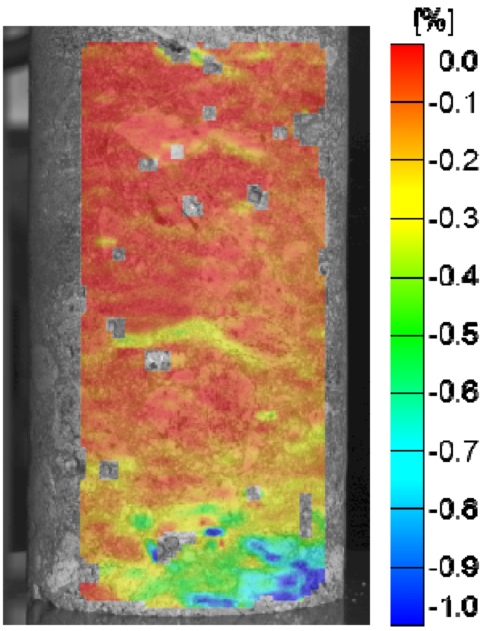

0-16Sh-4

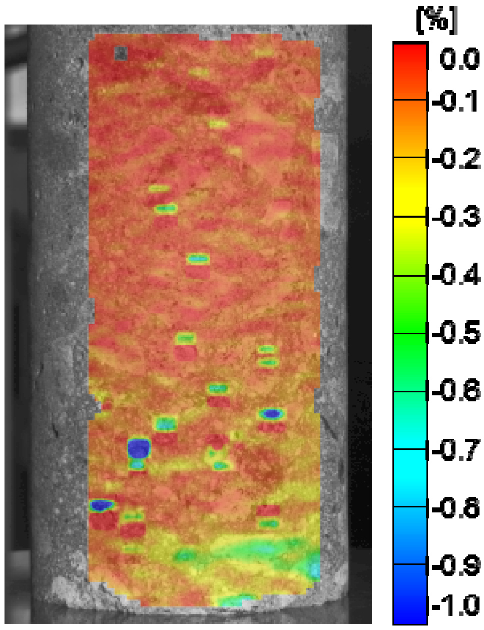

0-16Sh-7

Figure D 3 *Axial compressive strain field for specimens in group 0-16 Sh.*

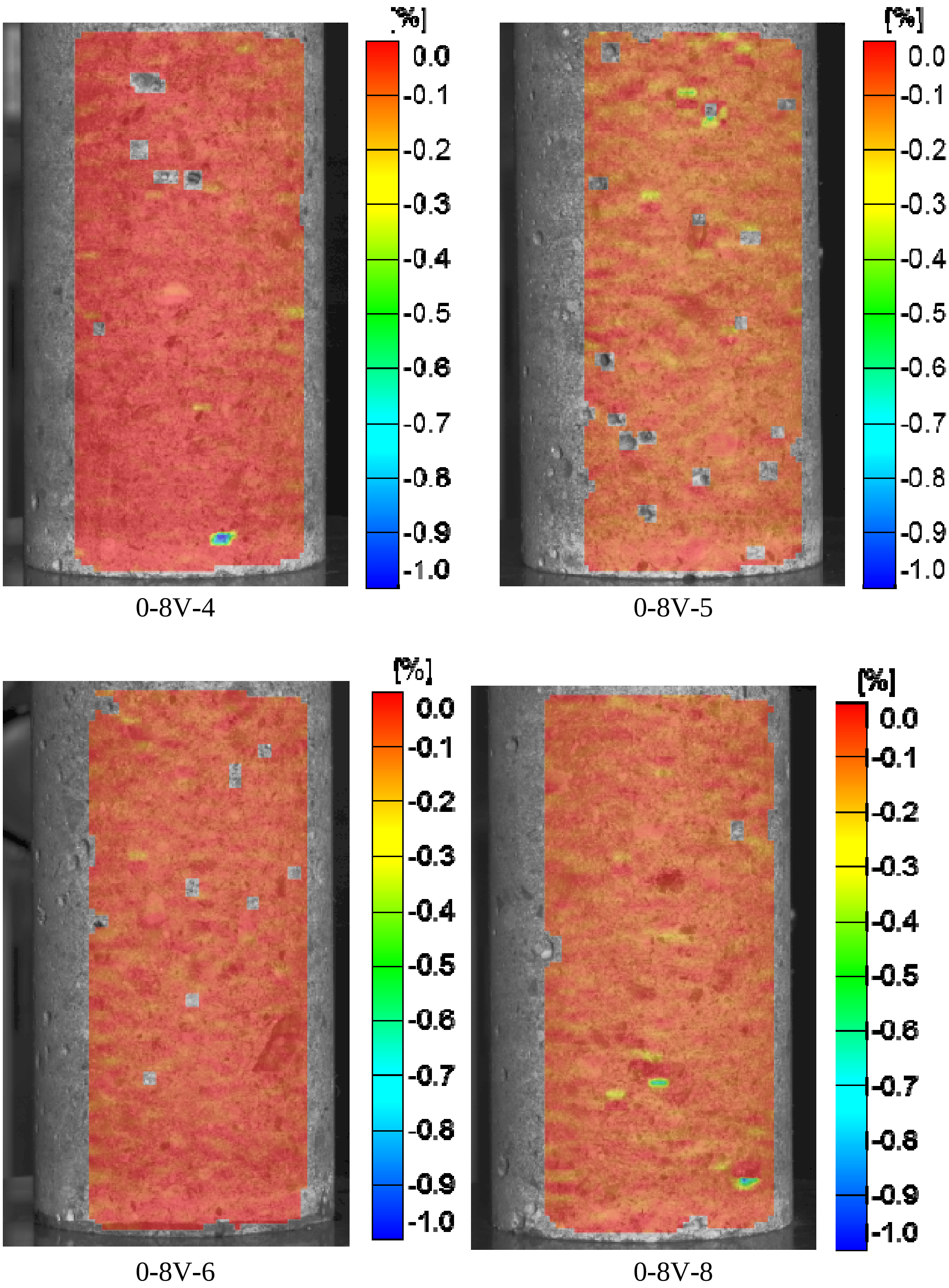

Figure D 4 *Axial compressive strain field for specimens in group 0-8 V.*

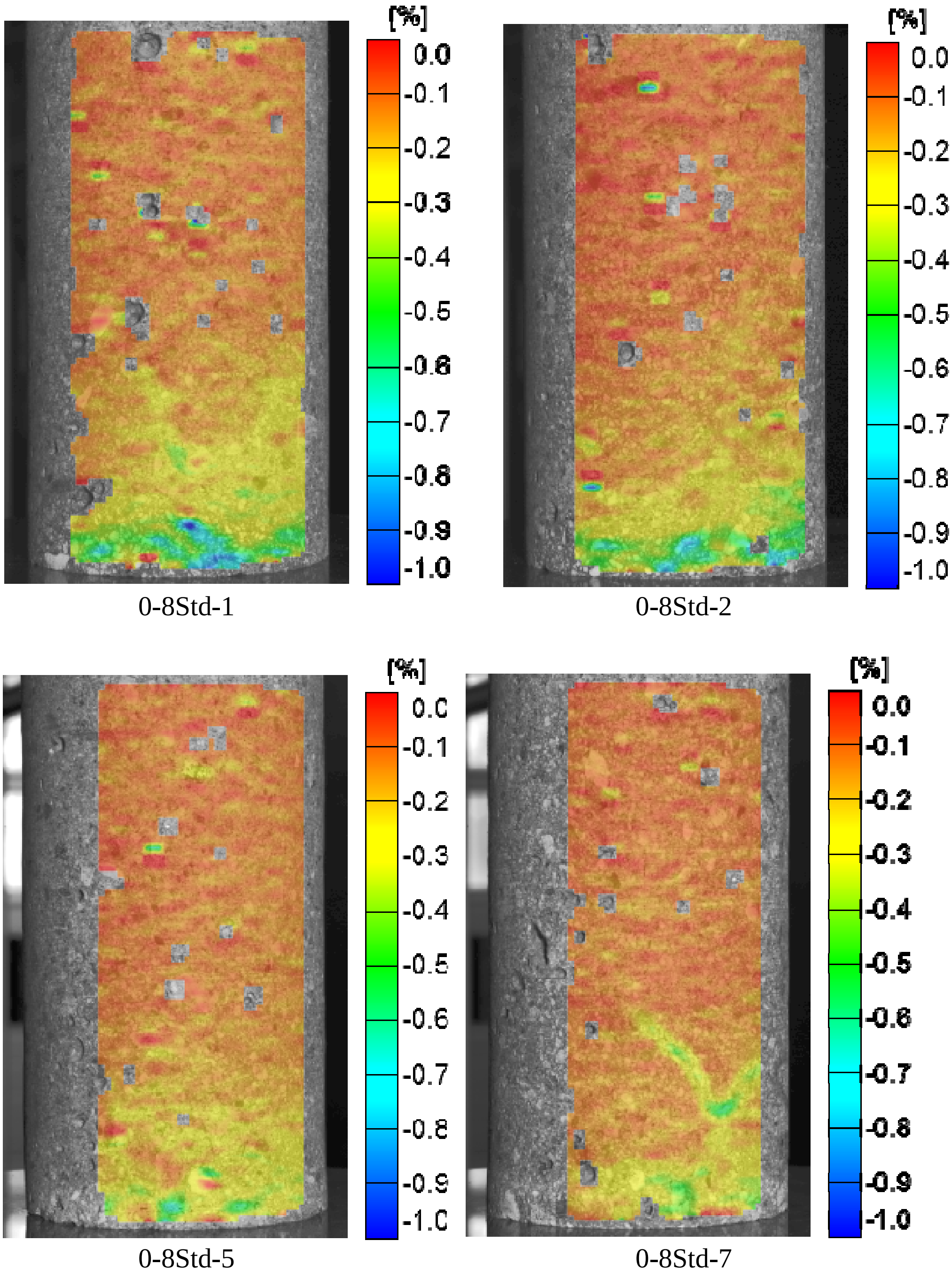

Figure D 5 *Axial compressive strain field for specimens in group 0-8 Std.*

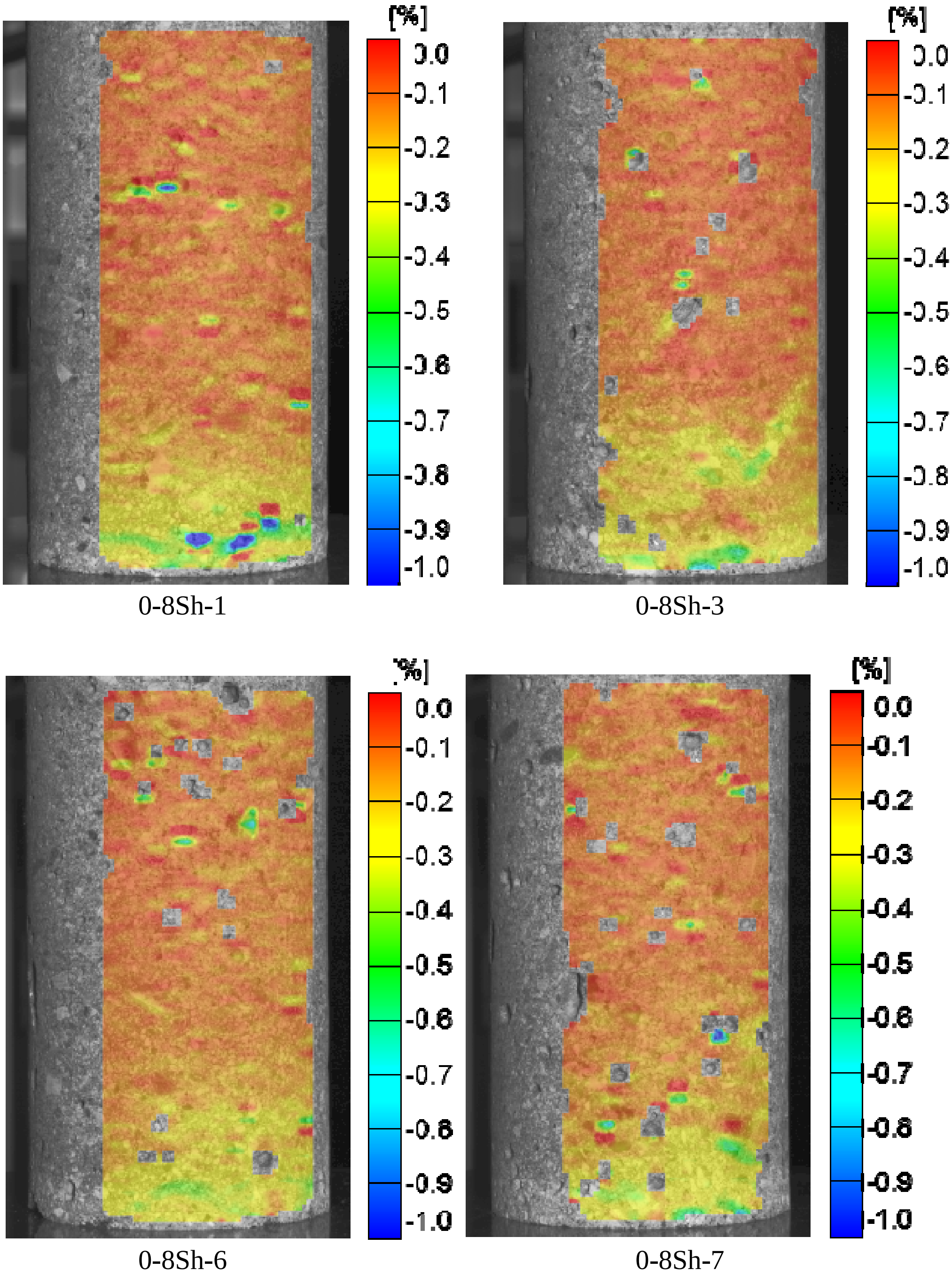

Figure D 6 *Axial compressive strain field for specimens in group 0-8 Sh.*

E. Strain depth

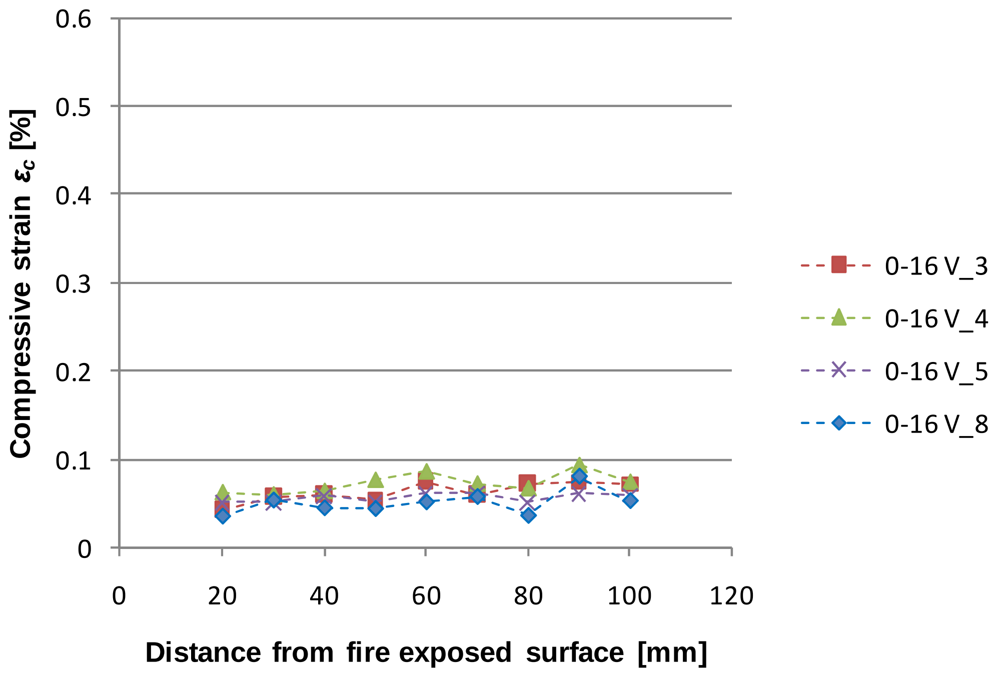

Figure E 1 *Axial compressive section strain ε_(c,s) vs. distance from fire exposed surface for specimens in group 0-16 V. The axial compressive stress was 20 MPa.*

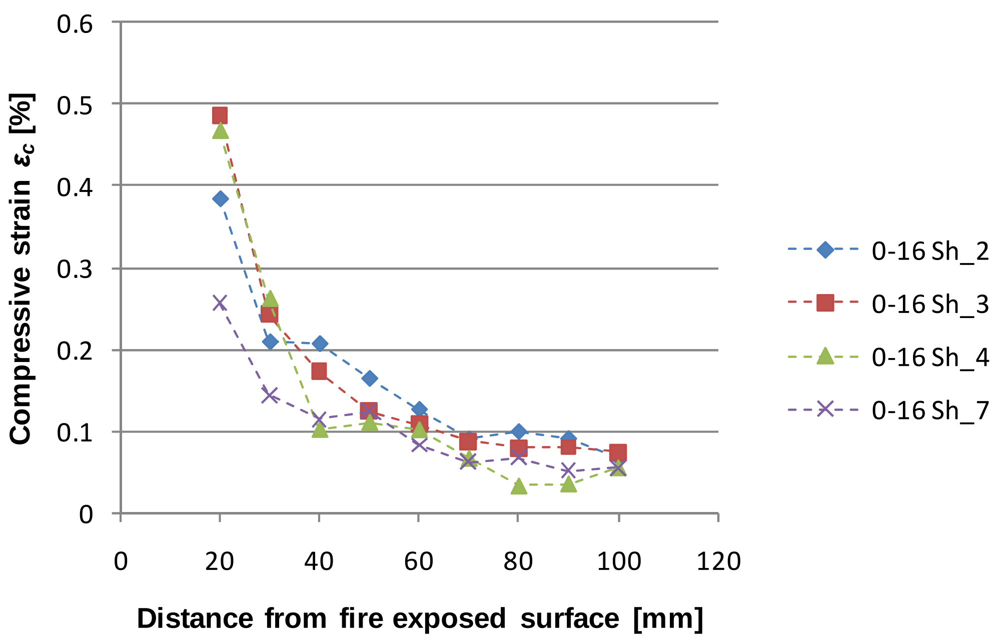

Figure E 2 *Axial compressive section strain ε_(c,s) vs. distance from fire exposed surface for specimens in group 0-16 Sh. The axial compressive stress was 20 MPa.*

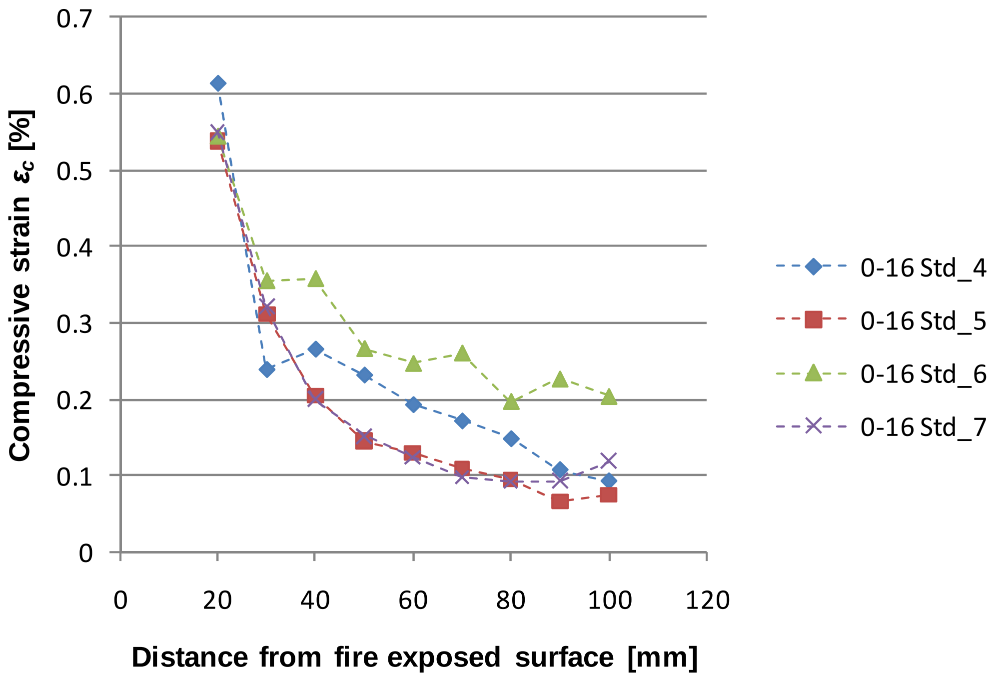

Figure E 3 *Axial compressive section strain ε_(c,s) vs. distance from fire exposed surface for specimens in group 0-16 Std. The axial compressive stress was 20 MPa.*

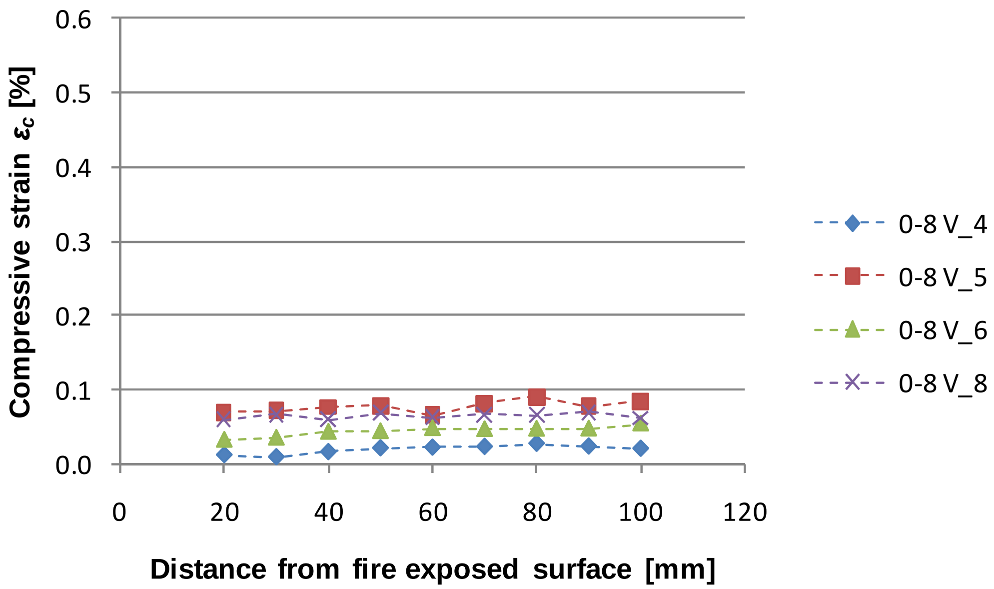

Figure E 4 *Axial compressive section strain ε_(c,s) vs. distance from fire exposed surface for specimens in group 0-8 V. The axial compressive stress was 20 MPa.*

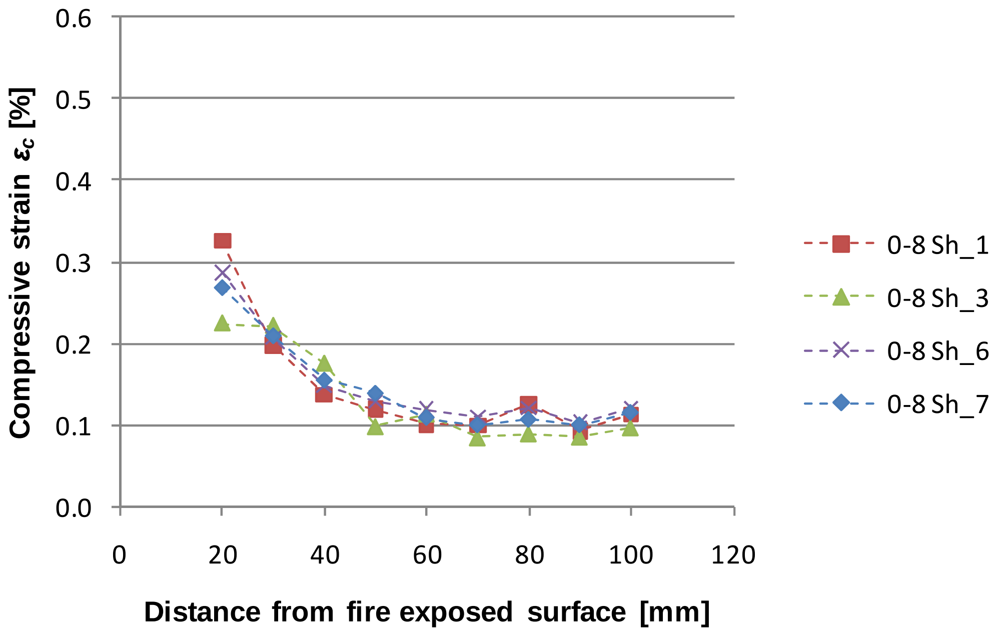

Figure E 5 *Axial compressive section strain ε_(c,s) vs. distance from fire exposed surface for specimens in group 0-8 Sh. The axial compressive stress was 20 MPa.*

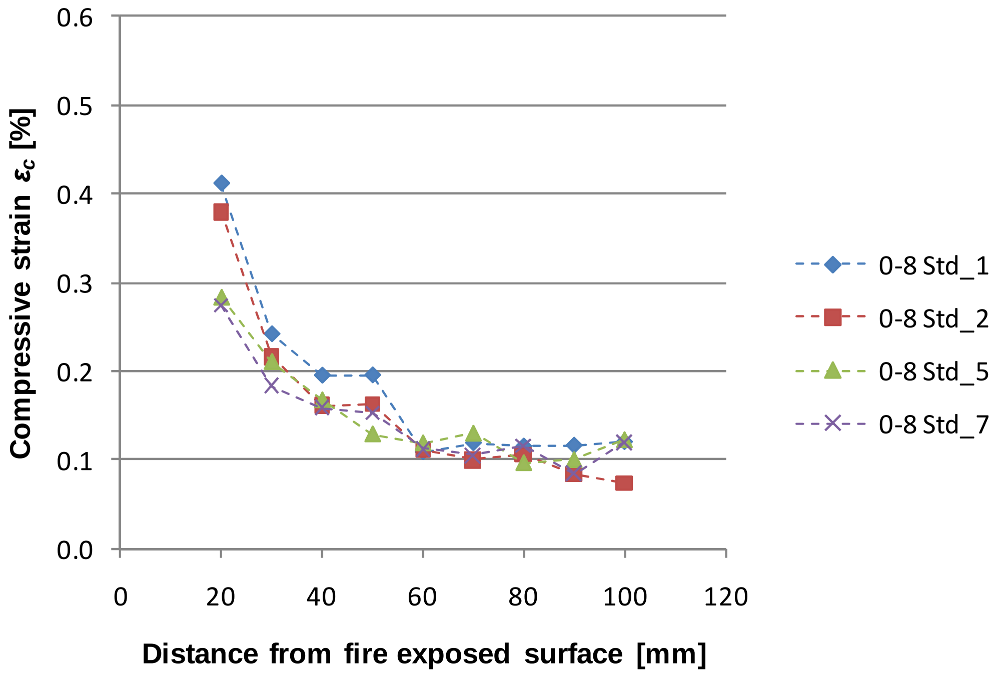

Figure E 6 *Axial compressive section strain ε_(c,s) vs. distance from fire exposed surface for specimens in group 0-8 Std. The axial compressive stress was 20 MPa.*

F. Stress-deformation

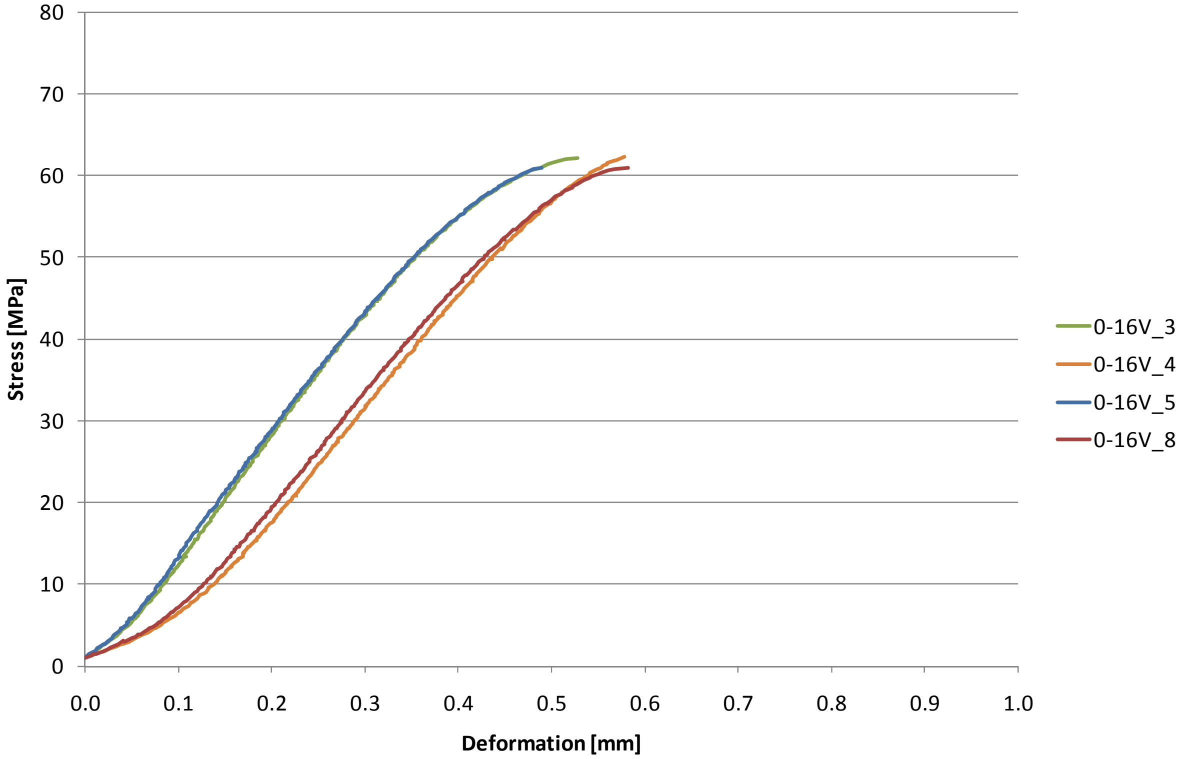

Figure F 1 *Compressive stress vs. axial deformation for specimens in group 0-16 V.*

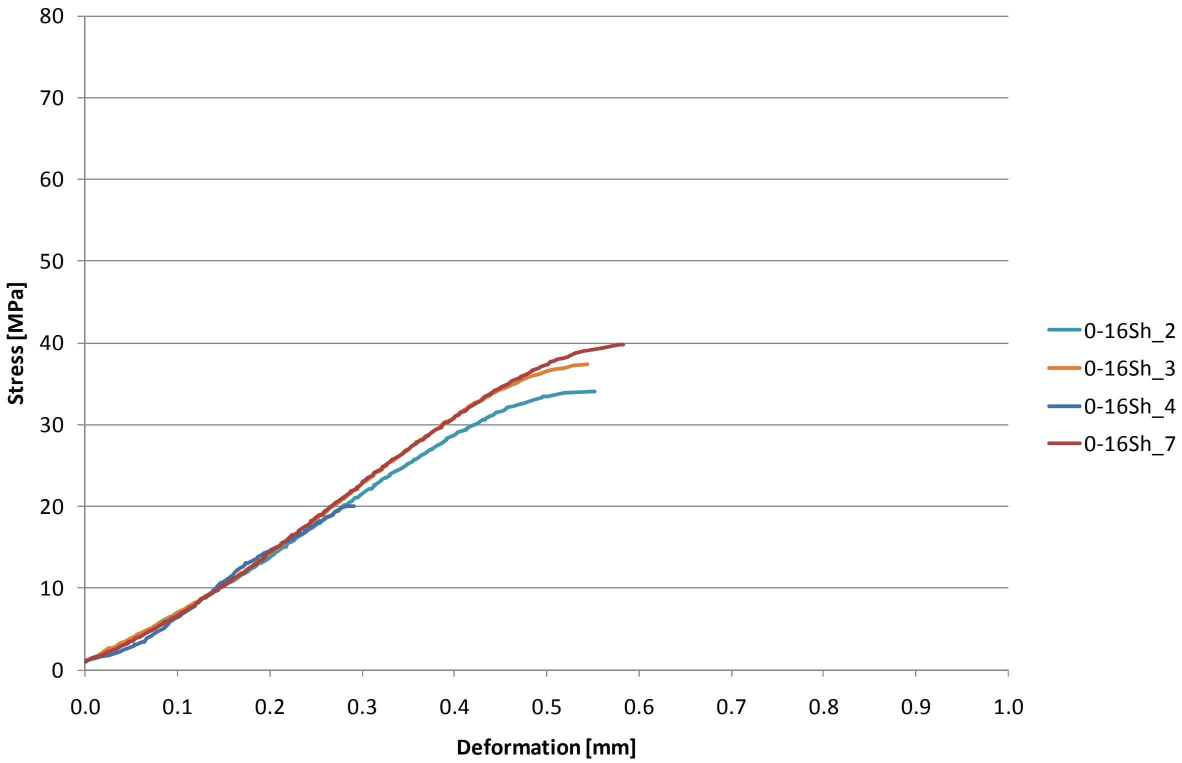

Figure F 2 *Compressive stress vs. axial deformation for specimens in group 0-16 Sh.*

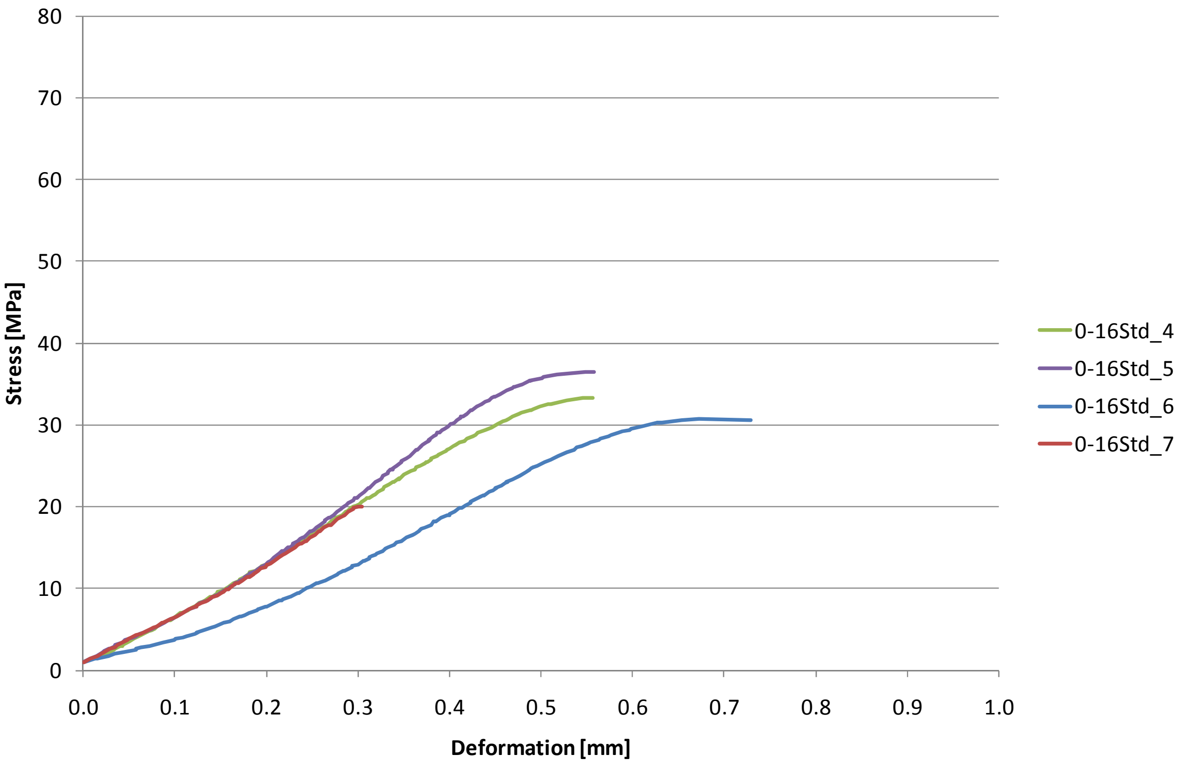

Figure F 3 *Compressive stress vs. axial deformation for specimens in group 0-16 Std.*

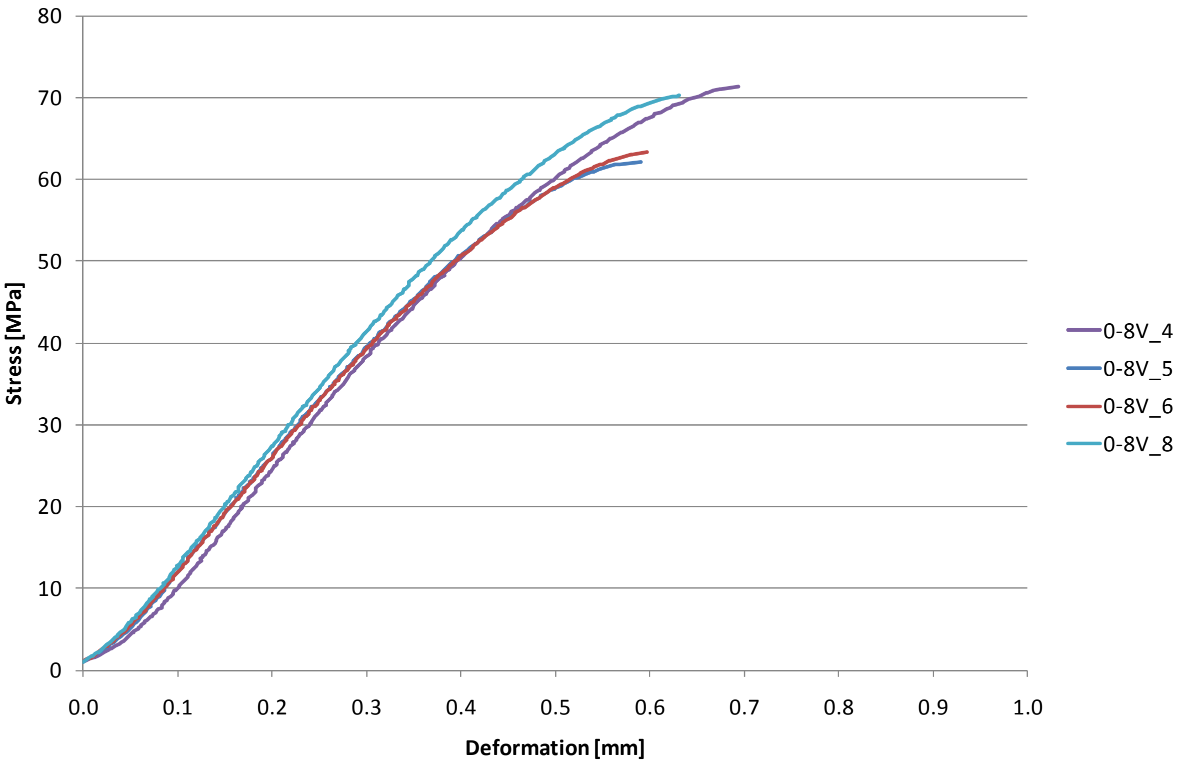

Figure F 4 *Compressive stress vs. axial deformation for specimens in group 0-8 V.*

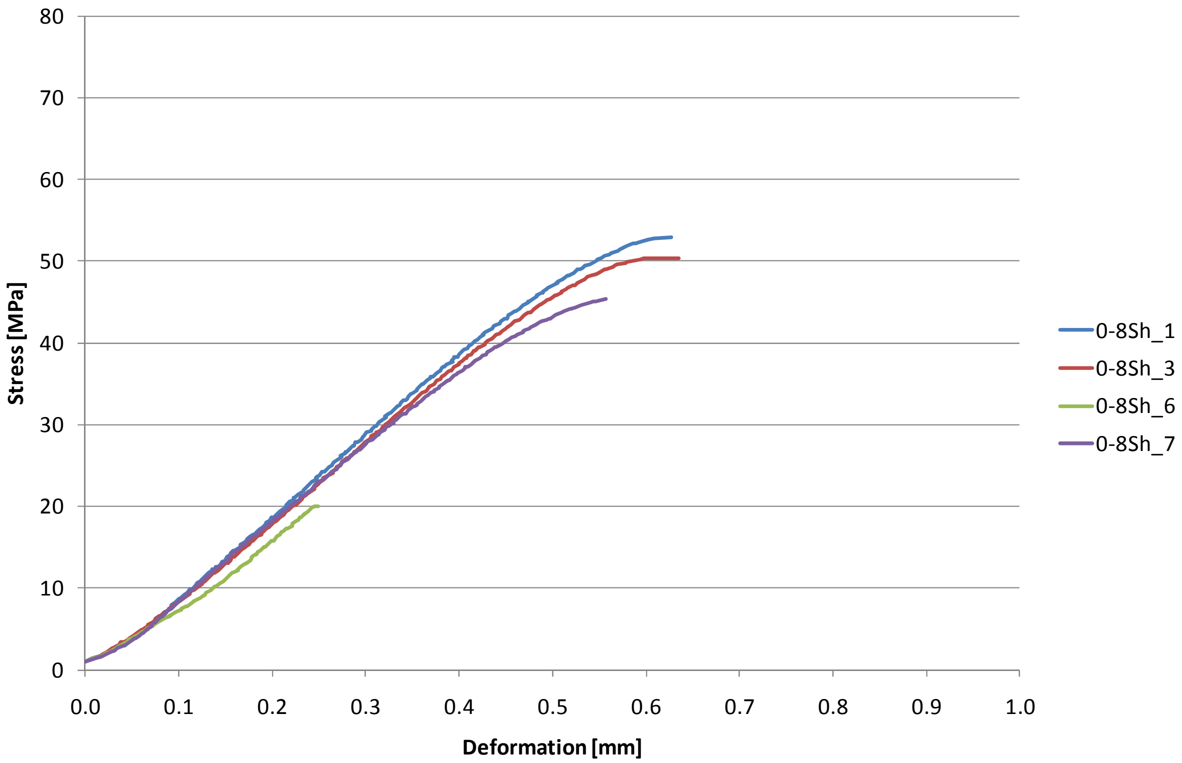

Figure F 5 *Compressive stress vs. axial deformation for specimens in group 0-8 Sh.*

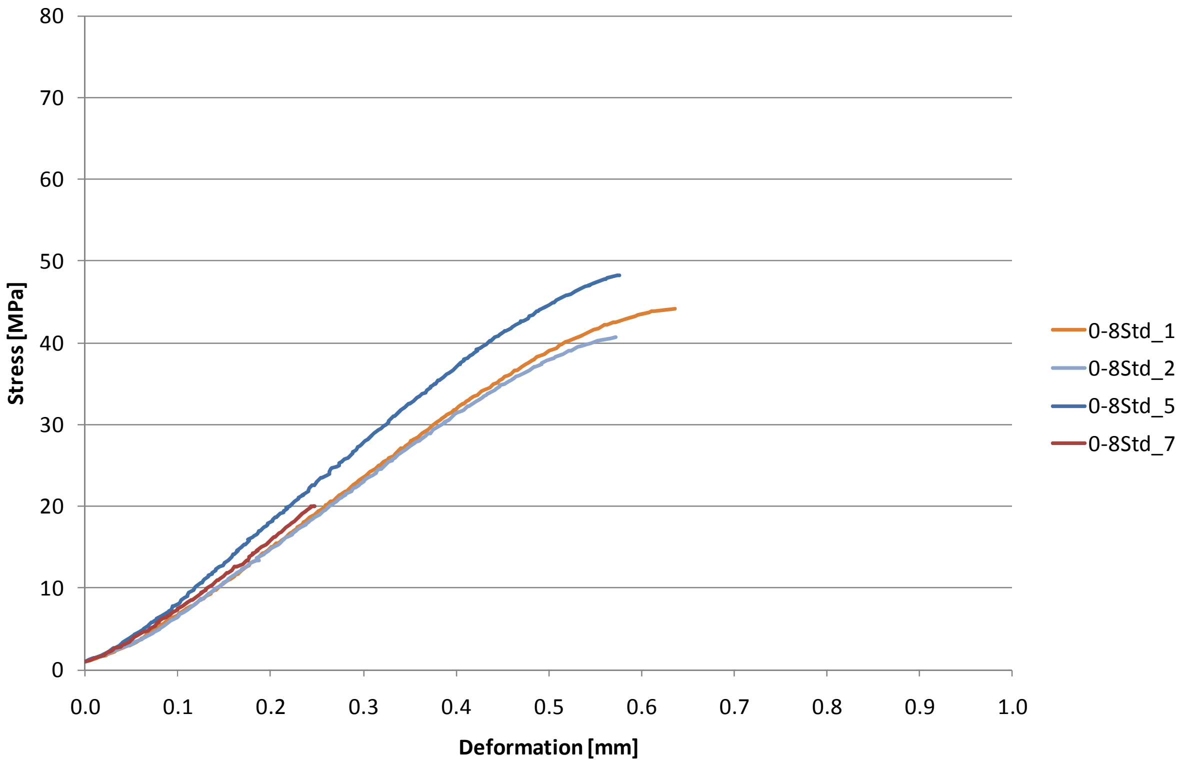

Figure F 6 *Compressive stress vs. axial deformation for specimens in group 0-8 Std.*

SP Technical Research Institute of Sweden

Our work is concentrated on innovation and the development of value-adding technology. Using Sweden's most extensive and advanced resources for technical evaluation, measurement technology, research and development, we make an important contribution to the competitiveness and sustainable development of industry. Research is carried out in close conjunction with universities and institutes of technology, to the benefit of a customer base of about 9000 organisations, ranging from start-up companies developing new technologies or new ideas to international groups.

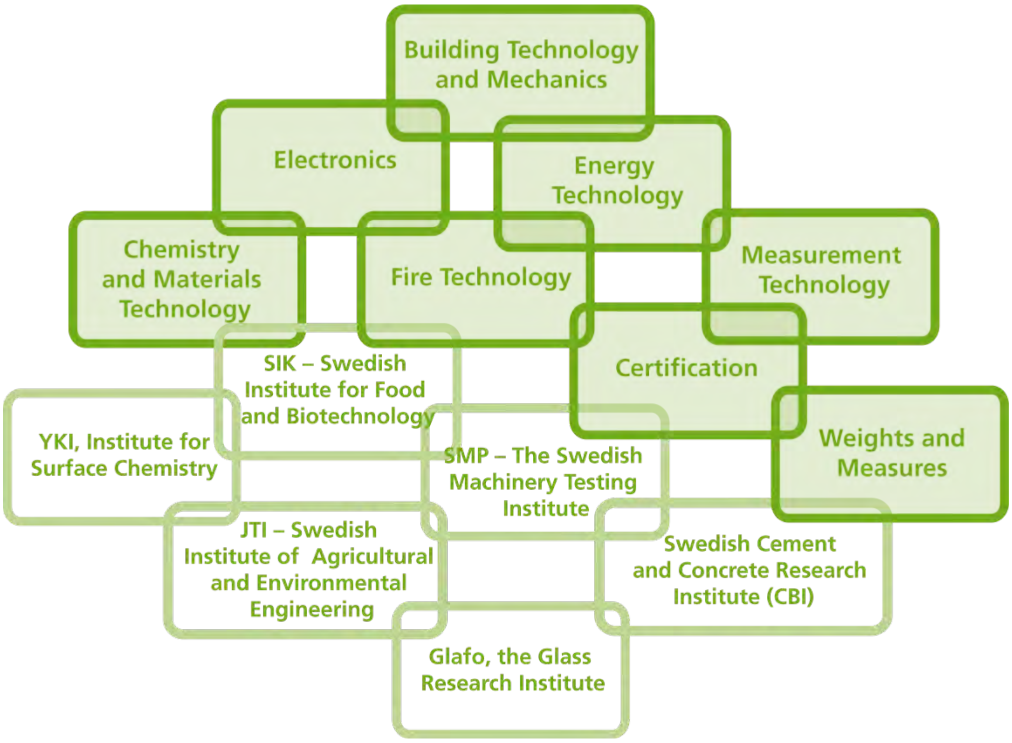

SP Technical Research Institute of Sweden
Box 857, SE-501 15 BORÅS, SWEDEN
Telephone: +46 10 516 50 00, Telefax: +46 33 13 55 02
E-mail: info@sp.se, Internet: www.sp.se
www.sp.se

Fire Technology
SP Report 2011:19
ISBN 978-91-86622-50-3
ISSN 0284-5172

More information about publications published by SP: **www.sp.se/publ**